Geological setting and alteration characteristics of the Hillside mineralising system, Yorke Peninsula

Ben Cerlienco

Centre for Tectonics, Resources and Exploration
Department of Geology and Geophysics
School of Earth and Environmental Sciences
University of Adelaide, South Australia
benjamin.cerlienco@student.adelaide.edu.au

26 October, 2009

Table of Contents

Abstract

The Hillside Cu-Au deposit of the Yorke Peninsula, South Australia is attributable to the iron oxide-copper-gold (IOCG) family of deposits. It has clear genetic affinities with other IOCG deposits of the Gawler Craton and defines the southernmost occurrence of this style of mineralisation in the Olympic Cu-Au province. A broad study on the mineral paragenesis and geochemistry of the deposit was carried out on drill core provided by Rex Minerals, the holder of the Hillside tenement. The deposit is hosted by the Palaeoproterozoic metasedimentary and metavolcanic Wallaroo Formation, and the highly brecciated Mesoproterozoic Arthurton Granite; a Hiltaba Suite equivalent. These breccias are expressions of the Pine Point Fault Zone, which is the dominant structural control on mineralisation. Coastal outcrops are dominated by the Arthurton Granite and Wallaroo Group basement with overlying Stansbury and St Vincent sedimentary sequences. The alteration mineralogy is divisible into four assemblages; a garnet dominated calcsilicate assemblage, an epidote-quartz vein assemblage, a K-feldspar-carbonate-quartz-chlorite-sericite assemblage related to the mineralisation, and later carbonates veins that also host minor mineralisation. Ore mineral paragenesis occurs in an overlapping sequence; the first mineral precipitated was magnetite which was later extensively martitised, with hematite followed by pyrite, then chalcopyrite and later bornite. A later phase of copper and uranium minerals occur with the carbonate veins. Iron oxide chemistry and sulphur isotopes from the sulphides support this paragenesis. Bulk rock composition was found to have a decrease in silica and increase in iron oxide with progressive alteration, while alkali metals (Na, K) and aluminium were also lost from the rock and alkali earths (Mg, Ca) were gained during alteration. Trace element and rare earth element plots show no strong changes that correlate to progressive alteration. Temperature of formation as estimated by TitaniQ thermometry has two major peaks; 450°C-465°C and 495°C-500°C, likely corresponding a primary and a recrystallised quartz stage. Chlorite thermometry is in agreement with several samples; however others overestimate the temperature by an unacceptable amount. It is suggested mineralisation is genetically linked to the intrusion of the Arthurton Granite and activation of the Pine Point Fault, which together supplied both the heat source and plumbing to allow the flow of metal bearing fluids, possibly of magmatic origin. Descriptions of the mineralisation exploited in the historic Hillside Mine are different in their ore mineralogy and likely correspond to a later hypogene or supergene enrichment phase.

1. Introduction

The Hillside Cu-Au deposit is a historically exploited orebody located in the south-east of the Moonta-Wallaroo district of the Gawler Craton, approximately 12 km south of Ardrossan, South Australia (Figure 1). The deposit and surrounding region, occasionally referred to as the 'Pine Point Copper Belt', has been the focus of recent exploration drilling targeting iron oxide-copper-gold (IOCG) style mineralisation along the Pine Point Fault Zone. The Pine Point Fault Zone is a major crustal weakness that runs approximately N-S through the east coast of the Yorke Peninsula and is associated with several small historical Cu-Au workings, including the more substantial Hillside and Parara Mines. Despite the possible economic significance of these deposits, very little has been published on the host rock geology, alteration and structural controls of these deposits, with no information regarding the pressure-temperature conditions of formation and geochemistry. The relationship to other deposits in the broader region is also poorly understood, with the Moonta-Wallaroo Cu-Au mines and the large IOCGs of the north eastern Gawler Craton possibly having genetic affinities. There is a considerable need to determine these characteristics and assess the relationship with these deposits, which will in part aid assessment of the IOCG potential of the rest of the Pine Point Copper Belt and Yorke Peninsula.

The iron oxide-copper-gold (IOCG) class of deposit has come to the forefront of exploration in many regions of the world including the Gawler Craton due to the promising size and grades of the larger deposits. Although the IOCG deposit class includes the barren magnetite-apatite deposits of the Swedish 'Kiruna subtype'(Gandhi 2004), the deposits of the Gawler Craton have extensive polymetallic enrichment consisting primarily of Cu, Au, Ag, U and REE which are hosted within hydrothermal breccias, vein stockworks, and disseminations under strong structural control (Hitzman 2000; Hitzman & Valenta 2005; Corriveau 2006). Associated with this style of mineralisation is an extensive hydrothermal alteration halo consisting of focussed potassic, hydrolytic and iron oxide alteration with a larger regional sodic-calcic footprint (Skirrow *et al.* 2002; Barton & Johnson 2004). The deposits of the Gawler Craton commonly are spatially and temporally associated with the Mesoproterozoic Hiltaba Suite granitoids; an extensive series of granitoids which are often cited as the source of metals and fluids in proximal deposits (Ferris *et al.* 2002; Pollard 2006). The ore bearing fluids of IOCG deposits are highly saline, being of meteoric, metamorphic or magmatic origin (Barton & Johnson 2004). The host rock is variable, and does not constitute a defining characteristic of the deposits, although it does determine in part the chemistry and mineralogy produced by hydrothermal activity (Hitzman *et al.* 1992). There appears to be no single tectonic environment in which these deposits form, with several settings currently invoked to explain their formation (Hitzman 2000; Skirrow 2008).

The Gawler Craton has been the focus of exploration for IOCG style mineralisation in South Australia since the discovery of the world-class Olympic Dam deposit and the smaller but significant Prominent Hill deposit. This has led to the discovery of many prospective and subeconomic IOCG style occurrences throughout the northern and central Gawler Craton including the Oak Dam, Emmie Bluff, Carrapateena, Acropolis and Punt Hill prospects (Bastrakov *et al.* 2007). With these discoveries, targeted IOCG exploration has also increased on the Yorke Peninsula in the south east Gawler Craton, where high grade Cu-Au has been mined in the past on the north west of the peninsula. Recent re-examinations of these deposits suggest they may also be referrable to the IOCG deposit class (Skirrow 2008). Exploration on the eastern margin of the peninsula has been intermittent since the 1950s, although exploration targeting IOCGs has only been in effect since the 1990s. The presence of Hiltaba Suite granitoids and crustal-scale structures make the area extremely attractive coupled with the knowledge that high grade copper was mined in the region historically.

1.1 Mining and exploration history

The area 1-2 kilometres north of Pine Point contains three visible historical workings; the Hillside, Phillip’s and Hart’s Mines as shown in Figure 1. Hart’s Mine was only a small working cut into the coastal cliff face; however both Phillip’s and Hillside Mines had shafts sunk. Records of these mines are scarce for the period prior to 1916; however it is believed the first of these workings was Hart’s Mine, which was opened in 1847. The Hillside Mine was opened at an unknown later date after discovery of copper ore during ploughing, which led to the cutting of two shallow shafts and some open cut work prior to 1916 (Wade & Cochrane 1954). Work appeared to have ceased between 1916 and the next Department of Mines inspection in 1929, although was recommenced soon after, following the formation of a new company that worked the deposit. The two shafts of the Hillside Mine were extended to 26 m and 48 m between 1929 and 1932, with a further winze extending the depth to 54 m. There is no record of the date when mining was ceased; however it must have occurred soon after the last inspection in April 1932 (Wade & Cochrane 1954). During this sporadic period of mining, the Hillside Mine was recorded as having produced 57 tons of handpicked copper ore with an average grade of 13% Cu, which produced approximately 8 tons of copper (Wade & Cochrane 1954; Drexel 1979). Two lodes of between 0.3 and 4 m width were recognised, with the eastern lode having well defined walls which dipped west at 80°, while the western lode was much less well defined. Copper ore occurred in irregular shaped lenses, with most ore consisting of chalcopyrite and bornite, as well as occasional patches of rich malachite and chalcocite with lesser covellite and atacamite also recorded (Wade & Cochrane 1954).

Exploration has continued in the region intermittently, with the Department of Mines (Woodmansee 1957), Shaw River Minerals (Drexel 1979), BHP, CRA and Dampier Mining Co. (Dampier Mining Co. Ltd *et al.* 1986), MIM Exploration Pty Ltd (MIM Exploration Pty Ltd 1997), Avoca Resources (Avoca Resources Limited 2006) and most recently Rex Minerals (Rex Minerals 2009b) all investigating the region. The latter two companies have both recognised the IOCG characteristics of the mineralisation and further potential of the region. Earlier scintillometer and rock chip surveys also confirming the presence of uranium in the region, although initially concluded it was of low grade and not economically viable (Mumme 1955; Rowley 1955; MIM Exploration Pty Ltd 1997). The current holder of the tenement in which the Hillside Mine is located is Rex Minerals, who have initiated an exploration project utilising geophysical data and diamond drilling. Magnetic and gravity surveys were used to identify drilling targets within the clearly delineated Pine Point Fault Zone, in which the current Hillside target is located. Drilling has identified five separate, broadly parallel smaller faults running approximately N-S; the Dart, Zanoni, Marion, Parsee and Songvaar faults. The Dart, Zanoni, Marion and Parsee host copper mineralisation, while the Songvaar has significant intervals of uranium mineralisation. Grades in the Dart Zone range from 0.2-1.5% Cu over 7-70 m intervals, in the Zanoni from 0.2-3.2% Cu over 8-259 m and 0.2% Cu over 99 m in the Parsee (Rex Minerals 2009b).

1.2 Geological setting

The Pine Point Copper Belt is located on the south-eastern margin of the Gawler Craton; a large and complex Precambrian basement crustal block (Figure 2). The craton records several phases of rift and collision dating back to the Late Archaean (2560-2500 Ma) (Hand *et al.* 2007), with several tectonic subdomains assignable based on the structure and tectonic history (Ferris *et al.* 2002). The area of interest falls into the Olympic Domain, a region dominated by the Palaeoproterozoic (~1740-1760 Ma) Wallaroo Group metasedimentary and metavolcanic package (Hand *et al.* 2007). The Wallaroo Group is intruded by the Mesoproterozoic (1595-1570 Ma) Hiltaba Suite granitoids, which are believed to be genetically linked to much of the IOCG mineralisation in the area (Ferris *et al.* 2002; Zang *et al.* 2002). In a mineral deposit scheme, the Pine Point Copper Belt is in the southern Olympic Cu-Au province (Figure 2) which incorporates much of the Olympic Domain, as well as part of the Mt Woods Inlier, Cleve Domain, Spencer Domain and Gawler Range Volcanics Domain (Skirrow *et al.* 2002). The Olympic province incorporates two operating IOCG mines; the supergiant Olympic Dam and smaller but significant Prominent Hill, and many prospective occurrences including the Oak Dam, Emmie Bluff, Carrapateena, Acropolis and Punt Hill deposits (Fairclough 2005; Bastrakov *et al.* 2007; Belperio *et al.* 2007).

The Pine Point Copper Belt is located in what is often referred to as the Moonta-Wallaroo Subdomain (or district), an area historically associated with high grade Cu-Au (Conor 1995). Many of these deposits were associated with significant earlier hydrothermal iron oxide alteration, and may be attributable to the overarching IOCG deposit class (Ruano *et al.* 2002; Skirrow *et al.* 2002). The geology of the Moonta-Wallaroo region consists of Wallaroo group metasediments and metavolcanics which overlie the mid-Palaeoproterozoic Gleesons' Landing Granite in the south west of the peninsula. The Wallaroo Group here is also intruded by Hiltaba Suite Granitoids and rarer associated mafics. The basement is largely covered by Cambrian and Tertiary sediments of the Stansbury and St Vincent Basins, with the land surface covered by quaternary alluvial, colluvial and aeolian sediments. Alteration in the region has been studied and extensively described (Conor 1995; Zang 2002; Zang *et al.* 2002), consisting primarily of calcsilicate, magnetite-biotite, chlorite dominated assemblages and later epithermal and carbonate veining. Mineralisation is associated with both the biotite and chlorite dominated assemblages (Zang *et al.* 2002).

1.3 Local geology and previous studies

The geology of the region immediately around the Hillside prospect is poorly understood due to a shallow blanket of recent sediment and regolith cover. Very limited outcrop occurs inland, with the coastal cliffs providing the most useful mappable outcrop. A series of shallow drillholes sunk by several exploration companies along the road network in the early 1980s allow a means of mapping the subsurface (See Appendix A, Map B). These were percussion-drill (RC) holes and as such the quality of the rock description is quite poor and difficult to effectively map out different units within the Palaeo-Mesoproterozoic basement.

1.3.1 Proterozoic

The basement in the immediate region has previously been inferred as undifferentiated Wallaroo Group and Hiltaba Suite Graintoids based on geophysical interpretation (Raymond 2001), with mapping and inspection of the beach outcrop confirming this (Teakle 1983; Zang *et al.* 2006). The outcrop exposed along the beach north of Pine Point has been referred to the Aagot Member of the Wandearah Formation and consists of layered metasandstones and metasiltstones (Zang *et al.* 2006). A rhyolite was also described from thin section of rocks from the mullock heaps around Hillside and Hart's Mines and referred to the Moonta Porphyry, indicating Wallaroo Group-aged volcanics are also present in the immediate vicinity (Drexel 1979). John Drexel also described these rhyolites to be host rock to mineralisation in the area.

The Mesoproterozoic Hiltaba Suite granites which intrude the Wallaroo Group are represented in the region by the 1582 ± 7 Ma Arthurton Granite (Creaser & Cooper 1993) which is variably classed as an adamellite to quartz monzonite, and has a quartz, microcline, plagioclase, mica, sphene, tourmaline, magnetite and chlorite composition (Conor 1995; Zang 2002). Two mafic units are known from the wider region, the Renowden Metabasalt Member of Wallaroo Group age and the Mesoproterozoic Curramulka Gabbronorite, however the extent of mafics around the Hillside mineralisation is unknown.

1.3.2 Palaeozoic

There is a hiatus in the geological record from the Mesoproterozoic until the Cambrian, when the Stansbury Basin formed. The basal unit of the Stansbury Basin is the Winulta Formation, a sandstone, conglomerate, siltstone and dolomitic unit (Zang *et al.* 2006) which was extensively intersected between Rogues Point and Ardrossan during percussion drilling and to a lesser extent east of Port Julia to the south (Dampier Mining Co. Ltd *et al.* 1986). This is stratigraphically overlain by the Kulpara Formation a thick bedded limestone and dolomite unit (Zang *et al.* 2006) which is also intersected in the same areas as the Winulta Formation, although more proximal to the coast. In his petrographic report in 1979, John Drexel found several marble and calcsilicate assemblages which hosted Cu mineralisation at Hillside, Phillip's and Hart's Mines which he attributed to the Kulpara Formation (Drexel 1979). Two later formations; the Coobowie Limestone and Ramsay Limestone have been intersected in diamond holes in the Port Julia region and appear to unimportant as host rocks.

The top of the Stansbury Basin is represented by the Middle Cambrian Yuruga Formation, a thick red-brown sandstone, comglomerate and breccia unit which is present along the beach north of Pine Point (Teakle 1983). The basal conglomerates and breccias are thought to represent uplift of basement along the Pine Point Fault Zone before passing into fluvial sandstone deposits (Zang *et al.* 2006). Mapping by Raymond Teakle indicates the presence of numerous small folds in the region south of where the Pine Point Fault outcrops, which may be due to later reverse faulting along the Pine Point Fault Zone. The Yuruga Formation also appears unimportant in terms of hosting mineralisation, however indicates that the Pine Pont Fault Zone has been crucial in the landscape and sedimentary history of the region, and has been active since its formation.

1.3.3 Cenozoic

The Tertiary sedimentary record of the eastern Yorke Peninsula has been extensively studied and reported by Stuart (1970). The Muloowurtie Formation, Throoka Silts and Rogue Formation are all present in the Pine Point region (Stuart 1970), with all but the Throoka Silts definitely intersected in dill core. These sediments occupy grabens created by extension along major pre-existing faults, including the Pine Point Fault Zone, with two graben faulting events recognised in the region (Zang *et al.* 2006). More recent reactivation of the Pine Point Fault Zone has resulted in reverse faulting and elevation of the eastern Yorke Peninsula coast. The Quaternary sedimentary record comprises calcretes, fossiliferous limestones and recent reworked alluvium, colluvium and sand dunes in the terrestrial environment. The marine environment is dominated by recent beach sands, silts and fossiliferous limestones (Zang *et al.* 2006).

1.3.4 Structural setting

The Pine Point Fault Zone is the dominant structural feature of the region, and encloses the Hillside mineralisation. Despite this, little has been published on this major crustal weakness. The most information published on the fault zone was in a report commissioned by PIRSA and undertaken by SRK Consulting, who used integrated geophysical methods to better understand the architecture of the Stansbury Basin. The report produced good qualitative information, although quantitative information regarding the fault's movements is scarce. The Gawler Craton, including the Wallaroo Group, preserves structures related to the 1850-1700 Ma Kimban Orogeny, which are truncated to the east by the Pine Point Fault. This truncation appears to be the first record of movement along the fault zone, and separates the Gawler Craton from the St. Vincent Block (as per Teasdale 2001). Although an exact date on this truncation and therefore fault activation has not been produced, it is suggested to be of Mesoproterozoic age. The fault was reactivated during the Neoproterozoic as a normal fault of unknown orientation and again in the early Cambrian as an east-dipping oblique normal fault (Teasdale *et al.* 2001). Compressional stresses during the Delamarian Orogeny caused the fault zone to reactivate once more as a high angle oblique reverse fault with dextral movement, thrusting the Cambrian Stansbury Basin strata over the Proterozoic basement (Teakle 1983; Zang *et al.* 2006). Structural evidence for the fault movement at this period comes from the coastal outcrops north of Pine Point which show this relationship. The fault switched back to normal movement during the Tertiary at least twice, forming grabens in which the Tertiary formations were deposited. The most recent movement was the reactivation as a reverse fault which contributes to the Yorke Peninsula's current topography (Zang *et al.* 2006).

Project aims

The aim of this study was to broadly extend the understanding of both the local geology and the mineralisation based on diamond core obtained by Rex Minerals. However at the onset of the project, the nature of the mineralisation was entirely unknown, so a preliminary core logging study was undertaken to further assess what analytical methods were to be used. Some of the fundamental properties of mineralisation which were aimed to be determined were the host rock identity, alteration and mineralisation paragenesis, pressure-temperature conditions of formation, structural controls on mineralisation and an understanding of how rock composition changed with alteration. This information was used to compare the Hillside mineralisation to other IOCG deposits and prospects within the Gawler Craton

2. Preliminary core logging study

A preliminary core logging study was undertaken to assess what methods were to be used in analysis of the mineralisation. Emphasis was placed on determining the original host rocks and the paragenesis of the alteration that overprinted them. In consultation with Rex Minerals, HDD013 was chosen as it intersected every major lithological unit known from core thus far. Logs of magnetic susceptibility and core structure were provided by Rex Minerals.

2.1 Preliminary results

2.1.1 Host rocks

Much of the core from below 500 m was altered to a state that the original rock was impossible to determine, however isolated sections of relatively unaltered host rock allowed for two main rock types to be recognised. The first, and most proximal to the surface, is a grey metasedimentary rock that shows both metasandstone and schistose lithologies (Figure 3). This unit extended from the base of the weathering zone (14 m) to around 260 m depth, although heavy alteration and the more regular intrusion of felsic rock types towards the base made it difficult to assign a definitive depth. The metasediments range from light grey muscovite and/or quartz-rich layers to black biotite and amphibole rich sections, with darker minerals generally concentrated in distinct bands which likely define a regional foliation plane. Based on structural core logs, this plane has a dip of 0-15° and a strike approximately north-south. Structure in the metasediments becomes more chaotic downhole towards the felsic intrusions, where plastic deformation and gneissic texture is quite common. This unit is part of the Wallaroo Group, possibly corresponding to the Doora Member based on the abundant schist lithology (Zang 2002).

The second and most voluminous host rock was a felsic intrusive of a granitic composition, with pods of coarse quartz-feldspar ± tourmaline pegmatite and fine grained quartz-feldspar aplite also present (Figure 3). This unit is extremely altered and brecciated, making accurate hand specimen identification very difficult. Small pegmatite veins extend throughout the metasedimentary sequence, however the main intrusive body begins at around 270 m depth and continues to the end of the hole (752 m). Heavy alteration makes the upper boundary difficult to recognise. Pegmatite and aplite dykes also cut the main intrusive body in places and commonly contain tourmaline. This unit is the Arthurton Granite, a Mesoproterozoic Hiltaba Suite equivalent intrusive body which is known from much of the Yorke Peninsula (Zang 2002).

Amongst the main intrusive body, several pockets of possible metasediments (or volcanics) were identified, although the extremely heavy alteration again made identification difficult. Several highly mafic zones were also observed and initially logged as mafic dykes.

2.1.2 Alteration

Alteration was most prevalent throughout the felsic intrusive, although the metasediments did show several alteration assemblages in places. The alteration sequence as seen in core is summarised below with the first being the earliest and the last the latest:

- Orange-red hematite rich feldspar – possibly albite.
- Pistachio green Epidote-rich veins, with associated or later chlorite overprint
- Quartz vein sequences – milky to smoky in colour
- Initial carbonate veining
- Brecciation associated with main stage of ore mineral formation (Magnetite – Hematite - Pyrite – Chalcopyrite sequence).
- Chlorite veining and alteration
- Later carbonates and carbonate-hematite breccias

The structure of the breccias and mineralisation was avoided due to its complexity, with Rex Minerals already having released initial ore body structure and morphology data to the stock market (Rex Minerals 2009a).

2.2 Preliminary study recommendations

Diamond core logging gave a first overview of the host rock and alteration present at Hillside, and also gave the study focus as to what further work was to be done. Samples taken from the core were made into thin and polished thick sections by Pontifex Petrographic Services Ltd. Thin sections were used to ascertain the host rock types more clearly and to further describe alteration paragenesis. The temperature conditions of the mineralisation and alteration process were determined using the TitaniQ method and backed up with the chlorite geothermometry method, using the abundant chlorite in the alteration assemblage. The associated pressure conditions were to be found using fluid inclusion studies analysed by Dr. Andreas Schmidt Mumm, however a lack of suitable inclusions meant this was not possible. The sulphur isotope compositions of the sulphide minerals were determined, as was the trace element content of the iron oxide minerals. Bulk rock composition was determined using XRF, which showed changes in elemental abundances as the rock progressed from unaltered to entirely metasomatised. A detailed map of the coastal outcrop was also produced to further understand the geology of the immediate region.

3. Field mapping

3.1 Mapping procedures

A 1.5 km stretch of beach outcrop north of Pine Point was mapped to help ascertain the geological history of the immediate region (Appendix A). This mapping focussed on distinguishing lithological units, largely ignoring structural aspects which are obscured by the intensely weathered nature of most outcrops. Previous mapping by Raymond Teakle has already deduced the structure of most sedimentary units. Mapping was carried with Google Earth derived true-colour satellite photos as base maps. The 1.5 km section was divided into five 280 m x 430 m A4 sized sheets to allow relatively small scale features to be mapped on. Outcrop mapping was supplemented by face-mapping the coastal cliffs, which was done on the same paper as the outcrop mapping, making it straightforward to correlate the two. The map ranges from the north (Latitude 34°32'15.18"S, Longitude 137°53'8.50"E) to the south (Latitude 34°33'1.74"S, Longitude 137°53'4.67"E) in an approximately north south orientation. The map and face-maps were digitised using Inkscape, a freeware vector-based drawing platform.

3.2 Mapping results

Mapping showed several distinct lithologies along the coast, with most of these also seen in the diamond core (Appendix A, Maps A and B). The oldest units are two metasediments of Wallaroo Group age, a feldspathic metasandstone and a strongly laminated siltstone. The siltstone occurs as what appears to be a boulder lying discordantly over (or in) the underlying metasandstone. Both lithologies are cut by several later fault planes, indicating this is likely a depositional feature predating faulting. Lack of further siltstone outcrop prevents determination of the relationship between the two lithologies. Scree around the Hart’s Mine pit contains feldspar dominated rhyolite which is likely of Wallaroo Group age also.

The Arthurton Granite is also extensively found along the beach, although is commonly extremely altered and weathered. The granite commonly shows a quartz-K-feldspar-plagioclase mineral assemblage, with mafic minerals quite rare. The granite is frequently cut by pegmatite and aplite dykes to the south of the mapping area, with the granite itself being quite coarse grained. Associated with these felsic intrusions are intermingled pods of more mafic material consisting predominantly of plagioclase and hornblende. Several highly weathered amphibolites are present in outcrop as well, although their relationship to the granites is unclear. It should be noted that due to the foliation, alteration and weathering of the granites and metasandstones, they are indistinguishable in places and mapped accordingly.

The Proterozoic basement is unconformably overlain by the Cambrian Yuruga Formation; which ranges in lithology from basal channel sedimentary breccias and conglomerates to more homogenous sandstones and arkoses at the top. Granitic clasts are common in the conglomerates, indicating the granite must have been exposed at the surface during the mid-Cambrian. This unit has previously been mapped by Raymond Teakle, however he did not recognise the unit in this mapped area (Teakle 1983). Cenozoic sediments include ferruginous fossiliferous sandstone attributed to the Eocene Rogue Formation and several Quaternary units on the cliff tops.

4. Analytical procedures

4.1 Petrography

During the core-logging process, samples of each host rock and alteration type from HDD013 was sampled for production of thin and polished thick sections for identification of minerals and assemblages. Production of thin sections was carried out by Pontifex Petrographic Services Ltd. Thin sections were investigated with a transmitted light microscope and polished thick sections with both transmitted and reflected light.

4.2 Mineral Geochemistry

Quartz

Quartz veins are associated with most stages of the alteration in the deposit, however they are predominantly associated with magnetite, later hematite and sulphide bearing stages. The concentration of the trace element Ti in quartz has been demonstrated to be an accurate and highly reliable geothermometer, with precision usually greater than ± 5°C (Wark & Watson 2006). The technique requires the quartz to be saturated in Ti, normally demonstrated by the presence of Ti-bearing mineral phases in equilibrium with quartz; typically rutile, ilmentite, titanate or T-magnetite. The technique has been demonstrated to be applicable to most, but not all, situations where hydrothermal quartz is analysed (Rusk *et al.* 2008).

Suitable quartz bearing samples were studied by both reflected and transmitted light to ascertain the petrographic relationship between quartz and the ore minerals. In all cases, quartz was associated with hematite or one of the sulphide phases. This also corresponds to the gangue mineral assemblage associated with quartz and the ore minerals, which is described later. Only two samples were found to have very fine rutile crystals where Ti-saturation could confidently be assumed.

The temperature of quartz precipitation is calculated by the formula:

$$\mathrm{T}\ (°\mathrm{C}) = \frac{-3756}{\log\left[\frac{X_{\mathrm{Ti}}^{\mathrm{qtz}}}{a_{\mathrm{TiO_2}}}\right] - 5.69} - 273 \qquad \text{(Eq. 1)}$$

Where $a_{\mathrm{TiO_2}}$= 1 when Ti-minerals are paragentically associated with the quartz (Wark & Watson 2006).

-LA-ICPMS operating procedures-

The titanium composition of 76 grains of hydrothermal quartz were analysed using a New Wave Research Merchantex Products UP-213 Laser Ablation System coupled with an Agilent 7500 Series ICP-MS housed at Adelaide Microscopy, University of Adelaide. Laser settings used during the analyses were: continuous beam at 5 Hz, a 65 µm spot diameter and 75 % power level. An internal Si^{29} standard was implemented. Quartz grains were selected prior to analysis using microscopy to ensure the zone was free of contaminations, particularly sulphides and oxides. Zones of finer grained, recrystallised quartz noticed in cross-polarised light were avoided where possible. The spots on the slide analysed are presented in Appendix B.

During analysis, NIST-612 glasses were used as standards and NIST-614 glass used as an unknown to fit a linear curve of ratios to the data. Three NIST-612 standards were run followed by 2 NIST-614 samples, again followed by a NIST-612. Ten quartz samples were then run, with 4 quartz grains per sample selected for analysis. Two of these had 3 points in the grain and immediate vicinity sampled and the other two only 2 points sampled. During this analysis the following elements were analysed, to eliminate and identify contaminants and sub-microscopic mineral inclusions (chlorite, carbonates, sulphides etc): Na^{23}, Al^{27}, Si^{29}, P^{31}, K^{39}, Ca^{43}, Ti^{49}, Fe^{56} and Fe^{57}.

Iron oxides

The composition of both hematite and magnetite was analysed for two main purposes; to determine whether the chemistry supported the paragenetic sequence elucidated from petrography and to determine if the Ti levels of each would support the fluid being Ti saturated. This was critical for TitaniQ thermometry as described later.

-LA-ICPMS operating procedure-

Magnetite and hematite were analysed in a way similar to quartz using the same LA-ICPMS equipment with the same settings except for the following: Fe^{57} as the internal standard and a 40 µm spot diameter for sample 7152, due to the small size of the remnant magnetite crystals. Fe^{56}, the more common isotope of iron was unavailable for use due to interference from other isotopes. The extremely dense 'network' of veins and fractures along which martitisation had occurred made finding a sample of suitable size to be analysed with the laser difficult. Invariably there was minor contamination between the oxides. Elements analysed were: Al^{27}, Si^{29}, P^{31}, Ca^{43}, Ti^{49}, V^{51}, Cr^{52}, Fe^{56}, Fe^{57}, Co^{59}, Ni^{60}, Cu^{65}, La^{139}, Ce^{140}, Pr^{141}, Nd^{146}, Sm^{147}, Eu^{153}, Gd^{157}, Dy^{163}, Ho^{165}, Er^{166}, Yb^{172}, Pb^{208}, Bi^{209} and U^{238}.

Chlorite

Chlorite is a common hydrothermal mineral throughout the Hillside mineralising system, which can be used as a geothermometer (de Caritat *et al.* 1993). Chlorite geothermometry is based around the manner in which the chemical composition of the mineral changes with temperature, although polytypism and chlorite-carbonate equilibria can also be used, but were not attempted here. The geothermometers used here work on the systematic increase in Al^{IV} and decrease in Si^{IV} in the tetrahedral sites with temperature, as well as an increase in the combined amount of Fe and Mg and decrease in Al^{VI} in the octahedral sites (de Caritat *et al.* 1993). For further information, the reader is referred to de Caritat *et al* 1993.

Three equations were used to calculate temperature of formation in the present study, each being based on these temperature dependant exchanges.

(Cathelineau & Neiva 1985) $$T = -61.92 + 321.98\,\mathrm{Al}^{\mathrm{IV}} \qquad \text{(Eq. 2)}$$

(Kranidiotis & MacLean 1987) $$T = 106\,\mathrm{Al}_{\mathrm{C}}^{\mathrm{IV}} + 18 \qquad \text{(Eq. 3a)}$$

Where $\mathrm{Al}_{\mathrm{C}}^{\mathrm{IV}}$ is a corrected $\mathrm{Al}^{\mathrm{IV}}$ value which accounts for variation in Fe/(Fe + Mg) and is calculated according to:

$$\mathrm{Al}_{\mathrm{C}}^{\mathrm{IV}} = \mathrm{Al}^{\mathrm{IV}} + 0.7(\mathrm{Fe}/[\mathrm{Fe{+}Mg}]) \qquad \text{(Eq. 3b)}$$

(Jowett 1991) $$T = 319\ \mathrm{Al}_{\mathrm{C}}^{\mathrm{IV}} - 69 \qquad \text{(Eq. 4a)}$$

where $\mathrm{Al}_{\mathrm{C}}^{\mathrm{IV}}$ is again a corrected $\mathrm{Al}^{\mathrm{IV}}$ value which accounts for variation in Fe/(Fe + Mg) and is calculated according to:

$$\mathrm{Al}_{\mathrm{C}}^{\mathrm{IV}} = \mathrm{Al}^{\mathrm{IV}} + 0.1(\mathrm{Fe}/[\mathrm{Fe{+}Mg}]) \qquad \text{(Eq. 4b)}$$

-Electron microprobe operating procedures-

The composition of 93 chlorite grains was determined using a Cameca SX 51 Electron Microprobe equipped with SAMx analysis and control software at Adelaide Microscopy, University of Adelaide. An accelerating voltage of 15 kV and beam current of 20 nA was employed during analysis. All formulas were calculated with the aid of a spreadsheet developed by A.G. Tindle based on 28 oxygens and with $\mathrm{Fe}^{2+}/\mathrm{Fe}^{3+}$ and OH^{-} calculated assuming full site occupancy (Tindle 1999). Chlorite composition was considered in the compositional framework of both (Hey 1954) and (Wiewióra & Weiss 1990).

Sulphides

Sulphide samples for use in sulphur isotope work were selected on their mineralogical variation and their relationship to different host rocks and alteration sequences, in an attempt to capture as much mineralogical variation as possible. All samples were pyrite or chalcopyrite, with one sample of bornite attempted; however the low volumes prevented the sample being correctly analysed. The sulphides were drilled out using a tungsten carbide drill bit on a small mounted dental drill, with either pyrite or chalcopyrite exclusively targeted in each sample. There were several samples of core containing both chalcopyrite and pyrite, which had both minerals sampled.

The powdered sulphides were transferred to 2 mL vials after drilling, before preparation of samples for the mass spectrometer. Approximately 200 mg of sulphide sampled was placed in a small tin capsule, along with around 300 mg of vanadium pentoxide to allow for more complete combustion. The capsules were sealed off and moulded into small spherical balls for placement in a Fisons Optima Mass Spectrometer. Along with the samples, several standards were also prepared in a similar manner; IAEA S-1, IAEA S-2, IAEA S-3 and Tas Barite, which were used for calibration purposes.

4.3 Whole rock geochemistry

Six samples of core which were thought to represent a gradational change from unaltered granite/volcaniclastics to heavily altered versions of these rocks were prepared for major, trace and rare earth element XRF analysis. Samples of rock were crushed and milled so that 90 % passed through a 106 µm sieve. A total of 70 g of each was then split from the milled rock and submitted to Adelaide Geoanalytical, Amdel Limited for analysis of REE element concentration. Major and trace element samples were prepared at the University of Adelaide and analysed by John Stanley.

Major element analysis

The samples were dried in an oven at 110°C for over two hours to remove absorbed moisture. They were then weighed into alumina crucibles and ignited overnight in a furnace at 960°C, to yield the Loss on Ignition (LOI) values. This comprises organic material, CO_2 from carbonate minerals, H_2O^+ (water in combination with the crystal structure), and possibly S, Cl and other volatiles. Nominally 1g of the ignited material was then accurately weighed with nominally 4g of flux (commercially available as type 12:22, comprising 35.3% lithium tetraborate and 64.7% lithium metaborate). The sample-flux mixture was fused using a propane-oxygen flame, at a temperature of approximately 1150°C, using Pt-Au crucibles, and cast into a preheated mould to produce a glass disc suitable for analysis (Stanley, *pers comm*., 2009).

The samples were analysed with a Philips PW 1480 X-ray Fluorescence Spectrometer, using an analysis program calibrated against several international and local Standard Reference Materials (SRM's). A dual-anode (Sc-Mo) X-ray tube was used, operating at 40kV, 75mA (Stanley, *pers comm*. 2009).

Trace element analysis

About 10g of sample powder was mixed with nominally 1ml of binder solution (Poly Vinyl Alcohol) and pressed to form a 30 mm diameter pellet. This was allowed to dry in air and was heated for a further 1 to 2 hours in a 60°C oven to ensure that the pellet was completely dry before analysis.

The samples were analysed using a Philips PW 1480 XRF Spectrometer, using several analysis programs covering suites of from 1 to 7 trace elements, with conditions optimised for the elements being analysed. The programs were calibrated against many (30 or more in some cases) local and international SRM's. The dual-anode Sc-Mo tube (operated at sufficient voltage to excite the Mo) and an Au tube were used for the analyses. Matrix corrections are made using either the Compton Scatter peak, or mass absorption coefficients calculated from the major element data. Due to technical limitations at the time of analysis, Cu was not included in the analysis (Stanley, *pers comm*. 2009).

Rare Earth Element analysis

REE contents were determined by AMDEL Laboratories. A 0.2 g sub-sample of analytical pulp was dissolved in a hydrofluoric/multi-acid digest, and then analysed by ICP-MS. AMDEL Laboratories work to documented procedures in accordance to ISO 9001 Quality Management Systems standard.

5. Results

5.1 Petrography

The full report of thin section petrography can be found in Appendix B.

5.1.1 Host rocks

Relatively unaltered samples of the Doora Member and the Arthurton Granite were thin sectioned to gain a better understanding of their lithology. The Doora metasediment proved to be a fine grained quartz-feldspar sandstone with foliation defining amphiboles (Figure 4A-B). No muscovite or obvious biotite was present in the sample. Coincident with the amphibole foliations are bands of much coarser grained quartz which may represent recrystallised grains. Further sections on the mica and biotite bearing sections are needed to adequately describe the mineralogy of this unit.

A sample selected for use to determine the identity of what was logged as a mafic amphibolite was found to be a heavily chloritic metavolcanic in thin section (Figure 5A-B). The groundmass consists almost exclusively of recrystallised orthoclase, quartz and to a lesser extent microcline which have undergone extensive chlorite replacement. Accessory minerals include plagioclase, biotite, sphene, spinel and opaque minerals. This sample was taken from deep within the granite dominated zone, indicating that xenoliths of Wallaroo Group remain.

Unaltered granite observed in thin section has a relatively uniform composition across samples, consisting of K-feldpar, quartz and plagioclase dominated rocks (Figure 5C-D). Under the IUGS plutonic classification scheme these fall in the quartz monzonite and syenite fields. Accessory mafic minerals include amphibole, biotite chlorite, opaques, sphene, and in one sample abundant large titanate. Grain size is generally not large and may have been modified by shearing.

During core logging, one sample was taken under the assumption of being a porphyroblast bearing volcanic or intrusive rock, being entirely orange and grey in colour. In thin section this rock was found to be quartz bearing marble with large remnant K-feldspar and carbonate crystals (Figure 4C-D). Being in close proximity to the granite it appears the rock was reheated and recrystallised in places, with only the large feldspar porphyroblasts retaining the precursor rock’s chlorite defined foliation. This rock is either a carbonate rich (altered?) Wallaroo Group metasediment or part of the Kulpara Formation which has been down-thrust over a Wallaroo Group footwall.

5.1.2 Alteration

Hydrothermal alteration of the host rocks appears to be divisible into several distinct assemblages (Figure 11). The relative time of formation of some minerals is still difficult to constrain, namely due to extensive later overprinting or only being present in very small amounts in few slides.

Calcsilicate assemblage

The earliest alteration appears to be a calcsilicate assemblage that is only found in a narrow range of the core from 532–542 m depth. In core it has a dominantly green colour, and a mineralogy consisting nearly exclusively of andradite or grossular garnet (Figure 6 A-C-D) with rare actinolite and large euhedral epidote (Figure 6B). There is a possibility that early albite alteration seen elsewhere in other slides may correspond to this assemblage, however no direct contacts are observed between these. Garnet tends to be massive, often filling the entire slide, with epidote and actinolite occurring as small >0.2 mm crystals, often highly altered and unrecognisable.

Epidote assemblage

An epidote-quartz-carbonate and minor allanite assemblage is commonly observed in most slides. This has been observed to overprint the calcsilicate assemblage (Figure 7B), including alteration of earlier euhedral epidote to murky fine grained epidote along vein networks (Figure 6B). The assemblage appears to have two textural styles; the fine grained more epidote rich style described above and a larger more euhedral quartz-epidote-carbonate assemblage observed in larger veins. Carbonate and epidote in these latter assemblages tend to form bladed crystals in a more quartz dominated vein (7A, C, D). The main magnetite alteration is likely associated with either the epidote or calcsilicate assemblage, or alternatively may be referrable to its own stage. The extensive martitisation suffered by magnetite prevents observation of any other paragenetic minerals.

HSCCF assemblage

The main hematite and sulphide precipitating assemblage consists of a quartz-carbonate-K-feldspar-chlorite-sericite-hematite-sulfide assemblage that overprints the previous two stages (Figure 8 A-B). While several slides show this entire assemblage, quartz-K feldspar-sericite assemblages are most common. More massive sulphides, consisting of pyrite, chalcopyrite and rare bornite, tend to occur in quartz veins with rare carbonate, chlorite and feldspar. Heavy chlorite-only alteration occurs in many metasediments (Figure 8C), volcanics and granite breccias. Here chlorite appears to fill interstitial spaces and grain boundaries, often containing very fine almost submicroscopic opaques. Feldspar commonly has extensive red-brown hematite inculsions giving a very dusty, dirty appearance that helps distinguish it from quartz in plane-polarized light (Figure 8A). The opaque mineralogy and paragenesis is described later.

Carbonate veining

A series of fine carbonate veins and breccias cross cut all earlier alteration and mineralisation. There appear to be two sets of carbonates; a fine, relatively pure carbonate vein network which has very rare fine chalcopyrite associated with it (Figure 9A). The second is a carbonate-hematite (earthy red) breccia system that appears to be the last alteration stage present in the core.

5.1.3 Ore petrography

Ore mineral paragenesis was determined using polished thick sections and reflected light microscopy. Determination of ore mineral paragenesis is relatively straightforward, although the hematite and sulphide minerals tend to have transitions between precipitating minerals where the fluid fluctuated between the two minerals. Magnetite was the first ore mineral precipitated, and as stated above the timing in relation to gangue minerals is indeterminable. The second mineral was hematite (Figure 10A), which has caused extensive martititsation of magnetite along veins and fractures. Hematite then coprecipitated with pyrite before pyrite only was precipitated (Figure 10B). This is evidenced by small hematite inclusions often in the outer rims of pyrite; otherwise pyrite shows replacement and infilling textures in and around hematite. The system then moved to coprecipitate chalcopyrite with pyrite, with similar textures observed in the hematite-pyrite system occurring here also. In all slides from HDD013 the chalcopyrite was the last stage, however a piece of core from drill hole HDD027 containing fine bornite grains in a quartz vein was also taken to understand the relationship of bornite. It appears the same fluctuations between precipitation of chalcopyrite and bornite occurred with these two minerals (Figure 10C-D). No gold or uranium bearing minerals were observed.

A diagrammatic presentation of the paragenetic sequences is shown in Figure 11.

5.2 Mineral geochemistry

Quartz

Nine slides were used to analyse the Ti content of quartz, with a total of eighty points analysed. Ti content ranged from 1.14 ppm to 17.23 ppm (Table 1). Only four spot analyses showed Ti concentrations greater than 10 ppm, therefore these four values were considered outliers and discarded from the dataset. No spikes in elemental composition which would indicate the presence of mineral or fluid inclusions were observed. The revised data set ranges from 1.14 to 8.88 ppm. The dataset has an average of 3.86 ppm with a 95% confidence interval of 0.42 ppm. When a histogram of the Ti concentration data is produced, two obvious peaks are present; one with a mean around 3.0 ppm and the other at 6.5 ppm (Figure 13). This indicates there are two distinct populations of quartz based on Ti concentration.

Petrography indicated there would likely be some degree of contamination; predominantly from small chlorite and hematite inclusions scattered throughout the quartz in most slides.

The quartz composition data reflect this contamination, with Al commonly higher than 100 ppm and in several cases higher than 1000 ppm. Na, K and Ca were also elevated to levels greater than 100 ppm in some samples, although were not as consistently high as Al. These elements may represent fine, uniform mineral inclusions or precipitates on grain boundaries as a result of the penetrative recrystallisation of the quartz. Fe and P rarely are contaminating. Contamination will likely decrease the accuracy of any temperatures produced, therefore plots of Ti versus all other elements were produced to check whether Ti systematically increased with an increase with a contaminating element (Figure 12). No such pattern is observed, therefore the entire dataset was utilised.

Iron oxides

There is a distinct difference between the trace element composition of magnetite and hematite (Table 2-3), with hematite being more enriched in several trace and all rare earth elements. Magnetite only has a higher Ti and Al content than hematite, while hematite is enriched in Cu, Ni, Co, U and all rare earth elements (Figure 14-15). Several other elements including Si, P, Co and Cr show very little differences between the two minerals. Ca ranges between below detection level and 4.1%, and is excluded from analysis due to this wide and unexplained variation. No veins were found to cross cut the oxides analysed, which rules out the possibility of fine carbonate veining.

The Ti content of magnetite was reasonably high at between 300 and 1900 ppm, however hematite had a much lower content of 60-100 ppm (Table 2-3). Although the rare earth element data are incomplete, a spidergram of these elements normalised to chondrite shows the discrepancy between magnetite and hematite values (Figure 15). It should also be noticed that the REE contents of most magnetite samples analysed were below detection limit. The possibility of contamination between hematite and magnetite should also be recognised, with the fine network of martite veins likely cutting below the surface of grains.

Chlorite

Based on the data obtained, all chlorites analysed were members of the trioctahedral clinochore-chamosite $[(Mg_5Al)(Si_3Al)O_{10}(OH_8)\text{-}(Fe^{2+}_5Al)(Si_3Al)O_{10}(OH_8)]$ solid solution series as defined by (Wiewióra & Weiss 1990)(Table 4). Classification based upon the Si vs Fe/(Fe+Mg) ratio system of (Hey 1954) indicates most chorites fall into the pycnochlorite and diabantite fields, with a few falling into the brunsvigite, ripidolite and dapnite fields (Figure

16). All chlorites appeared to be in equilibrium with at least one stage of quartz, and often with sulphides and hematite.

Chlorite generally is found as small inclusions in the quartz, growing around earlier magnetite and hematite, as well as a later stage which appears to be associated with sub-millimetre fractures. It should be noted that digenetic or metamorphic chlorite was present in some sections that contained metasediments, however this was avoided for two reasons; (1) when analysed with the Microprobe EDX, significant quantities of Na, K and Ca were present indicating chlorite was interlayered with other sheet-silicate clay minerals and (2) because the temperature of metamorphism was not a focus of the present study. To avoid similar contamination in other chlorite samples, any analyses that showed a total Ca, Na and K oxide content of 0.5 wt% were discarded. Several authors argue these cations have no place in the chlorite crystal structure and their presence indicates contamination with other silicates.(de Caritat *et al.* 1993) The filtered and recalculated chlorite data used in temperature calculations is present in Table 5

Sulphides

The sulphides have a $\delta^{34}S$ range of -5.77 to 2.4 ‰ CDT with a mean of -1.77 ‰ CDT (Table 6). The highest frequency of values falls between -3 and -4 ‰ CDT, however the distribution of values is far from normal (Figure 17). The peak of values between -3 and -4 ‰ CDT is isolated and the values higher form a steadily increasing tail. When the first batch of samples were run, a value of -25.07 was obtained and presumed to be erroneous. When the sample was redrilled and rerun, a value of -26.73 was obtained, excluding experimental error. In considering the dataset however, these values were excluded due to their outlier effects.

There is a discrepancy in the values from sulphur taken from pyrite and those from chalcopyrite. Overall there is a slight trend of pyrite having more negative values and chalcopyrite having positive values, although this is not clear cut.

5.3 Whole rock geochemistry

The major element data (Table 7) for the whole rock analyses show several strong trends from the least altered to the most altered rock as identified by visible alteration (Figure 18). When iron oxide values are plotted against silica values, a very strong, slightly curvilinear trend is observed ($R^2 = 0.91$), with silica decreasing and iron increasing with increasing visible alteration (Figure 19). This gives confidence that silica can be used as a proxy for the degree of alteration in the rock. Plots for aluminium oxide vs silica show Al decreases with Si as alteration becomes more intense (Figure 21). Relationships between alkali and alkali earth metals are not as strong, however still show convincing patterns (Figure 20). With increasing alteration, alkalis (K_2O and Na_2O) decrease, while alkali earths increase (CaO and MgO). MnO also shows an increase with increased alteration. Several other major elements including Ti and P show no obvious patterns.

Trace and rare earth elements do not show any strong correlation with silica and therefore alteration, instead varying widely between samples (Table 8). A plot of trace and rare earth elements normalised against primitive mantle (Sun & McDonough) shows some broad scale trends between the unaltered granite and the more altered rocks. Several elements including Ti, Zr, Y, La and Ce are heavily enriched in the altered rocks, while most others show no discernable patterns (Figure 22). A spiderplot of rare earth elements normalised to chondrite shows a relatively flat pattern (Figure 23), with no strong preferential enrichment in either the light or heavy rare earth elements. All samples show a negative europium anomaly and most show a negative cerium anomaly. There are no consistent, systematic trends between altered and unaltered rocks in the rare earth elements.

6. Interpretation of results

6.1 Hillside geological setting

The Hillside deposit is hosted by Wallaroo Group metasediments and the Arthurton Granite, with the primary mineralisation strongly controlled by the Pine Point Fault Zone. The exact units of the Wallaroo Group are still not well constrained; partly because of the alteration and also because the stratigraphy and contacts of the units are still relatively poorly known. As mentioned previously, it appears the schistose unit may be attributable to the Doora Member; however this unit has never been described from this far south before. A second alternative is that the entire metasedimentary unit is of the Aagot Member, and the schistose units are previously undescribed. The feldspathic metasandstone observed in coastal outcrop appears not to be present in core; however with extensive alteration and brecciation, it may be confused with granite if it is indeed present. The marble present in slide 010 is unlikely to be of Cambrian age, as this would require a substantial amount of movement along a fault to be present at this depth. No other possible Cambrian units have been observed in drill core above the marble, which tends to rule out this possibility. Instead it is likely to be a calcareous unit of the Wallaroo Group sedimentary package, or possibly a metamorphosed highly carbonate altered rock.

The metavolcanics observed in thin section are also poorly understood. The identity of these volcanics is also unknown; there are several distinct Palaeoproterozoic volcanic units mapped to the east and north on the Yorke Peninsula which are candidates to be the unit(s?) present at Pine Point. The extreme alteration observed in HDD013 prevents description and identification of the unit; therefore other holes will need to be observed to find unaltered volcanics. Alternatively, several unaltered rhyolites were found as scree on the northern mapped section of the beach; however their relation to the stratigraphy is unknown.

The Arthurton Granite is well understood, with extensive published lithological and geochemical descriptions available (Zang, 2002). The presence of granitic clasts in the Yuruga Formation suggests the granite was at the surface during the mid-Cambrian when this unit was deposited. The nature of the pegmatite and aplite dykes that are observed to cross cut the granite in coastal outcrop are less well understood in relation to their timing and genetic links with the main granite body. Pods of more mafic material described from the coast are also undescribed in literature; as are the larger enclaves of amphibolitic material. The extent of mafics in the mineralised area is also poorly understood, with highly chloritic rocks confusing identification of igneous mafic rocks.

Mineralisation is strongly controlled by the faults running in an approximately north-south orientation, however the movements and timing of these faults in relation to mineralisation is wholly unknown. The timing of fault activation in relation to the granites is also only partly understood; mineralisation occurs in brecciated granite therefore the fault movement and mineralisation must have occurred at some period after pluton emplacement. Therefore the granite gives a maximum age on mineralisation, but no minimum age can yet be constrained.

6.2 Alteration and ore paragenesis of the deposit

While several distinct assemblages are observed as per above, the use of only a single drill hole obviously prevents any interpretation on the lateral and overall vertical extent of each type of alteration. The rather haphazard and widely spaced nature of the samples prevents any meaningful depth analysis.

6.2.2 Alteration assemblages

There are at least three alteration assemblages clearly documented from thin sections as described previously; a calcsilicate, epidote and HSCCF assemblages. There is some doubt as to the alteration that occurred in the period between the calcsilicate and HSCCF stages, with magnetite and possibly an amphibole stage also present, however this was indeterminable in all sections analysed.

The ore paragenesis of primary mineralisation associated with the HSCC assemblage was relatively straightforward, with overlaps in the dominant mineral precipitated suggesting a gradual change in fluid composition. Such a change is also supported by the isotopic composition of the sulphide minerals. Petrography suggests chalcopyrite formed after pyrite, and a trend of chalcopyrite containing more of the heavier sulphur isotope than pyrite is also observed. In an evolving fluid, the fluid would preferentially take light sulphur isotopes from the source as it is kinetically favoured. As the source is depleted of the lighter isotope, the heavy isotope becomes more enriched in the fluid; thus minerals formed from this fluid have a heavier isotopic signature. The iron oxide mineral chemistry also suggests that magnetite was relatively barren with respect to Cu, and not involved with the mineralising stage, while hematite has higher Cu and U levels, suggesting it may have been more closely related to the copper mineralising stage. There still is no obvious answer as to how long before hematite magnetite was precipitated; whether magnetite was part of the overall HSCCF assemblage is still not known. There is no record of hematite being replaced by or surrounded by magnetite, suggesting magnetite occurred well before hematite. Gold was not observed in polished section, but based on Rex Mineral’s assay results is likely associated with primary copper mineralisation.

Carbonate veining and minor brecciation with earthy hematite are the only later stages, with very minor chalcopyrite and pyrite identified from one such vein. The mineral assemblage of bornite-chalcopyrite-chalcocite-malachite and minor covellite and atacamite reported from the Hillside Mine by Wade and Cochrane is not seen in any core examined. They further reported it to be associated with carbonates, suggesting this is some form of supergene or hypogene enrichment zone in which primary mineralisation was mobilised and concentrated by later fluid activity. No uranium minerals were observed in primary mineralisation either and the confinement of high uranium values to a single copper-poor shear zone may suggest it is not part of the primary mineralisation. Observations by Rowley in the 1950s tend to support this, with pitchblende replacing Cu mineralisation, including covellite, in rocks from the Hillside Mine. This suggests that uranium was introduced at a later stage than the proposed hypogene enrichment, or at least at a later stage in the fluid evolution. The presence of malachite and atacamite is also indicative that supergene enrichment locally acted on these copper lodes.

6.3 Geothermobarometry of alteration

6.3.1 TitaniQ thermometry

Under the assumption of titanium saturation, the temperature for each quartz spot was calculated (Table 9). The raw results give a mean temperature of 461.6°C with a 95% confidence interval of 455.2°C-468°C. A histogram in bins increasing by 5°C shows that the mean is not necessarily the best way to treat the data however, as two populations of quartz temperatures become obvious in the approximately bimodal plot (Figure 24); one from 450°C-465°C and the other at 495°C-500°C. An examination of the petrography of these sections indicates no obviously different petrographic features. The two populations of data are separated by a relatively poorly represented range of temperatures between 470°C-490°C. The upper range of temperatures has a slightly negative skew, with the tail reaching a temperature of 519°C. The lower temperature population has a strong positive skew, with the tail reaching a minimum temperature of 405°C.

6.3.2 Chlorite thermometry

The results are summarised in Table 10, with the total mean temperature of all samples being nearly identical for the geothermometers of Cathelineau (554.2°C) and Jowett (553.6°C), with very similar standard deviations of 83.6°C and 86.3°C respectively. The geothermometer of Kranidiotis & MaClean produced a much lower temperature range, with a mean of 249.1°C and standard deviation of 36.1°C. When analysing the mean temperature of the individual samples, it is apparent that the chlorite data suggests a wide range of temperatures from ~490°C-720°C, which is markedly different to the relatively narrow TitaniQ temperature range.

In contrast to the bimodal distribution of quartz temperatures, the chlorite temperatures had a single peak, but had strong negative skews, with the peak at ~480°C in the Cathelineau and Jowett thermometers (Figure 25), with very few values below this. In comparison with the TitaniQ values, the Kranidiotis & MaClean values underestimate the temperature by 110°C-260°C, which is unacceptable (Figure 26). The Cathelineau and Jowett temperatures overestimated the temperature in comparison to TitaniQ, however in some cases the margin was much smaller, ranging from 7°C-285°C. This discrepancy has been attributed to the effect variability in the host rocks has on the chlorite composition (de Caritat, 1993). The Kranidiotis & MaClean thermometer is calibrated for Al rich rocks, which are not present at Hillside and thus the thermometer produces an anomalous temperature.

7. Discussion

7.1 Geology of the Moonta-Wallaroo district

The geological setting of the Hillside mineralisation broadly agrees with what is observed elsewhere in the Moonta-Wallaroo district. The presence of Wallaroo Group metasediments and metavolcanics with felsic intrusive is a common setting for mineralisation and alteration elsewhere in the region, and makes up the basement of the district (Zang, 2002). The presence of the Doora Member would serve to extend the southernmost known limit of this lithology; however the accuracy of this placement is still uncertain. The “Doora Member” at Hillside preserves amphibole defined foliations dipping 0-15° and a striking approximately north-south. Zang (2002) summarises this same foliation elsewhere dipping 40-50° at a strike of around 40-60° N, suggesting there is some discrepancy between these fabrics. The volcanics of the deposit likely represents the Moonta Porphyry according to Drexel (1979); however it may be attributable to other formations such as the Mona Volcanics, Wardang Volcanics or other undifferentiated members of the Weetulta Formation. Much of the shallow drilling in the 1980s around the deposit recorded ‘gneiss’ in the chip logs. This likely corresponds to either more intensely altered Wallaroo Group metasediments of possibly foliated granite, however no such deformed granite was seen (mostly due to alteration).

7.2 IOCG alteration in the Gawler Craton

The Hillside Mineralisation displays some alteration characteristics similar to other areas of the Yorke Peninsula and the wider Gawler Craton. Three of the four broad alteration assemblages described appear to be equivalent to alteration stages described by Zang (2002). The calcsilicate (garnet-actinolite-epidote) assemblage correlates with an albite-actinolite-magnetite dominated assemblage which represents the ‘type’ Oorlano Metasomatite (Zang 2002). The major difference with other units on Yorke Peninsula is the overwhelming abundance of garnet, with actinolite and epidote relatively rare. Also, no obvious magnetite or albite are observed with this assemblage; however may prove to be present in other sections.

In the wider Gawler Craton, it corresponds to the CAM (calcsilicate-alkali feldspar-magnetite) as defined by Skirrow (2002) it appears this stage rarely has any major associated mineralisation, although minor Fe and Cu sulphides are occasionally present.

The main mineralisation bearing stage at Hillside (quartz-carbonate-K-feldspar-chlorite-sericite + hematite-Fe and Cu sulphides) is rarely seen elsewhere on the Yorke Peninsula and generally weak in nature (Zang, 2002). In the wider Olympic Domain, this alteration has been defined as the HSCC assemblage, consisting of hematite-sericite-chlorite-carbonate ± Fe and Cu sulphides as well as U and REE bearing elements (Skirrow, 2002). This assemblage is dominant in the Olympic Dam deposit and is associated with the main mineralising event. It is is also seen at Emmie Bluff and possibly Prominent Hill, suggesting areas with such mineralisation have the potential for IOCG mineralisation (Bastrakov, 2007). The Hillside assemblage appears to be very similar to that described by Skirrow; however no U or REE minerals have been observed in association, instead they either predate or postdate this stage.

The later carbonate dominated stage which is likely associated with a hypogene and/or supergene enrichment stage producing a bornite-chalcopyrite-chalcocite-covellite-malachite-atacamite followed by pitchblende is common only in the Moonta-Wallaroo district, and is not described from the northern Olympic Domain. It is typically a minor and late epithermal overprint dominated by argillic, carbonate, chlorite, silica and adularia alteration. Minor pyrite, chalcopyrite, chalcocite, covellite and bornite are reported from these later epithermal veins elsewhere on the peninsula, which suggests these patches of enriched material are partly hypogene in nature. Based on observations by Rowley (1955), it appears the pitchblende was introduced at a later stage in the fluid evolution, although with this copper and uranium mineral assemblage not seen during the course of this study, this remains speculative.

Of somewhat more interest is the presence of the epidote-quartz-carbonate-allanite assemblage, which appears to not be documented anywhere else in the Olympic Domain. As described previously it overprints the calcsilicate assemblage and is overprinted itself by the HSCCF assemblage. There appears to be absolutely no associated iron oxides or sulphides and no copper sulphides. Also of note is the absence of a biotite-magnetite alteration stage, which is commonly found elsewhere in the Olympic Domain including the Moonta-Wallaroo district, and represents focussed potassic alteration. Also of note is the rarity of albite, which is often found in several assemblages and as part of a regional Na-Ca alteration footprint, however abundant K-feldspar is present.

7.2 Alteration geochemistry of IOCG deposits

There is relatively little published on the elemental changes in the altered rocks that contain the deposits in the Gawler Craton, however the sulphur isotopes have been previously used to compare the deposits (Figure 27). These data are usually accompanied by ƐNd values, however this information was not gathered during this study but can be found in (Taylor 2009). The analysis of sulphur isotope data from various locations in the Olympic Cu-Au Province has shown that Olympic Dam has a lighter sulphur isotope signature (-10 to -5 ‰ CDT) than many of the other barren or subeconomic prospects (~ -5 to 10 ‰ CDT). The Hillside deposit has a range between -5.77 and 2.29 ‰ CDT, placing it closer to the heavier values associated with the unproven prospects. Bastrakov suggests that the sulphur isotope values of these subeconomic deposits fall into two groups; -4 to +4‰, and +5 to +12‰. The Hillside deposit would therefore fit into the former group. This difference in isotope signatures is due to differences in the fluid sources, with Olympic Dam thought to have a more mantle derived origin than the subeconomic prospects. The source of mineralisaing fluids at Hillside is not discussed here, but can be found in Taylor (2009)

Temperature data for the mineralising fluids of the Olympic Province are scarce, with Bastrakov calculating a range between 250 and 800°C for several of the subeconomic prospects in the region (Bastrakov *et al.* 2007). The Olympic Dam deposit records a decrease in temperature from 400°C to 200°C as the fluid moved from precipitating magnetite to hematite (Oreskes & Einaudi 1992). There has been little research into if or how the temperature of formation affects grade, but the Hillside deposit does fit into the temperature range of the other Gawler Craton deposits.

7.3 Genetic model for the Hillside mineralisation

Combining the findings of this project with existing data from other Gawler Craton IOCG deposits, a preliminary genetic model can be constructed for the Hillside mineralisation. The initiation of fluid flow and mineralisation is still obscure, however is likely to be related to the intrusion of the Arthurton Granite and the initiation or reactivation of the Pine Point Fault Zone. Elsewhere in the Olympic Cu-Au province, the Hiltaba Suite Granitoids are spatially and temporally associated with both highly mineralised and barren systems, with deep crustal fractures needed to focus mafic and ultramafic fluids. Hillside has both the granite and the crustal fracture required for such a system, although the extent of mantle derived mafics in the region is still highly unclear. It is likely the granite acted as a heat source and plumbing for the mineralising fluids to move through the Pine Point Fault Zone, probably supplied by a deep mafic metal source. The fluid evolved from an iron oxide to a sulphide dominated composition, precipitating magnetite, then hematite, pyrite, chalcopyrite and bornite. As the sulphur source was gradually depleted, the sulphur carried by the fluid evolved to a heavier isotopic composition.

Based on the description of mineralisation from the historic Hillside Mine and observations elsewhere on the Yorke Peninsula, it is likely that a second phase of mineralisation occurred during a subsequent reactivation of the Pine Point Fault Zone. This mineralisation appears to be distinct in its mineralogy and association with a late carbonate assemblage. This saw several Cu rich lodes form, with these consisting of chalcocite, malachite, covellite and atacamite. Uranium in the form of pitchblende replaces these copper minerals, and apparently occurs as a later stage mineral in these assemblages. If this phase is related to the epithermal (shallow level) deposits observed elsewhere on Yorke Peninsula, it could correlate with the period that the Arthurton Granite was exposed and eroded at the surface to form the Yuruga Formation. Being the Yuruga Formation is known to be of Cambrian age, this would suggest an origin related to compression during the Delamarian Orogeny. This second phase was not observed and remains obscure, with supergene enrichment possibly acting on these lodes also.

8. Conclusion

The Hillside Cu-Au deposit can be confidently placed within the geological and mineralogical framework of other IOCG deposits of the Gawler Craton, with this research establishing several fundamental paramaters of the mineralisation. These include host rock lithology, alteration paragenesis, bulk rock and mineral geochemical trends as well as paleotemperature. The mineralisation is genetically linked to the Arthurton Granite based on other deposits in the Olympic Domain, and is strongly controlled by the Pine Point Fault. There are two phases of mineralisation; the primary stage which has been described from core for the first time here, and a later hypogene enrichment which appear to produce small lodes of high grade copper, such as those exploited in the Hillside Mine itself. The primary mineralisation shows an evolution in the fluid composition from magnetite to hematite, then pyrite, chalcopyrite and bornite. This similarity in geological setting, alteration mineralogy and isotope geochemistry clearly link Hillside with the IOCGs of the northern Gawler Craton

There are clearly several unanswered questions relating to the deposit; the primary one of these is related to the timing of mineralisation. Allanite and epidote provide dateable minerals, and REE phosphates such as monazite and xenotime might also be expected. Dating may also help determine whether there are two distinct stages of mineralisation as outlined above. Another major question relates to the genesis of mineralisation, and the role of different fluids in the formation. Current models of the formation of Olympic Dam propose a fluid mixing model, with magmatic fluids intermingling with meteoric fluids, causing sudden deposition of metals (Haynes *et al.* 1995). If suitable fluid inclusions can be located, analysis should shed light on the state of the fluids in the deposit. Suitable fluid inclusions should also be searched for to determine the pressure conditions, which was unable to be achieved during this study. Other questions relate to the spatial variation and extent of alteration, and to whether some of the problems previously raised may be determined by further sampling of other drill holes. The presence of mafic intrusives remains enigmatic; with thin sections showing chloritic metasediments may be mistaken for these. A short time before this document was submitted Rex Minerals announced the discovery of further enrichment zones consisting of both minerals observed in this study, as well as malachite, cuprite, native copper and minor chalcocite. This mineralisation, which is similar to that recorded from the old Hillside Mine, has now been intersected in drill core and should allow further analysis of this enrichment, and how it relates to the primary mineralisation described in this report.

Acknowledgements

I would like to first and foremost thank my supervisor Andreas Schmidt Mumm for his guidance throughout the year, in both the field and laboratory. Rex Minerals both funded this research, as well as provided accommodation and invaluable support in the field. Particular thanks go to Hamish and Andy, who patiently answered our questions during core logging. I thank both Ben Wade and Angus Netting at Adelaide Microscopy for their tutorials and guidance in the use of the Electron Microprobe and LA-ICPMS, as well as John Stanley who both guided us through various devices within the university and carried out XRF analysis. Galen Halverson is also thanked for his aid in preparation and analysis of stable isotopes. Lastly, I would like to thank Courtney Taylor for being an eternal drain on my sanity, as well as providing endless entertainment by getting stuck in the Pine Point Beach quicksand in the search for ever more distal (and unimportant) outcrop.

References

AVOCA RESOURCES LIMITED 2006. Fourth Quater Activities Report.

BARTON M. D. & JOHNSON D. A. 2004. Footprints of Fe-oxide(-Cu-Au) systems. *SEG 2004: Predictive Mineral Discovery Under Cover. Centre for Global Metallogeny, Special Publication* **33**, 112-116.

BASTRAKOV E. N., SKIRROW R. G. & DIDSON G. J. 2007. Fluid evolution and origins of iron oxide Cu-Au prospects in the Olympic Dam district, Gawler craton, south Australia. *Economic Geology* **102**, 1415-1440.

BELPERIO A., FLINT R. & FREEMAN H. 2007. Prominent Hill: A hematite-dominated, iron oxide copper-gold system. *Economic Geology* **102**, 1499-1510.

BOYNTON W. V. 1984. Cosmochemistry of the rare earth elements: meteorite studies. *In:* Henderson P. ed. *Rare Earth Element Geochemistry,* pp. 63-114. Elsevier, Amsterdam.

CATHELINEAU M. & NEIVA D. 1985. A chlorite solid solution geothermometer The Los Azufres (Mexico) geothermal system. *Contributions to Mineralogy and Petrology* **91**, 235-244.

CONOR C. H. H. 1995. Moonta–Wallaroo region, an interpretation of the geology of the Maitland and Wallaroo 1:100 000 map sheet areas. *South Australia. Department of Primary Industry and Resources. Open File Envelope 8886*.

CORRIVEAU L. 2006. *Iron Oxide Copper-Gold (±Ag ±Nb ±REE ±U) Deposits: A Canadian Perspective*. Mineral Deposits of Canada:Deposit Synthesis. Geological Survey of Canada.

CREASER R. A. & COOPER J. A. 1993. U-Pb Geochronology of Middle Proterozoic Felsic Magmatism Surrounding the Olympic Dam Cu-U-Au-Ag and Moonta Cu-Au-Ag Deposits, South Australia *Economic Geology* **88**, 186-197.

DAMPIER MINING CO. LTD, BHP MINERALS LTD & CRA EXPLORATION PTY LTD 1986. Open File Envelope No. 3567: EL 499, EL 906 And EL 1112, Curramulka-Pine Point Area

DAVIDSON G. J., PATERSON H., MEFFRE S. & BERRY R. F. 2007. Characteristics and origin of the Oak Dam East breccia-hosted, iron oxide Cu-U-(Au) deposit: Olympic Dam region, Gawler craton, South Australia. *Economic Geology* **102**, 1471-1498.

DE CARITAT P., HUTCHEON I. & WALSHE J. L. 1993. Chlorite Geothermometry: A Review. *Clays and Clay Minerals* **41**, 219-239.

DREXEL J. F. 1979. Mineral occurrences south of Ardrossan - Hillside, Phillips and Harts mines. *South Australia. Department of Mines and Energy. Report Book, 79/77.*

FAIRCLOUGH M. 2005. Geological and metallogenic setting of the Carrapateena FeO-Cu-Au prospect - a PACE success story. *MESA Journal* **38**, 4-7.

FERRIS G. M., SCHWARZ M. P. & HEITHERSAY P. 2002. The Geological Framework, Distribution and Controls Of Fe-Oxide-Cu-Au Mineralisation In The Gawler Craton, South Australia. Part I - Geological And Tectonic Framework. *In:* Porter T. M. ed. *Hydrothermal Iron Oxide Copper-Gold & Related Deposits: A Global Perspective* **2** PGC Publishing, Adelaide.

GANDHI S. S. 2004. Magmatic-hydrothermal Fe oxide ± Cu ± Au deposits: Classification for a digital database and an overview of selected districts [abs]. Paper presented at IAVCEI General Assembly 2004, Pucon, Chile (unpubl.).

HAND M., REID A. & JAGODZINSKI L. 2007. Tectonic framework and evolution of the Gawler craton, southern Australia. *Economic Geology* **102**, 1377-1395.

HAYNES D. W., CROSS K. C., BILLS R. T. & REED M. H. 1995. Olympic Dam Ore Genesis - A Fluid Mixing Model. *Economic Geology and the Bulletin of the Society of Economic Geologists* **90**, 281-307.

HEY M. H. 1954. A new review of the chlorites. *Mineralogical Magazine* **30**, 227.

HITZMAN M. W. 2000. Iron Oxide-Cu-Au Deposits: What, Where, When, and Why. *In:* Porter T. M. ed. *Hydrothermal Iron Oxide Copper-Gold & Related Deposits: A Global Perspective*, pp. 9-25. **1**, Adelaide.

HITZMAN M. W., ORESKES N. & EINAUDI M. T. 1992. Geological characteristics and tectonic setting of Proterozoic iron-oxide (Cu-U-Au-REE) deposits. *Precambrian Research* **58**, 241-287.

HITZMAN M. W. & VALENTA R. K. 2005. Uranium in iron oxide-copper-gold (IOCG) systems. *Economic Geology* **100**, 1657-1661.

JOWETT E. C. 1991. Fitting iron and magnesium into the hydrothermal chlorite geothermometer. *GAC/MAC/SEG Joint Annual Meeting (Toronto, May 27-29, 1991), Program with Abstracts* **16**, A62.

KRANIDIOTIS P. & MACLEAN W. H. 1987. Systematics of chlorite alteration at the Phelps Dodge massive sulfide deposit, Matagami, Quebec. *Economic Geology* **82**, 1898-1911.

MIM EXPLORATION PTY LTD 1997. Open File Envelope No. 9166. EL 1785 Maitland. First Partial Relinquishment Report For The Period 7/9/1992 To 6/3/1996.

MUMME I. A. 1955. Ground scintillation survey at the Hillside, Harts and Parara copper mines, and a copper prospect on section 39 Hd of Muloowurtie, Ardrossan. *South Australia. Department of Mines. Report Book, 39/22*.

ORESKES N. & EINAUDI M. T. 1992. Origin of hydrothermal fluids at Olympic Dam; preliminary results from fluid inclusions and stable isotopes. *Economic Geology* **87**, 64-90.

POLLARD P. J. 2006. An intrusion-related origin for Cu-Au mineralization in iron oxide-copper-gold (IOGG) provinces. *Mineralium Deposita* **41**, 179-187.

RAYMOND O. L. 2001. *Yorke Peninsula (Moonta Subdomain) Geophysical Interpretation of Pre-Neoproterozoic Basement Geology 1:250 000 Scale Map (Second Edition)*. Geoscience Australia, Canberra.

REX MINERALS 2009a. *More High Grade Copper at Hillside, SA*. ASX and Media Release: 3 April, 2009.

REX MINERALS 2009b. Quarterly Activities Report - for the period ended 30 June 2009. Online

ROWLEY R. 1955. Uranium occurrence, Hillside copper mine, Ardrossan. *South Australia. Department of Mines. Report Book, 39/8*.

RUANO S. M., BOTH R. A. & GOLDING S. D. 2002. A fluid inclusion and stable isotope study of the Moonta copper-gold deposits, South Australia: evidence for fluid immiscibility in a magmatic hydrothermal system. *Chemical Geology* **192**, 211-226.

RUSK B. G., LOWERS H. A. & REED M. H. 2008. Trace elements in hydrothermal quartz: Relationships to cathodoluminescent textures and insights into vein formation. *Geology* **36**, 547-550.

SKIRROW R. G. ed. 2008. *'Hematite-group' IOCG±U ore systems: Tectonic settings, hydrothermal characteristics, and Cu-Au and U mineralizing processes*. Exploring for Iron Oxide Copper-Gold Deposits: Canada and Global Analogues Shortcourse Notes, GAC-MAC-SEG-SGA 2008, Quebec City, 29-30th May 2008 **X**. Geological Association of Canada.

SKIRROW R. G., BASTRAKOV E. N., DAVIDSON G. J., RAYMOND O. L. & HEITHERSAY P. 2002. The Geological Framework, Distribution and Controls of Fe-oxide Cu-Au Mineralisation in the Gawler Craton, South Australia. Part II - Alteration and Mineralisation. *In:* Porter T. M. ed. *Hydrothermal Iron Oxide Copper-Gold & Related Deposits: A Global Perspective*, pp. 33-47. **2** PGC Publishing, Adelaide.

STUART W. J. 1970. The Cainozoic stratigraphy of the eastern coastal area of Yorke Peninsula, South Australia. *Transactions of the Royal Society of South Australia* **94**, 151-178.

SUN S.-S. & MCDONOUGH W. F. 1989. Chemical and isotopic systematics of oceanic basalts: implications for mantle composition and processes. *Geological Society, London, Special Publications* **42**, 313-345.

TAYLOR C. 2009. Source of fluids and metals in the Hillside IOCG deposit. University of Adelaide, Adelaide (unpubl.).

TEAKLE R. P. 1983. Hydrocarbon Potential of the Cambrian Succession on Yorke Peninsual, South Australia. University of Adelaide, Adelaide (unpubl.).

TEASDALE J., PRYER L., ETHERIDGE M., ROMINE K., STUART-SMITH P., COWAN J., LOUTIT T., VIZY J. & HENLEY P. 2001. Western Stansbury Basin SEEBASE Project SRK Consulting & Primary Industries and Resources, South Australia, Adelaide.

TINDLE A. G. 1999. Mineral Recalculation Software:Chlorite (unpubl.). Online <www.open.ac.uk/earth-research/tindle/AGTWebData/Chlorite.xls >

WADE M. L. & COCHRANE G. W. 1954. Hillside copper mine, Ardrossan (21/10/52). *Mining Review, Adelaide* **97**, 55-59.

WARK D. A. & WATSON E. B. 2006. TitaniQ: a titanium-in-quartz geothermometer. *Contributions to Mineralogy and Petrology* **152**, 743-754.

WIEWIÓRA A. & WEISS Z. 1990. Crystallochemical classifications of phyllosilicates based on the unified systems of projection of chemical composition: II. The chlorite group. *Clay Minerals* **25**, 83-92.

WOODMANSEE W. 1957. Diamond drilling at the Hillside copper mine, Ardrossan. *South Australia. Department of Mines. Report Book, 41/61*.

ZANG W. L. 2002. *Late Palaeoproterozoic Wallaroo Group and early Mesoproterozoic mineralisation in the Moonta Subdomain, eastern Gawler*

Craton, South Australia. Report Book, 2002/001. Department of Primary Industries and Resources, South Australia.

ZANG W. L., COWLEY W. F. & FAIRCLOUGH M. 2006. *Maitland Special: SHEET SI53-12* 1:250 000 Geological Series — Explanatory Notes. PIRSA Publishing Services, Adelaide.

ZANG W. L., RAYMOND O. L. & CONOR C. H. H. 2002. Geology of Yorke Peninsula and Cu–Au mineralisation at Moonta and Wallaroo. *In: 16th Australian Geological Convention, Adelaide, Excursion Guide A1* Geological Society of Australia, Adelaide.

Table captions

Table 1: LA-ICPMS trace element in quartz dataset with the minimum detection limit filtered (in ppm). Blank spaces indicate value was below detection limit. Ti was the element targeted to calculate palaeotemperature using TitaniQ method. Remainder of elements analysed to detect possible contamination from silicates or sulphides. Sample names are composites of the slide number, the circle number (c1-4), and the spot ID (a-c).

Table 2: LA-ICPMS trace element values in magnetite with minimum detection limit filtered (in ppm). Data with < preceding them indicate value is below detection limit. Detection limit differs between each spot, and is calculated each time a spot is run. Magnetite was sampled to analyse Ti concentration, and to compare the magnetite with hematite to evaluate how fluid composition changed between the two stages. Samples are numbered by their slide number and the spot number (m=magnetite 1-9)

Table 3: LA-ICPMS trace element values in hematite with minimum detection limit filtered (in ppm). Data with < preceding them or blank cells indicate value is below detection limit. Hematite was sampled to analyse Ti concentration, and to compare the magnetite with hematite to evaluate how fluid composition changed between the two stages. Samples are numbered by their slide number and the spot number (h=hematite 1-9)

Table 4: Raw chlorite compositional data as determined by electron microprobe (in oxide %). Chlorite was analysed for use in chlorite thermometry which requires knowledge of Si, Al, Fe and Mg concentrations. Included here is subset of complete data showing elements involved in temperature-controlled cation exchange, as well as Ca, Na and K which indicate contamination of other sheet silicate if total greater than 0.5%. Samples are labelled by their slide number, the chlorite grain or group (chl1-3) and the spot number.

Table 5: Corrected chlorite microprobe data, displaying data required for chlorite thermometry calculations. Si and Al data are number of cations in chlorite formula. Al^{iv} and Al^{vi} represent the aluminium cations in the tetrahedral and octahedral sites respectively. The Fe/Fe+Mg ratio is also based on number of cations in chlorite formula.

Table 6: Summary of $\delta^{34}S$ (‰ CDT) of sulphide samples from Hillside. Samples differentiated by sulphide type. Sample names represent sampler (R=B. Cerlienco, G = C. Taylor), number represents core sample.

Table 7: Major element XRF data from unaltered to altered core (oxide %). HB001 is unaltered pegmatitic granite; HB028 is the most altered metasomatite, with a gradational visual change from right to left. Sample numbers correspond to core sample numbers

Table 8: Trace and rare earth element XRF data. A) Rare earth element concentration from bulk rock core samples (in ppm). Same data ordering and sample numbering as table 6; HB001 is unaltered pegmatitic granite; HB028 is the most altered metasomatite, with a gradational visual change from right to left. Data proceeded by < indicates element was below detection limit. B) Trace element concentration from bulk rock core samples (in ppm). Same data ordering as with REE table.

Table 9: TitaniQ thermometry calculated temperatures based on Ti concentration measured by LA-ICPMS. Table includes sample number as per naming of Table 1. Temperature calculations as per (Wark & Watson 2006).

Table 10: A summary of the three cation exchange-based chlorite thermometry calculations by sample. All data and sample names based on microprobe data in Table 4.

Figure captions

Figure 1: The location of the three visible historical workings; Hillside, Hart’s and Phillip’s Mines on the east coast of the Yorke Peninsula, South Australia. Drilling is occurring in the region south of Hillside Mine.

Figure 2: A map of the tectonic domains of the Gawler Craton, with the Olympic Cu-Au Province marked in by dashed lines. Note the Hillside mineralisation (triangle) occurs in the south eastern margin of the province. Modified from Skirrow et al, 2002.

Figure 3: Main unaltered host rocks in core. A) Quartz and mica rich metasandstones and schists. B) Pegamatitic quartz-feldspar granitoid with tourmaline.

Figure 4: Metasedimentary rocks of the Hillside deposit in thin section: A) Plane polarised light, 5 x magnification. Quartz and K-feldspar dominated metasediment with foliation defining amphibole lathes. B) Cross polarised light, 5 x magnification. Quartz and K-feldspar dominated metasediment, with bands of coarse grained ?recrystallised quartz parallel to foliation plane amphiboles. Cross-cut by later carbonate veins. C) Plane polarised light, 5 x magnification. Large euhedral K-feldspar crystals in a finer grained recrystallised calcite-quartz matrix (marble). D) Cross polarised light, 20 x magnification. Remnant primary carbonate containing chlorite foliations, surrounded by recrystallised quartz and carbonate.

Figure 5: Thin section pictomicrographs of host volcanics and granites. A) Plane polarised light, 5 x magnification. K-feldpar-biotite-opaque dominated recrystallised felsic volcanic with overprinting chlorite. B) Plane polarised light, 10 x magnification. Higher magnification of previous image, showing slight preferred orientation in biotite. C) Cross polarised light, 1.5 x magnification. Titanite bearing granite composed dominantly of quartz and sericitised K-feldspar. D) Cross polarised light, 5 x magnification. Heavily sericitised, coarse grained K-feldspar dominated granitoid.

Figure 6: Pictomicrographs of the calcsilicate assemblage. A. Plane polarised, 5 x optical magnification of the massive garnet being cut by K-feldspar, quartz and minor carbonate. B. A cross-polarized, 5 x magnification of a single large euhedral epidote crystal within garnet. Both the garnet and euhedral epidote are cut and overprinted by very fine grained epidote. Surrounding the garnet is a speckled assemblage consisting of Quartz, carbonate, chlorite, K-feldspar and opaques. C & D show the overprinting relationships of the K-feldspar-carbonate-hematite-chlorite assemblage.

Figure 7: Pictomicrographs of the epidote dominated assemblages. A) Plane polarised light at 5 x magnification. Epidote occurring coevally with quartz and after an opaque phase, as demonstrated by the filling of fractures with epidote and quartz. B) Plane polarised light, 10 x magnification. Fine grained epidote overprinting and altering garnet, giving a very dirty appearance. Both garnet and epidote are overprinted by K-feldspar and carbonate. C) Cross polarised light, 5 x magnification. A quartz vein overprinting a primary titanate crystal (granitic protolith), with alteration of titanate to epidote. Note overprinting of quartz-epidote vein by fine grained carbonate-K feldspar-quartz-chlorite vein at bottom left hand corner. D) Cross polarised light, 10 x magnification. Coarse grained epidote in a large quartz vein. Minor overprinting by a later chlorite stage.

Figure 8: Pictmicrographs of the HSCCF assemblage in transmitted light. A) Plane polarised light, 5 x magnification. A K-feldspar-carbonate-opaque (hematite?) assemblage overprinting the earlier garnet assemblage. B) Cross polarised light, 5 x magnification. A coarse grained carbonate-quartz vein with chlorite at the edges overprinting an earlier epidote-quartz assemblage. C) Cross polarised, 5 x magnification. Heavy chlorite-sericite alteration throughout a metavolcanic rock. D) Cross polarised light, 5x magnification. Quartz-K feldspar-sericite-carbonate-hematite assemblage.

Figure 9: Late carbonate veining. A) Plane polarised light, 5 x magnification. Carbonate using an earlier chlorite vein network in a metasediment rock. B) Cross polarised light, 5 x magnification. Carbonate veins cutting quartz rich metasediment.

Figure 10: Reflected light pictomicrographs of ore mineral assemblage. A) 5 x magnification. Martitised magnetite surrounded by pyrite. B) Two stages of pyrite differentiated by texture, with minor earlier hematite. Post dated by massive chalcopyrite. C-D) 10 x magnification. Bornite and chalcopyrite demonstrating two paragenetic sequences (chalcopyrite replaced by bornite, bornite surrounded by later chalcopyrite).

Figure 11: Summary of proposed mineral paragenesis of the four well recognised assemblages at Hillside. Note several minerals remain poorly understood in terms of their timing (albite and magnetite), and the ore minerals of the late stage hypogene/supergene assemblage are based on Wade and Cochrane (1954) and Rowley (1955).

Figure 12: Plots of Ti against all other elements sampled to check for systematic change in Ti with other elements, which may signify contamination. No such trends are observed.

Figure 13: Ti concentration in quartz histogram as measured by LA-ICPMS. Note any values greater than 10 ppm Ti were excluded as outliers. Note the slightly bimodal nature of the dataset. Data is not separated by samples, however TitaniQ temperature histogram does

Figure 14: Graphical comparison of trace elements in magnetite (red) and hematite (blue) as measured with LA-ICPMS. Values represent the maximum, average and minimum trace element values (from top dot to bottom dot) for each mineral. Note the similarity between Si, P, V, Cr, Co and Ni, and the discrepancy between Al, Ti and Cu.

Figure 15: Rare earth elements in magnetite (Red) and hematite (Black) normalised to chondrite (Boyan, 1984) as determined by LA-ICPMS. Not all elements are sampled, and thus produce a broken pattern. Note hematite is richer in all REE, with magnetite having both a negative cerium and europium anomaly.

Figure 16: Classification of chlorite from Hillside based on electron microprobe data under the scheme of Hay (1954). This scheme is based on the ratio of Fe and Mg to Si atoms. Sample spots are separated by colour. Most samples fall in the daphnite and pycnochlorite fields, with fewer in the brunsvigite and ripidolite fields

Figure 17: Histogram of sulphide (δ^{34}S [‰CDT]) values, separating different sulphide species by colour. Note the excessively negative values (-26 to -25 ‰ CDT) are treated as outliers. There is a trend of pyrite having a slightly heavier isotopic signature than pyrite.

Figure 18: Stacked major element oxide % totals normalised to 100% showing the increase and decrease of each element from unaltered granite (HB001) to the most altered metasomatite (HB028). Visual alteration levels increase from left to right. There is a decrease in SiO_2, Al_2O_3, K_2O and Na_2O and an increase in Fe_2O_3 (total) and to a weaker extent, CaO and MgO.

Figure 19: Inverse linear relationship between SiO_2 and Fe_2O_3T demonstrated in rocks of varying visible alteration. This relationship indicates silica is a good proxy for amount of visible alteration. HB012 and HB037 are reversed from the otherwise uniform pattern (HB037 shows less visible alteration than HB012).

Figure 20: Enrichment and depletion of alkali and alkali earth metals with changing silica levels. As demonstrated above, silica is a proxy for the amount of alteration; low silica levels

signify higher alteration. The alkali metals K and Na are depleted from the host rock (dominantly granitoids), while Mg and Ca are enriched. This is probably due to the addition of carbonate, chlorite and epidote to the system. Note the coefficient of determination ranges from 0.14 to 0.59, suggesting only a weak relationship is supported for these trends.

Figure 21: Depletion of aluminium from the host granitoid rock with decreasing silica levels. As demonstrated previously, silica is a proxy for the amount of visible alteration; low silica levels signify higher alteration. The coefficient of determination (0.66) is quite high, indicating moderate support for this relationship.

Figure 22: Trace and rare earth elements normalised to primitive mantle (Sun & McDonough 1989) and plotted in a spidergram. Samples include both those analysed during this study Listed from least to most altered in key) and two unaltered granites in the region (Pine Point and Parara) based on data collected previously

Figure 23: Rare Earth Elements normalised to chondrite (Boynton 1984) plotted in a spidergram. Samples include both those analysed during this study and two unaltered granites in the region (Pine Point and Parara)(Zang 2002). Note the relatively flat, primitive pattern of the spidergram. Straight lines over more than one segment indicate a value below detection limit (and therefore not plotted).

Figure 24: Histogram of the TitaniQ population from the Hillside samples, showing the higher (~495°C) and lower (~460°C) peaks. Note samples are divided by colour.

Figure 25: Temperature frequency histograms for two chlorite thermometry methods A) Cathelineau (1988) and B) Jowett (1991). Kranidiotis (1989) produces an unreasonably low temperature when compared to the TitaniQ measurements and is therefore not included here

Figure 26: Graphical comparison of the TitaniQ and chlorite temperatures, showing the significant underestimation of the Jowett (1991) method and the slight agreement between methods in samples 7155, 027 and 020

Figure 27: Graphical comparison of range of sulphur isotope data (δ^{34}S [‰CDT]) over several Gawler Craton IOCG deposits and prospects. Olympic Dam is the only deposits for which the resource is well defined and actively being exploited, the remainder are prospects or subeconomic in nature. Several have ranges included for both pyrite (blue) and chalcopyrite (red). Those in which no differentiation between sulphide species has been made

are black. Olympic Dam data from (Oreskes & Einaudi 1992), Oak Dam from (Davidson *et al.* 2007), remainder from (Bastrakov *et al.* 2007) except for Hillside (this study).

Tables

Sample	Na^{23}	Al^{27}	P^{31}	K^{39}	Ca^{43}	Ti^{49}	Fe^{56}	Fe^{57}
005c1a	157.74	287.29	18.87	39.96	90.02	2.65	27.15	9.68
005c1b	170.06	231.68	10.31	23.11	147.3	3.22	37.45	14.35
005c1c	120.42	203.85	12.75	16.97	176.68	2.99	16.29	8.6
005c2a	-	17.1	-	-	-	5.59	2.59	4.57
005c2b	204.99	16.89	10.32	3.12	245.73	3.48	54.37	22.96
005c3a	11.62	32.16	9.65	2.44	-	3.77	-	-
005c3b	214.64	15.56	-	-	114.67	2.94	13.85	5.64
005c4a	-	20.04	9.37	-	153.38	3.26	-	-
005c4b	26.01	19.12	15.6	-	-	3.81	50.57	18.5
005c4c	-	10.97	21.52	-	-	3.54	-	-
013c1a	32.99	816.3	17.21	200.13	-	3.53	4.38	-
013c1b	61.54	674.09	11.37	232.9	76.17	3.23	144.7	59.3
013c2a	101.52	167.57	23.21	57.25	-	2.09	7.75	10.88
013c2b	106.71	407.11	18.04	94.66	149.56	1.97	23.7	5.38
013c2c	138.44	117.07	11.89	41.4	162.7	1.48	-	-
013c3a	34.86	1382.92	21.5	419.59	201.93	6.96	-	-
013c3b	99.41	1193.41	19.05	366.22	102.65	3.99	12.33	-
013c4a	55.74	294.19	16.97	68.94	-	2.35	45.2	14.57
013c4b	87.05	946.53	9.06	205.53	-	3.75	-	-
013c4c	62.6	780.77	20.2	225.87	159.25	1.42	-	-
020c1a	-	84.4	15.84	-	-	1.52	-	-
020c1b	114.94	36.2	11.25	12.97	-	2.03	-	-
020c1c	60.82	12.1	20.41	4.64	-	2.39	9.93	-
020c2a	45.18	35.1	15.89	2.24	-	2.08	4.4	-
020c2b	54.59	19.42	16.83	2.26	-	5.39	-	-
020c2c	127.67	20.32	22.38	13.58	136.84	3.13	-	-
020c3a	-	69.15	11.97	-	-	2.92	19.46	10.84
020c3b	54.59	23.52	12.58	6.53	-	-	-	-
020c4a	-	14.82	17.39	-	-	2.06	-	-
020c4b	181.82	22	15.93	29.78	233.58	6.09	7.76	4.14
027c1a	23.41	777.69	20.99	322.4	-	4.65	62.2	29.13
027c1b	191.52	574.08	19.82	179.66	215.01	2.27	-	-
027c2a	172.77	1555.08	20.61	589.39	230.66	3.72	9.62	-
027c2b	63.36	1293.71	11.59	382.8	-	3.82	40.75	17.94
027c3a	82.62	580.6	13.67	177	120.92	1.77	6.52	5.47
027c3b	92.46	378.4	9.34	53.52	140.35	1.78	11.18	-
027c3c	80.82	704.79	20.15	116.66	122.32	-	1.68	-
027c4a	135.47	47.58	22	24.06	-	1.74	-	-
027c4b	29.67	86.65	19.22	22.28	96.19	1.65	4.1	-
027c4d	155.17	1438.91	15.65	628.04	200.83	1.57	-	-
7152a	227.72	514.24	12.55	44.51	157.38	3.5	89.96	25.3
7152a2	14.36	440.79	9.92	-	-	3.72	-	-
7152a3	74.59	381.58	11.84	-	-	3.25	-	-
7152c4a	49.49	23.65	10.33	4.29	44.41	-	6	1.88
7152c4b	18.58	15.48	9.59	-	-	8.26	8.27	2.27
7152c4c	168.23	214.49	10.73	27.97	115.36	6.82	-	-
7152c2a	68.6	84.66	16.32	14.41	122.35	3.42	7.46	-
7152c2b	115.22	30.27	21.99	3.73	188.62	7.91	56.93	22.12
7152c2c	136.81	18.12	15.99	35.48	-	8.88	10.91	-
7152c3a	197.92	21.39	10.51	5.17	-	6.04	-	-
7152c3b	133.74	40.79	16.84	10.65	-	2.98	3.11	-
7152c3c	512.09	25.12	16.88	25.71	273.5	6.18	-	-

7155c1a	5.04	10.22	10.2	-	-	-	11.7	5.93
7155c1b	102.08	35.87	11.83	14.83	-	7.39	46.3	18.5
7155c1c	56.63	12.82	10.91	17.09	98.16	-	35.03	13.99
7155c2a	62.73	66.95	-	11.21	-	3.94	18.38	7.11
7155c2b	59.83	32.5	21.03	4.36	-	2.66	-	-
7155c3a	46.21	37.92	19.42	-	-	5.29	36.27	12.23
7155c3b	136	48.99	14.49	28.41	106.32	3.68	3.97	-
7155c4a	19.87	43.85	14.94	4.56	-	2.59	-	-
7155c4b	52.63	24.59	13.91	6.05	92.45	3.06	-	-
7155c4c	127	32.88	10.75	19.5	207.57	2.94	6.99	-
7156c1a	187.01	37.76	13.39	7.89	-	6.59	-	-
7156c1b	-	11.06	15.37	-	-	7.4	12.63	-
7156c1c	107.76	20.78	10.13	3.37	162.41	6.44	15.1	4.88
7156c2a	74.11	14.57	10.97	-	375.68	6.46	2.56	-
7156c2b	37.9	16.48	16.93	-	138.8	7.05	6.4	-
7156c3a	240.33	58.4	14.73	21.09	164.75	4.91	7.69	2.77
7156c3b	97.56	18.36	14.76	-	154.59	6.2	56.8	17.32
7156c3c	78.84	85.57	13.44	16.39	261.55	6.45	20.23	8.49
7156c4a	-	19.03	19.15	-	165.53	3.61	3.44	-
7156c4b	15.49	22.53	19.32	-	-	4.57	26.33	11.92
7171c1a	89.58	187.59	-	36.81	151.52	-	160.36	68.6
7171c2a	-	13.33	10.59	-	-	6.65	-	-
7171c2b	29.19	32.52	11.02	-	127.24	6.49	49.3	23.31
7171c2c	7.96	20.29	12.34	-	-	5.97	-	-
7171c3a	95.55	29.96	10.68	12.69	-	4.43	66.65	28.34
7171c3b	75.2	34.85	13.44	8.78	-	3.59	13.66	3.97
7171c3c	220.71	27.86	11.86	35.8	180.69	4.42	36.56	17.98
7171c4a	74.43	19.71	14.98	12.9	-	4.21	5.74	-
7171c4b	116.09	17.27	10.8	18.17	-	3.25	6.05	-
7171c4c	10.24	11.24	13.16	-	-	5.94	-	-
7161av1	51.57	646.22	-	43.61	-	-	-	-
7161bv2	20.74	1418.98	-	57.02	-	1.98	-	-
7161cv3	8.37	1474.74	28.06	-	-	1.2	-	-
7161dv4	29.06	1083.43	-	35.91	-	1.62	-	-
7161ev5	60.18	1399.77	17.11	83.89	-	1.66	14.7	-
7161fv6	49.47	2046.77	19.5	162.14	-	2.4	-	-
7161gvb1	-	362.22	22.28	-	-	1.35	-	-
7161hvb3	-	669.6	-	4.45	-	1.14	-	-
7161ivb4	3.89	828.25	-	21.49	-	1.41	-	-
7161jvc5	-	19.89	-	-	-	1.48	-	35.16

Table 1

Pr^{141}	**Ce^{140}**	**La^{139}**	**Cu^{65}**	**Ni^{60}**	**Co^{59}**	**Fe^{57}**	**Fe^{56}**	**Cr^{52}**	**V^{51}**	**Ti^{49}**	**Ca^{43}**	**P^{31}**	**Si^{29}**	**Al27**	
<0.030	<0.035	<0.034	<0.78	26.32	9.89	8E+05	2E+06	2.5	238.6	697	<203.65	<15.52	251.5	945.5	**7161m1**
<0.0225	<0.030	<0.026	<0.78	16.81	15.26	8E+05	2E+06	2.37	223.2	755.6	<204.20	<15.76	434.7	967.6	**7161m2**
<0.0212	<0.028	0.039	<0.77	15.21	9.29	8E+05	2E+06	3.53	369.5	973.7	<185.39	15.84	383.9	1098	**7161m3**
<0.0234	<0.027	<0.026	<0.76	14.7	8.1	8E+05	2E+06	2.37	353.8	1912	<191.65	18.79	451.2	1090	**7161m4**
<0.0249	<0.028	<0.026	<0.76	14.82	10.64	8E+05	2E+06	1.35	363.9	1455	<190.93	<14.52	333.4	1065	**7161m5**
<0.0246	<0.028	<0.027	<0.78	18.66	11.55	8E+05	2E+06	10.37	411.6	1224	<189.10	<14.57	337.1	921.7	**7161m6**
<0.0224	<0.029	<0.026	<0.81	15.81	13.27	8E+05	2E+06	4.6	388.3	298.8	<200.95	<15.45	286.8	869.4	**7161m7**
<0.0234	<0.034	<0.028	<0.85	41.9	14.82	8E+05	2E+06	3.31	388.3	399.4	315.3	19.99	416	771.8	**7161m8**
<0.0257	<0.028	<0.031	<0.82	61.21	20.47	8E+05	2E+06	2.43	369.8	630.1	<203.71	<15.55	357.1	680.4	**7161m9**
0.061	0.403	0.318	<1.18	17.27	20.09	8E+05	3E+06	2.14	216.2	432	<306.03	38.2	422.8	471.6	**7156m1**
<0.035	<0.046	<0.042	<1.10	17.93	24.3	8E+05	3E+06	2.96	228	445.4	<277.58	<21.35	402	449.7	**7156m2**
<0.047	<0.056	<0.052	<1.18	18.41	28.98	8E+05	3E+06	2.51	235.8	646.2	<227.04	31.24	518.2	562.7	**7156m3**
<0.041	<0.049	0.098	<1.08	18.77	25.61	8E+05	3E+06	10.59	237	451.4	441.8	<21.69	1105	473.4	**7156m4**
<0.070	0.136	<0.091	2.09	18.99	21.46	8E+05	3E+06	3.83	211.3	577.6	<419.32	<37.89	556.9	517.9	**7156m5**
<0.039	<0.062	<0.055	<1.30	17.1	27.34	8E+05	3E+06	2.75	203.5	429.1	329.8	<25.76	661.3	611.7	**7156m6**
<0.038	<0.052	<0.043	<1.19	18.1	28.08	8E+05	3E+06	3.7	227.3	671.7	<261.58	<20.97	506.1	557.4	**7156m7**
<0.052	<0.064	<0.063	<1.52	24.65	10.62	8E+05	4E+06	3.25	30.01	147.4	600.3	<25.44	550.9	242.2	**7156m8**
<0.0041	<0.0053	<0.0054	<0.049	22.41	14.79	5E+05	8E+05	162.3	427.3	157	61.19	<5.30	45.85	112.6	**030a**
<0.0013	0.003	<0.0024	<0.11	23.57	11.33	5E+05	8E+05	140.4	412.9	76.25	<56.95	<6.14	100.6	78.24	**030b**
<0.0017	0.002	0.002	<0.079	23.17	14.81	5E+05	8E+05	135.5	448.2	109.1	<62.11	<5.59	53.18	141.4	**030c**
<0.0013	0.006	<0.0024	<0.098	23.15	13.89	5E+05	8E+05	137.2	430.4	104.4	<73.67	6.9	80.67	151.5	**030d**
0.005	0.042	0.014	0.156	26.1	11.73	5E+05	8E+05	183	454.1	62.03	<67.02	7.2	3254	3005	**030e**

	U^{238}	**Bi^{209}**	**Pb^{208}**	**Yb^{172}**	**Er^{166}**	**Ho^{165}**	**Dy^{163}**	**Gd^{157}**	**Eu^{153}**	**Sm^{147}**	**Nd^{146}**
7161m1	<0.035	<0.045	0.178	<0.126	<0.087	<0.031	<0.112	<0.159	<0.045	<0.156	<0.151
7161m2	<0.028	<0.031	<0.067	<0.113	<0.084	<0.023	<0.101	<0.171	<0.051	<0.172	<0.137
7161m3	0.038	<0.033	0.14	<0.108	<0.068	<0.0258	<0.095	<0.142	<0.038	0.151	<0.121
7161m4	0.044	<0.032	0.217	<0.115	<0.077	<0.0247	<0.099	<0.160	<0.038	<0.148	<0.128
7161m5	<0.026	<0.033	0.145	<0.107	<0.071	<0.0226	<0.096	<0.150	<0.043	<0.155	<0.128
7161m6	0.03	<0.036	0.222	<0.115	<0.074	<0.026	<0.106	<0.168	<0.042	<0.157	<0.121
7161m7	<0.026	<0.034	<0.074	<0.124	<0.080	<0.027	<0.105	<0.170	<0.043	<0.168	<0.131
7161m8	<0.029	<0.036	0.093	<0.135	<0.082	<0.031	<0.115	<0.177	<0.043	<0.169	<0.144
7161m9	<0.031	<0.036	0.114	<0.132	<0.084	<0.026	<0.114	<0.179	<0.051	<0.178	<0.152
7156m1	0.182	<0.061	0.82	<0.220	<0.145	<0.049	<0.188	<0.27	<0.085	<0.27	<0.254
7156m2	0.048	<0.056	1.04	<0.193	<0.122	<0.038	<0.182	<0.25	<0.071	<0.30	<0.200
7156m3	<0.056	<0.065	0.86	<0.228	<0.153	<0.046	<0.206	<0.29	<0.081	<0.33	<0.242
7156m4	0.056	<0.055	1.13	<0.206	<0.123	<0.044	<0.167	<0.28	<0.080	<0.26	<0.221
7156m5	<0.085	<0.104	10.15	<0.35	<0.23	<0.070	<0.27	<0.48	<0.134	<0.45	<0.41
7156m6	<0.059	<0.074	<0.140	<0.25	<0.154	<0.056	<0.200	<0.32	<0.082	<0.33	<0.28
7156m7	0.465	<0.061	0.74	<0.192	<0.126	<0.042	<0.182	0.3	<0.075	<0.28	<0.212
7156m8	<0.060	<0.071	<0.144	<0.25	<0.168	<0.059	<0.220	<0.31	<0.093	<0.40	<0.31
030m1	<0.0036	<0.0035	0.028	<0.0119	<0.0075	<0.0048	<0.0106	<0.0126	<0.0054	<0.0111	<0.0118
030m2	<0.0012	<0.0015	0.03	<0.0061	<0.0034	0.002	<0.0062	<0.0071	<0.0009	<0.0041	<0.0092
030m3	0.003	0.002	0.02	<0.0024	<0.0017	<0.0010	0.004	<0.0041	<0.0017	<0.0041	0.003
030m4	0.011	<0.0013	0.031	<0.0055	<0.0032	<0.0009	6E-04	<0.0064	<0.0010	<0.0064	<0.0067
030m5	0.012	<0.0011	0.013	<0.0041	<0.0020	<0.0006	<0.0048	0.011	0.002	0.008	0.021

Table 2

030h5	030h4	030h3	030h2	030h1	7156h2	7156h1	7161h1	
149.11	100.97	131	112.98	337.17	172.87	1361.8	430.9	Al^{27}
98.52	157.96	<44.63	101.36	387.87	669.77	1796.5	360.29	Si^{29}
<5.02	<5.27	<5.98	5.83	<4.83	<23.36	<25.59	<14.34	P^{31}
<82.20	<76.45	<76.75	68.63	<61.63	<324.88	41693.02	<190.41	Ca^{43}
171.91	53.87	92.06	69.43	86.75	62.37	619.74	309.78	Ti^{49}
561.66	495.09	500.21	445.41	486.89	40.99	315.1	69.44	V^{51}
145.55	158.79	161.52	149.08	147.57	1.85	2	1.67	Cr^{52}
761765	761765.1	761764.9	761765	761765	3702558	3637674	1822776	Fe^{56}
537860.8	526717.9	526425.2	512824.5	503478.4	761764.8	761764.8	761764.8	Fe^{57}
2.1	8.45	4.58	11.37	3.95	6.36	9.31	12.69	Co^{59}
23.25	24.02	20.04	24.69	22.51	11.75	34.93	154.36	Ni^{60}
<0.109	<0.120	<0.106	<0.103	<0.107	1.49	1836.47	<0.76	Cu^{65}
<0.00108	0.257	0.082	1.92	0.73	0.92	9.24	0.421	La^{139}
0.00207	0.446	0.112	4.21	0.784	1.47	13.1	0.546	Ce^{140}
<0.00143	0.0327	0.0126	0.449	0.0596	0.111	1.13	0.043	Pr^{141}
<0.0042	0.15	0.045	1.78	0.29	0.46	2.85	0.299	Nd^{146}
<0.0049	0.0305	0.021	0.306	0.05	-	0.42	0.203	Sm^{147}
<0.00166	<0.0028	0.004	0.0269	0.0107	-	0.107	-	Eu^{153}
<0.0070	0.0287	<0.0052	0.241	0.041	-	0.63	0.205	Gd^{157}
<0.0049	0.025	0.0119	0.166	0.0426	0.46	0.8	0.324	Dy^{163}
0.0006	0.0038	0.003	0.0279	0.0064	0.104	0.291	0.072	Ho^{165}
<0.0029	0.0124	<0.0048	0.061	0.0205	0.52	0.94	0.358	Er^{166}
<0.0042	0.0062	0.0102	0.034	0.0165	0.64	2.44	0.682	Yb^{172}
0.0526	0.55	0.496	0.0332	0.619	2.24	4.01	1.54	Pb^{208}
<0.00082	0.0193	<0.00122	<0.00066	0.0118	<0.070	<0.071	<0.038	Bi^{209}
0.00201	3.47	0.202	0.0506	2.96	7.43	4.65	9.82	U^{238}

Table 3

	chl test	005Chl_004	013Chl_001	013Chl_002	013Chl_003	013Chl_004	7152Chl_001	7152Chl_002
SiO_2	28.0387	29.2618	24.3682	26.5694	23.7297	24.0321	29.9853	30.0705
TiO_2	0.1699	0.2003	0.0265	0.0094	0.0144	0.0039	0.0201	0.0239
Al_2O_3	19.7337	18.1702	18.6696	18.3665	18.4873	18.3821	19.7516	18.7343
FeO	22.4286	23.0713	34.4389	29.461	38.7284	39.6615	15.4584	13.9906
MnO	0.184	0.742	0.9357	0.9716	0.9357	1.0456	0.1334	0.103
MgO	16.2833	16.4027	7.8202	11.9847	4.9801	4.4388	23.4888	23.575
CaO	0.0659	0.001	0.0001	0.0122	0.0001	0.0267	0.0474	0.0747
Na_2O	0.0324	0.0376	0.2204	0.0748	0.0814	0.0457	0.2669	0.0353
K_2O	0.1238	0.242	0.0001	0.0056	0.0013	0.0315	0.0045	0.008

	7152Chl_005	7152Chl_006	027Chl_001	027Chl_002	027Chl_003	020chl1_001	020chl1_004	020chl1_005
SiO_2	28.74	29.6373	31.4582	31.3363	30.4376	28.3022	34.0987	30.29
TiO_2	0.0155	0.0278	0.0002	0.0358	0.0269	0.0106	0.0326	0.0111
Al_2O_3	19.5008	19.9265	16.5159	15.36	15.3893	14.4278	15.2734	15.3534
FeO	12.0949	13.2178	17.6284	17.8493	17.4296	16.8369	14.9597	15.418
MnO	0.1585	0.1635	0.4776	0.3817	0.4122	0.3657	0.191	0.1444
MgO	22.902	24.2999	23.4442	22.4968	22.3733	22.1898	25.6276	23.1744
CaO	0.0652	0.1137	0.0559	0.0376	0.0953	0.0785	0.1108	0.0749
Na_2O	0.141	0.033	0.0304	0.0604	0.0501	0.2829	0.068	0.0369
K_2O	0.0001	0.0001	0.0111	0.036	0.0089	0.0018	0.0138	0.0213

	020chl1_006	020chl1_008	020chl1_010	020chl1_011	020chl2_002	020chl2_004	020chl2_005	020chl2_006
SiO_2	29.0059	30.5961	31.551	29.4043	30.648	30.277	30.7058	28.8746
TiO_2	0.0002	0.0202	0.0051	0.0002	0.0485	0.0111	0.029	0.0294
Al_2O_3	14.1856	16.7286	14.7589	15.6797	14.9426	15.0966	14.9623	13.8069
FeO	16.1732	19.6173	18.2159	19.4588	17.1692	17.7699	17.8608	18.7844
MnO	0.1573	0.4367	0.2111	0.3652	0.3147	0.3191	0.3193	0.3013
MgO	21.3405	21.7209	22.6264	21.7482	22.2094	22.1093	22.7002	21.6195
CaO	0.0297	0.0429	0.0573	0.0067	0.1234	0.0735	0.0458	0.0838
Na_2O	0.0414	0.2592	0.0396	0.0259	0.3267	0.0959	0.0644	0.1701
K_2O	0.0154	0.0088	0.0286	0.0127	0.0216	0.0207	0.0084	0.0233

	020chl2_007	020chl2_008	020chl2_009	020chl2_010	020chl3_001	020chl3_002	020chl3_003	020chl3_004
SiO_2	30.1173	30.9103	31.5168	31.2777	30.0422	30.0604	29.3179	28.1603
TiO_2	0.0096	0.0559	0.084	0.0351	0.011	0.0128	0.0064	0.0002
Al_2O_3	13.926	15.0627	15.6744	15.1242	15.2669	15.3234	15.8133	15.8761
FeO	20.8815	19.8117	17.3323	16.6384	20.6065	20.4887	19.4288	21.447
MnO	0.6423	0.4459	0.3283	0.2896	0.3793	0.3457	0.4369	0.4132
MgO	19.7451	21.3184	22.9624	22.9127	21.1034	20.6286	21.1295	19.0843

CaO	0.0522	0.1266	0.1349	0.0996	0.0066	0.0228	0.0817	0.071
Na_2O	0.3336	0.1985	0.0398	0.0936	0.0103	0.0003	0.0302	0.0037
K_2O	0.0394	0.0246	0.0234	0.0132	0.0048	0.0009	0.0307	0.0031

	020chl3_005	**020chl3_006**	**020chl3_007**	**020chl3_008**	**020chl3_009**	**020chl3_010**	**7155chl2_001**	**7155chl2_002**
SiO_2	30.1469	30.269	24.1813	28.6643	28.5827	30.5078	31.0691	19.7755
TiO_2	0.0002	0.0002	0.0163	0.0002	0.0263	0.0336	0.0401	0.0002
Al_2O_3	15.6275	15.5229	13.6071	15.7689	15.6504	15.4534	15.8989	9.9196
FeO	17.3734	17.5954	20.2248	20.8086	22.1201	17.1003	16.8445	19.165
MnO	0.343	0.4036	0.2569	0.4103	0.4976	0.3802	0.3212	0.1459
MgO	22.6233	22.4735	18.1762	19.6216	18.6103	22.5021	23.8305	15.4888
CaO	0.0659	0.0401	0.0236	0.0606	0.0359	0.0955	0.042	0.076
Na_2O	0.0164	0.013	0.029	0.0548	0.0336	0.048	0.083	0.0188
K_2O	0.0004	0.0057	0.0218	0.0001	0.0105	0.0106	0.0141	0.0001

	7155chl2_003	**7155chl2_004**	**7155chl2_005**	**7155chl3_001**	**7155chl3_002**	**7155chl3_003**	**7155chl3_007**	**7155chl3_010**
SiO_2	30.5063	31.2398	31.4106	30.7489	31.8783	32.0158	30.8096	31.0835
TiO_2	0.0055	0.0002	0.0002	0.0002	0.1733	0.0002	0.0002	0.0037
Al_2O_3	14.8386	15.5999	15.5067	15.1502	15.1761	14.5847	14.7376	15.1469
FeO	16.1307	16.3215	16.0306	16.8286	16.0582	18.1725	19.0561	17.3375
MnO	0.3386	0.4233	0.3067	0.336	0.435	0.2562	0.2622	0.3494
MgO	23.2708	23.7128	23.9683	23.1792	23.4018	22.3735	21.5249	23.8225
CaO	0.1062	0.088	0.0622	0.0382	0.1157	0.0753	0.1017	0.084
Na_2O	0.0003	0.0591	0.0283	0.1012	0.1066	0.0842	0.0035	0.2076
K_2O	0.0001	0.0001	0.0128	0.0326	0.0198	0.0224	0.0061	0.0123

	7161chl1_001	**7161chl1_002**	**7161chl1_003**	**7161chl1_004**	**7161chl1_005**	**7161chl1_007**	**7161chl2_001**	**7161chl2_002**
SiO_2	27.4752	26.3191	27.3009	25.6753	26.7189	29.3943	25.8628	26.2734
TiO_2	0.0072	0.0413	0.0002	0.0004	0.0018	0.0032	0.0088	0.0412
Al_2O_3	17.4672	18.2713	15.8888	16.0054	15.9917	15.9075	18.0953	17.8453
FeO	27.9873	30.2027	25.7332	29.4872	25.7671	16.7325	32.2186	31.112
MnO	0.1664	0.1278	0.2329	0.1422	0.1303	0.165	0.1092	0.1536
MgO	14.2771	12.2482	15.6776	12.023	14.8264	21.4786	11.0966	12.0284
CaO	0.0084	0.0046	0.0468	0.0223	0.0019	0.0002	0.0002	0.0324
Na_2O	0.044	0.0371	0.0754	0.018	0.0467	0.0491	0.0491	0.0056
K_2O	0.0013	0.0001	0.0333	0.0171	0.0009	0.0001	0.003	0.0001

	7161chl2_003	**7161chl2_004**	**7161chl3_001**	**7161chl3_003**	**7161chl3_004**	**7161chl3_005**	**7161chl3_006**	**7161chl3_007**
SiO_2	25.2664	26.0226	27.3029	24.2021	32.0119	29.616	27.2968	29.401
TiO_2	0.0002	0.0062	0.0103	0.0002	0.0002	0.0156	0.0002	0.0002

Al_2O_3	17.7365	17.9618	15.9402	11.3831	14.4139	14.146	15.5114	14.7174
FeO	31.7431	30.8555	25.5545	14.0068	15.5939	15.8385	29.5559	16.8864
MnO	0.1695	0.1913	0.2377	0.1749	0.1842	0.15	0.1717	0.2219
MgO	11.3762	11.7552	15.1966	17.5647	21.2108	20.7394	12.7521	21.4711
CaO	0.0231	0.1001	0.0963	0.0903	0.0965	0.0505	0.0659	0.0124
Na_2O	0.0401	0.0378	0.0944	0.0386	0.0587	0.1444	0.0203	0.0367
K_2O	0.0026	0.0073	0.0091	0.0241	0.0167	0.007	0.0069	0.0057

	7161chl3_009	**7161chl3_010**
SiO_2	28.3474	31.6303
TiO_2	0.0002	0.0074
Al_2O_3	13.5607	15.8829
FeO	16.196	15.8416
MnO	0.232	0.2417
MgO	20.1461	23.1402
CaO	0.1046	0.0736
Na_2O	0.0244	0.0409
K_2O	0.0101	0.0145

Table 4

Fe/Fe+Mg	**Si**	**Al^{vi}**	**Al^{iv}**	
0.435908492	5.799640542	2.636657859	2.200359458	**chl test**
0.441065828	6.005702569	2.426837222	1.994297431	**005Chl_004**
0.712516975	5.513937216	2.505603944	2.486062784	**013Chl_001**
0.579678924	5.749126631	2.444163994	2.250873369	**013Chl_002**
0.813534511	5.490262648	2.535331971	2.509737352	**013Chl_003**
0.833691071	5.538778308	2.53780753	2.461221692	**013Chl_004**
0.269659226	5.838105273	2.386093557	2.161894727	**7152Chl_001**
0.24978071	5.97305332	2.37561387	2.02694668	**7152Chl_002**
0.22856683	5.86035082	2.57038426	2.13964918	**7152Chl_005**
0.2338158	5.8197556	2.4449905	2.1802444	**7152Chl_006**
0.2966935	6.1746774	2.0032192	1.8253226	**027Chl_001**
0.3080205	6.3008674	1.9521223	1.6991326	**027Chl_002**
0.30413597	6.22625332	1.94429387	1.77374668	**027Chl_003**
0.30736637	6.05634706	1.71988902	1.94365294	**020chl1_001**
0.24669991	6.49422909	1.93924358	1.50577091	**020chl1_004**
0.27180309	6.24022494	1.97757652	1.75977506	**020chl1_005**
0.29833645	6.28634921	1.91864865	1.71365079	**020chl1_006**
0.33629609	6.09374486	2.03006617	1.90625514	**020chl1_008**
0.31113818	6.36296081	1.88078675	1.63703919	**020chl1_010**
0.33601384	6.06401343	1.8801116	1.93598657	**020chl1_011**
0.30250879	6.28691552	1.91262543	1.71308448	**020chl2_002**
0.31078041	6.2359102	1.90802514	1.7640898	**020chl2_004**
0.30624225	6.25954788	1.86052832	1.74045212	**020chl2_005**
0.33457217	6.15258458	1.63815063	1.84741542	**020chl2_006**
0.37237936	6.33207679	1.79290146	1.66792321	**020chl2_007**
0.3427014	6.27054961	1.8814633	1.72945039	**020chl2_008**
0.29749245	6.27980954	1.97213404	1.72019046	**020chl2_009**
0.28947008	6.32741734	1.94559871	1.67258266	**020chl2_010**
0.35393001	6.17236363	1.87181418	1.82763637	**020chl3_001**
0.35783208	6.20172818	1.9332205	1.79827182	**020chl3_002**
0.34031412	6.07972882	1.94697587	1.92027118	**020chl3_003**
0.38668642	6.00763618	2.0002522	1.99236382	**020chl3_004**
0.30110929	6.17335078	1.95027122	1.82664922	**020chl3_005**

Fe/Fe+Mg	Si	Al^{vi}	Al^{iv}	
0.305194988	6.194607807	1.944568694	1.805392193	**020chl3_006**
0.400487847	5.739103734	1.585690673	2.260896266	**020chl3_007**
0.373028638	6.058755727	1.990244917	1.941244273	**020chl3_008**
0.400061341	6.074515606	1.99884845	1.925484394	**020chl3_009**
0.298910016	6.232073202	1.961410622	1.767926798	**020chl3_010**
0.283955839	6.188077831	1.926636891	1.811922169	**7155chl2_001**
0.437782999	5.625773677	1.019895186	2.374226323	**7155chl2_002**
0.28000111	6.27740652	1.88228883	1.72259348	**7155chl2_003**
0.27858069	6.25342678	1.94225113	1.74657322	**7155chl2_004**
0.2728494	6.2791082	1.941532	1.7208918	**7155chl2_005**
0.2894295	6.2515505	1.8892016	1.7484495	**7155chl3_001**
0.2779658	6.3558582	1.9364642	1.6441418	**7155chl3_002**
0.3130392	6.43218457	1.89884294	1.56781543	**7155chl3_003**
0.33185565	6.32479387	1.89903959	1.67520613	**7155chl3_007**
0.29124264	6.21931482	1.79926428	1.78068518	**7155chl3_010**
0.52376033	5.87214897	2.28004517	2.12785103	**7161chl1_001**
0.58043791	5.71826656	2.40446825	2.28173344	**7161chl1_002**
0.47972835	5.96019153	2.05271552	2.03980847	**7161chl1_003**
0.57914391	5.853328	2.1552823	2.146672	**7161chl1_004**
0.49367736	5.93808288	2.13099121	2.06191712	**7161chl1_005**
0.30413475	6.15860196	2.09805409	1.84139804	**7161chl1_007**
0.61961729	5.68021328	2.3680452	2.31978672	**7161chl2_001**
0.59202478	5.72650234	2.31380677	2.27349766	**7161chl2_002**
0.61224574	5.61627526	2.27327035	2.38372474	**7161chl2_003**
0.59556952	5.70785924	2.3555331	2.29214076	**7161chl2_004**
0.48544428	5.994095	2.12583788	2.005905	**7161chl3_001**
0.3091002	6.33334267	1.8519732	1.66665733	**7161chl3_003**
0.29201625	6.60794986	2.14267286	1.39205014	**7161chl3_004**
0.2999423	6.39730248	2.0165558	1.60269752	**7161chl3_005**
0.56527689	6.05023928	2.10957766	1.94976072	**7161chl3_006**
0.30615006	6.24710456	1.94076476	1.75289544	**7161chl3_007**
0.31083308	6.34397022	1.9315973	1.65602978	**7161chl3_009**
0.27749669	6.31995403	2.07639553	1.68004597	**7161chl3_010**

Table 5

Sample	**δ^{34}S (‰ CDT)**	**Sulfide type**
RS2	1.8	Ccp
RS5	2.29	Ccp
RS6	-0.27	Ccp
RS10	2.05	Ccp
RS11	-5.43	Ccp
GS7	-3.56	Ccp
GS23	-3.41	Ccp
GS2	-3.85	Ccp
GS15	-3.81	Ccp
GS25	-3.12	Ccp
GS8	-0.37	Ccp
GS19	-1.64	Ccp
GS2b	-3.42	Ccp
RS4	2.4	Ccp, minor contaminating Py
RS9	1.67	Ccp, minor contaminating Py
RS7	-5.77	Py
RS8	-3.29	Py
RS12	-3.78	Py
RS13	-3.65	Py
GS26	-25.07	Py
GS262	-26.73	Py
GS22	0.79	Py
GS24	-2.80	Py

Table 6

HB028	**HB030**	**HB019**	**HB012**	**HB037**	**HB001**	**Sample Name**
522.40	586.10	516.30	475.10	688.00	28.90	**Depth (m)**
25.93	31.11	43.13	56.59	48.95	73.39	**SiO_2 %**
3.20	9.22	6.44	8.62	11.82	15.19	**Al_2O_3 %**
55.92	38.96	21.92	11.33	16.50	0.27	**Fe_2O_3T %**
0.21	0.23	0.06	0.11	0.14	0.02	**MnO %**
4.58	5.35	5.65	8.73	2.89	0.17	**MgO %**
4.81	7.36	1.44	1.74	5.78	1.40	**CaO %**
0.12	0.19	0.18	0.13	2.69	4.77	**Na_2O %**
0.04	2.08	1.81	1.74	3.77	3.51	**K_2O %**
0.37	0.20	0.16	0.39	1.05	0.01	**TiO_2 %**
0.02	0.29	0.51	0.15	0.16	0.28	**P_2O_5 %**
0.53	0.36	0.73	1.48	0.49	0.13	**SO_3 %**
4.97	4.85	5.95	4.64	5.27	0.67	**LOI %**
100.69	100.19	87.96	95.65	99.48	99.80	**Total %**

Table 7

HB028	HB030	HB019	HB012	HB037	HB001	B)
44.7	42.5	132.6	138.4	104.5	18.5	**Zr**
4.9	7.0	5.9	11.4	14.2	41.0	**Nb**
26.0	13.4	18.6	29.6	82.0	7.2	**Y**
15.7	93.3	4.9	7.5	39.5	150.6	**Sr**
2.4	143.6	54.0	43.0	175.4	155.3	**Rb**
-0.5	1.0	5.5	62.3	15.5	8.1	**U**
2.1	6.8	5.0	11.8	12.9	0.2	**Th**
3.3	0.0	12.6	5.1	3.0	4.6	**Pb**
14.2	24.1	26.7	24.9	13.5	12.2	**Ga**
63	81	* -43	22	44	1	**Zn**
36	26	287	71	24	1	**Ni**
5	111	110	304	661	344	**Ba**
7.1	8.6	4.7	9.3	29.8	1.3	**Sc**
76	74	245	104	44	47	**Co**
68	41	47	50	247	6	**V**
68	70	33	73	161	7	**Ce**
-2	7	-2	23	59	1	**Nd**
7	25	-2	28	58	2	**La**
46	57	10	35	70	3	**Cr**

HB028	HB030	HB019	HB012	HB037	HB001	A)
17	37	8	65	175	6	**Ce**
13	25	5	34	65	3	**La**
6	2	5	6.5	12	4.5	**Dy**
5	1	4	5	8	3	**Er**
2	<0.5	1.5	2.5	2.5	2	**Eu**
9	2	8	11	13	8	**Gd**
1.5	<0.5	1.5	1.5	2.5	1	**Ho**
2	<0.5	1.5	1.5	1.5	1	**Lu**
11.5	14	7.5	35	65	7.5	**Nd**
3	4	2	9	20	1	**Pr**
7.5	2.5	6	11	12.5	6.5	**Sm**
0.5	<0.5	0.5	0.5	1	0.5	**Tb**
1	<1	1	1	1	<1	**Tm**
7	1	6	7	7	4	**Yb**
1	4.5	6.5	12.5	13	1	**Th**
1.5	1.5	4.5	60	13	10.5	**U**
23	13	19.5	29	75	8.5	**Y**

Table 8

Sample	Ti (ppm)	TitaniQ
005c1a	2.65	440.153
005c1b	3.22	451.797
005c1c	2.99	447.323
005c2a	5.59	486.926
005c2b	3.48	456.544
005c3a	3.77	461.503
005c3b	2.94	446.312
005c4a	3.26	452.547
005c4b	3.81	462.162
005c4c	3.54	457.598
Mean		456.287
013c1a	3.53	457.423
013c1b	3.23	451.985
013c2a	2.09	426.46
013c2b	1.97	423.131
013c2c	1.48	407.467
013c3a	6.96	501.85
013c3b	3.99	465.059
013c4a	2.35	433.157
013c4b	3.75	461.172
013c4c	1.42	405.258
Mean		443.296
020c1a	1.52	408.898
020c1b	2.03	424.816
020c1c	2.39	434.131
020c2a	2.08	426.189
020c2b	5.39	484.501
020c2c	3.13	450.079
020c3a	2.92	445.904
020c3b		
020c4a	2.06	425.643
020c4b	6.09	492.689
Mean		443.65
027c1a	4.65	474.828
027c1b	2.27	431.165
027c2a	3.72	460.672
027c2b	3.82	462.326
027c3a	1.77	417.184
027c3b	1.78	417.494
027c3c		
027c4a	1.74	416.244
027c4b	1.65	413.339
027c4d	1.57	410.642
Mean		433.766
7152a	3.5	456.897
7152a2	3.72	460.672
7152a3	3.25	452.36
7152c4a		
7152c4b	8.26	513.923
7152c4c	6.82	500.442
7152c2a	3.42	455.475
7152c2b	7.91	510.835
7152c2c	8.88	519.14
7152c3a	6.04	492.131
7152c3b	2.98	447.122
7152c3c	6.18	493.685
Mean		482.062
7155c1a		
7155c1b	7.39	506.034
7155c1c		
7155c2a	3.94	464.265
7155c2b	2.66	440.374
7155c3a	5.29	483.26
7155c3b	3.68	459.999
7155c4a	2.59	438.808
7155c4b	3.06	448.714
7155c4c	2.94	446.312
Mean		460.971
7156c1a	6.59	498.076
7156c1b	7.4	506.129
7156c1c	6.44	496.496
7156c2a	6.46	496.709
7156c2b	7.05	502.743
7156c3a	4.91	478.363
7156c3b	6.2	493.905
7156c3c	6.45	496.603
7156c4a	3.61	458.808
7156c4b	4.57	473.707
Mean		490.154
7171c1a		
7171c2a	6.65	498.7
7171c2b	6.49	497.026
7171c2c	5.97	491.343
7171c3a	4.43	471.707
7171c3b	3.59	458.464
7171c3c	4.42	471.562
7171c4a	4.21	468.455
7171c4b	3.25	452.36
7171c4c	5.94	491.003
Mean		477.847
7161av1		
7161bv2	1.98	423.415
7161cv3	1.2	396.421
7161dv4	1.62	412.341
7161ev5	1.66	413.668
7161fv6	2.4	434.373
7161gvb1	1.35	402.58
7161hvb3	1.14	393.774
7161ivb4	1.41	404.883
7161jvc5	1.48	407.467
Mean		409.88
Average	3.62367	
Std Dev	1.87673	1.46548
95% CI	0.41125	2.28798

Table 9

Sample	Cathelineau (1988)	Kranidiotis (1987)	Jowett (1991)	Sample	Cathelineau (1988)	Kranidiotis (1987)	Jowett (1991)
chl test	646.5517384	283.5825127	646.8201481	**020chl3_005**	526.2245163	233.9671269	523.306488
005Chl_004	580.2038869	262.1226122	581.2508805	**020chl3_006**	519.3801784	232.0170406	516.6558298
013Chl_001	738.5424953	334.3914147	746.7833197	**020chl3_007**	666.0433797	287.3712024	665.0014711
013Chl_002	662.8162073	299.6047532	667.5203624	**020chl3_008**	563.121831	251.4506178	562.1565366
013Chl_003	746.1652327	344.3964201	757.5579663	**020chl3_009**	558.0474653	251.7858973	557.9914785
013Chl_004	730.5441605	340.7493769	742.7244651	**020chl3_010**	507.3170705	227.5793638	504.5038781
7152Chl_001	634.1668642	267.1695556	629.2465472	**7155chl2_001**	521.4826998	231.1332731	518.061363
7152Chl_002	590.7162908	251.3900762	585.5639943	**7155chl2_002**	702.5333916	302.1514888	702.3434748
7152Chl_005	627.0042421	261.7624716	620.8393694	**7155chl2_003**	492.7206475	221.3709909	489.4393544
7152Chl_006	640.0751063	266.4550451	633.9567025	**7155chl2_004**	500.4416448	223.8074487	497.0435808
027Chl_001	525.7973695	233.4988566	522.7424324	**7155chl2_005**	492.1727351	220.6599519	488.6683725
027Chl_002	485.1667102	220.963178	482.8491502	**7155chl3_001**	501.0457745	224.8113156	497.9881952
027Chl_003	509.190956	228.5840371	506.5271283	**7155chl3_002**	467.4607862	212.9040973	464.348353
020chl1_001	563.8973733	246.8337961	560.8302747	**7155chl3_003**	442.8852117	207.4159443	441.1190723
020chl1_004	422.9081172	195.9168497	419.2106471	**7155chl3_007**	477.4628689	220.1955384	475.9769498
020chl1_005	504.692373	224.7039457	501.0387621	**7155chl3_010**	511.4250128	228.3628326	508.3292113
020chl1_006	489.8412829	221.7835485	487.1715361	**7161chl1_001**	623.2054749	282.4152255	626.4924333
020chl1_008	551.8560292	245.0162145	549.8232342	**7161chl1_002**	672.7525321	302.9322371	677.3889357
020chl1_010	465.1738798	214.6126078	463.140811	**7161chl1_003**	594.8575296	269.815541	597.0022348
020chl1_011	561.4289559	248.1468034	559.2985574	**7161chl1_004**	629.265451	288.5197103	634.2630592
020chl2_002	489.6589414	222.0331073	487.1239801	**7161chl1_005**	601.9760744	273.1940745	604.499869
020chl2_004	506.0816325	228.0534246	503.6585399	**7161chl1_007**	530.9733405	235.7549903	528.1078728
020chl2_005	498.4707735	225.2110993	495.9733538	**7161chl2_001**	685.0049287	309.8729954	690.7777558
020chl2_006	532.9108165	238.6512893	530.9983708	**7161chl2_002**	670.1007776	302.9189907	675.1313449
020chl2_007	475.1179152	222.4304087	474.9464056	**7161chl2_003**	705.5916914	316.1034566	710.9388309
020chl2_008	494.9284356	226.7501846	493.626848	**7161chl2_004**	676.103481	305.1581789	681.1915694
020chl2_009	491.946924	222.4141282	489.2307655	**7161chl3_001**	583.9412921	266.6458958	586.3693678
020chl2_010	476.6181636	216.7724417	473.7879629	**7161chl3_003**	474.7103285	217.6009122	472.523986
020chl3_001	526.5423593	237.9910626	525.3063704	**7161chl3_004**	386.292303	187.2249199	384.3793118
020chl3_002	517.0875612	235.1679538	516.0635547	**7161chl3_005**	454.1165486	210.1416564	451.8286695
020chl3_003	556.3689146	246.8000529	554.4225269	**7161chl3_006**	565.8639572	266.6181818	571.0060031
020chl3_004	579.581304	257.8826978	578.8993566	**7161chl3_007**	502.4772735	226.5232513	499.9398321
				7161chl3_009	471.2884691	216.6029714	469.1890756
				7161chl3_010	479.0212016	216.6751271	475.786809
				Mean	554.2327406	249.1446117	553.6164378
				Std Dev	83.59047384	36.11526452	86.31053544
				Median	526.3834378	235.461472	524.3064292

Table 10

Figures

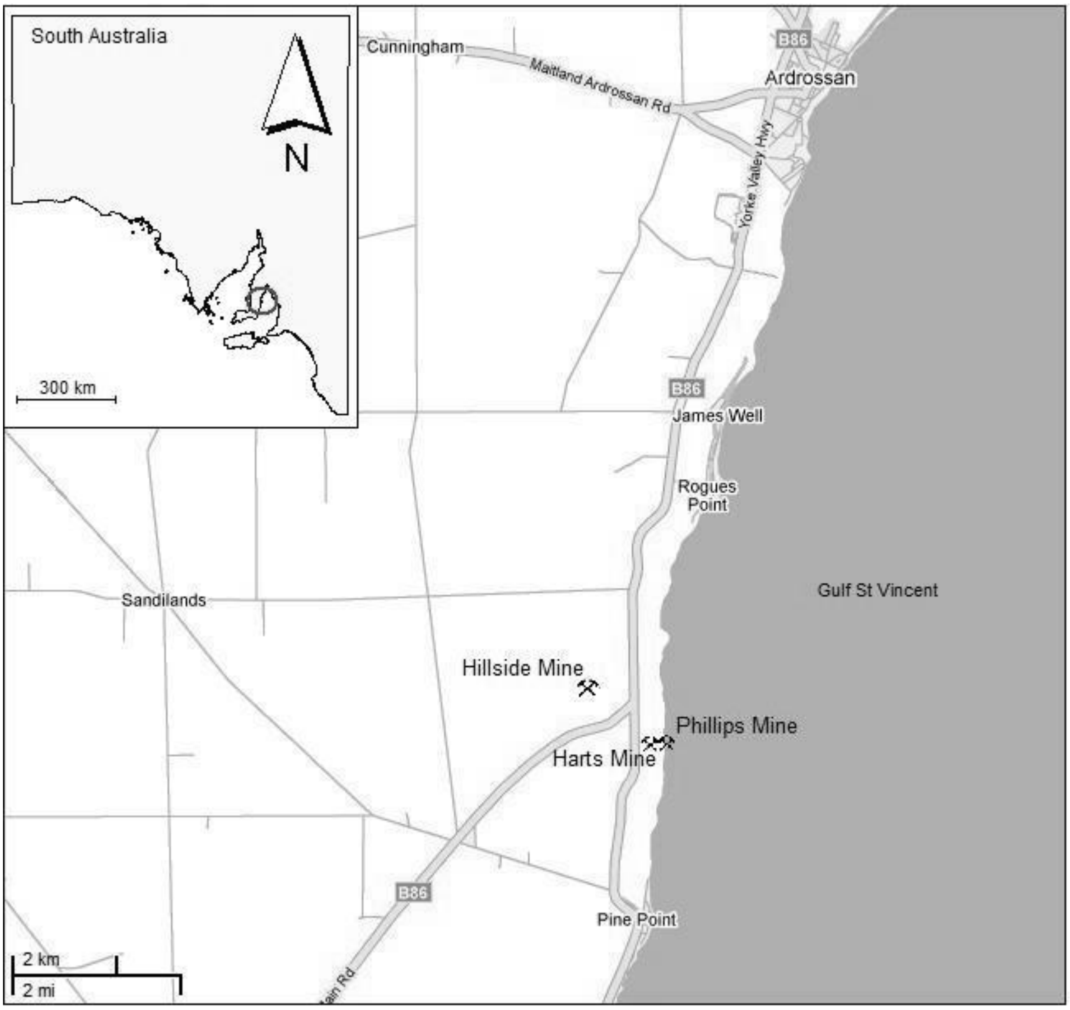

Figure 1

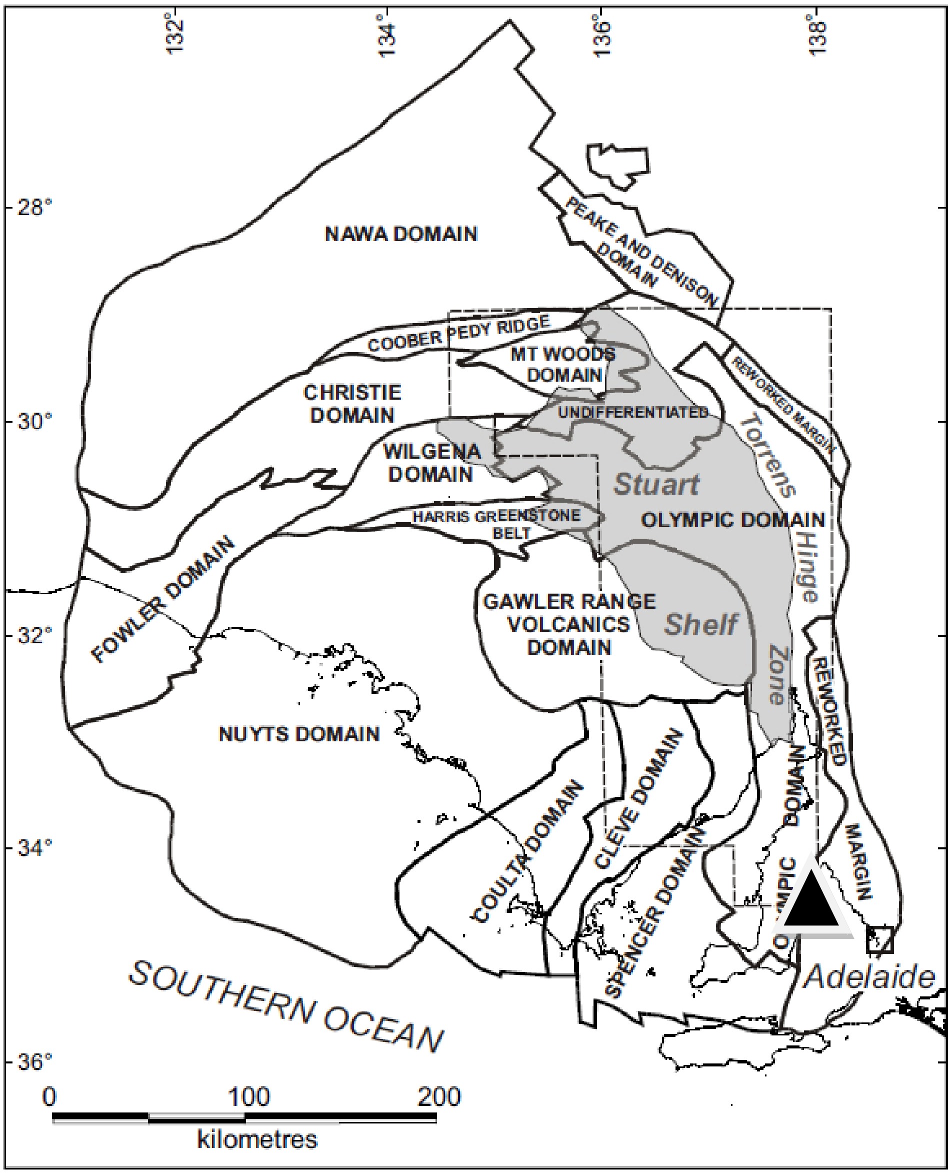
132°
134°
136°
138°
28°
30°
32°
34°
36°
NAWA DOMAIN
PEAKE AND DENISON DOMAIN
COOBER PEDY RIDGE
MT WOODS DOMAIN
CHRISTIE DOMAIN
UNDIFFERENTIATED
REWORKED MARGIN
Torrens
WILGENA DOMAIN
Stuart
OLYMPIC DOMAIN
HARRIS GREENSTONE BELT
Hinge
FOWLER DOMAIN
GAWLER RANGE VOLCANICS DOMAIN
Shelf
Zone
REWORKED
NUYTS DOMAIN
CLEVE DOMAIN
COULTA DOMAIN
SPENCER DOMAIN
O MPIC DOMAIN
MARGIN
Adelaide
SOUTHERN OCEAN
0
100
200
kilometres

Figure 2

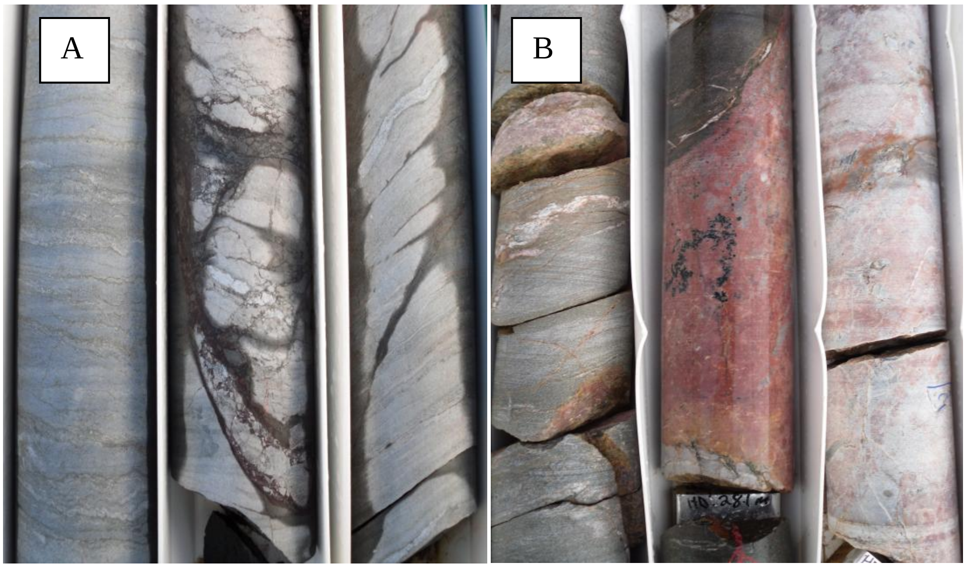

Figure 3

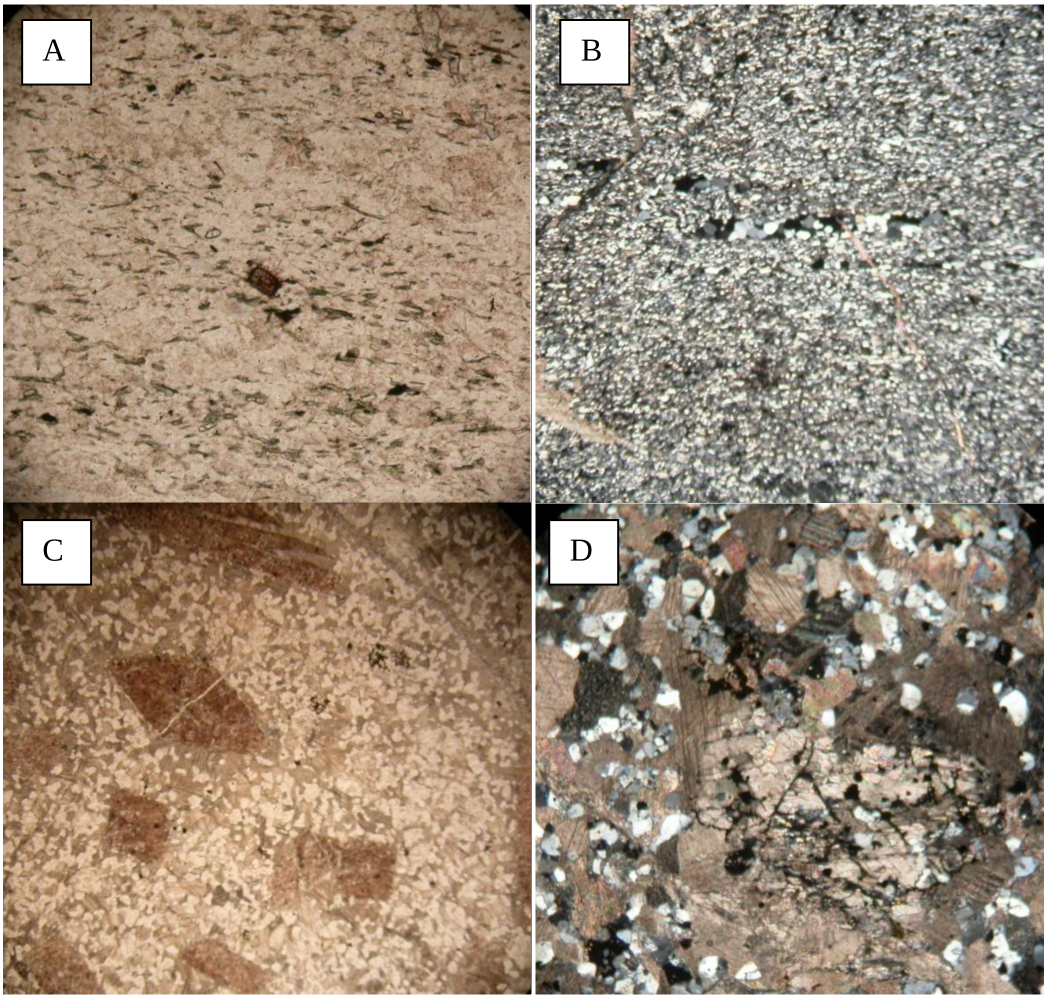

Figure 4

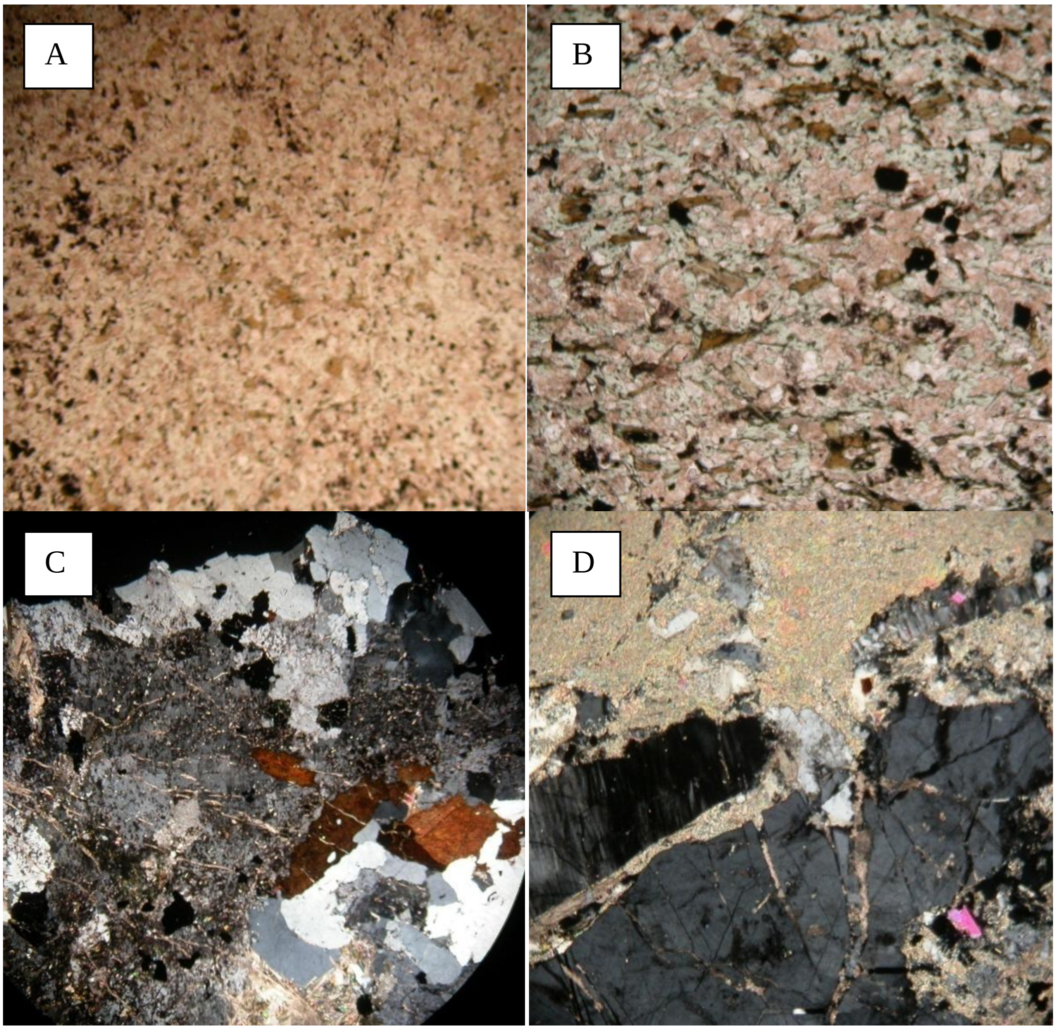

Figure 5

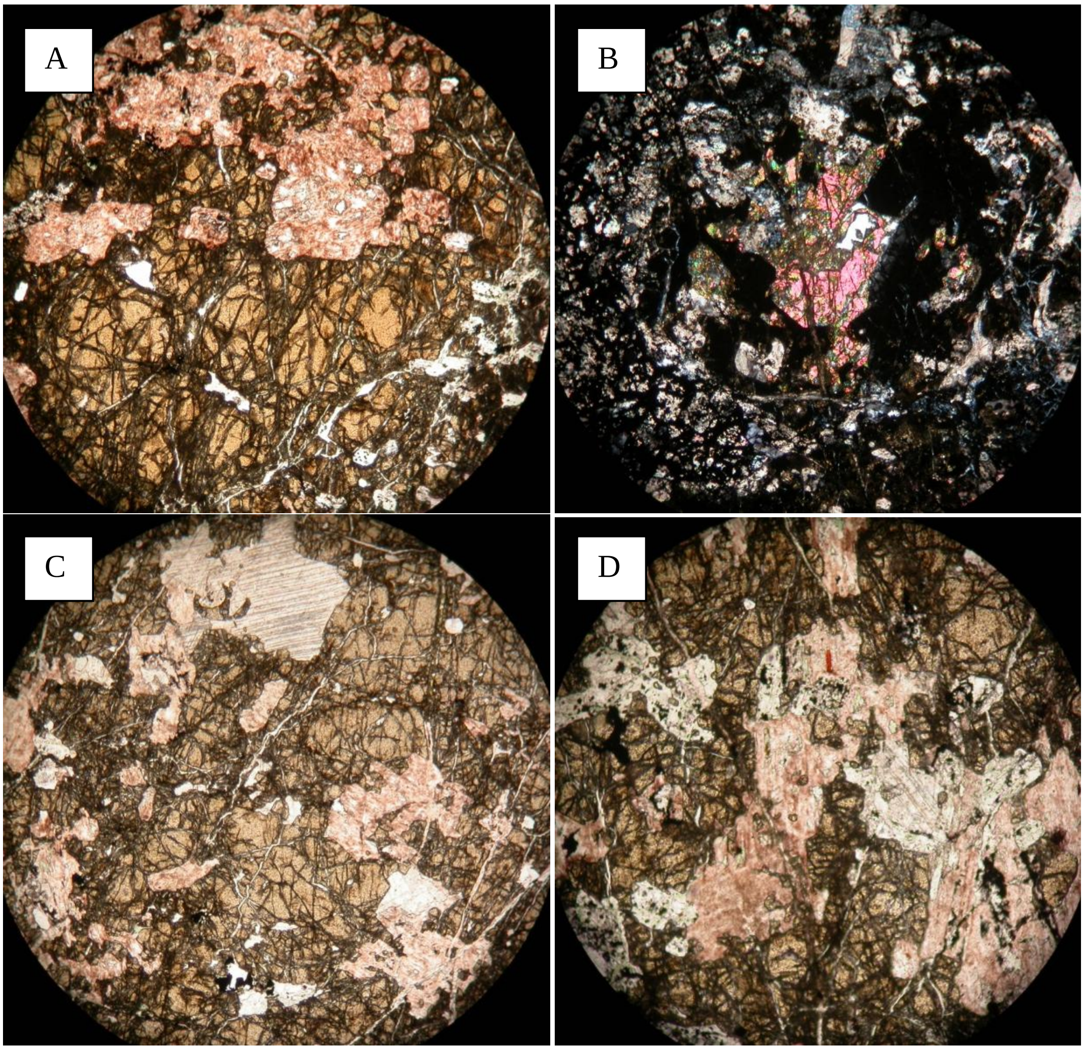

Figure 6

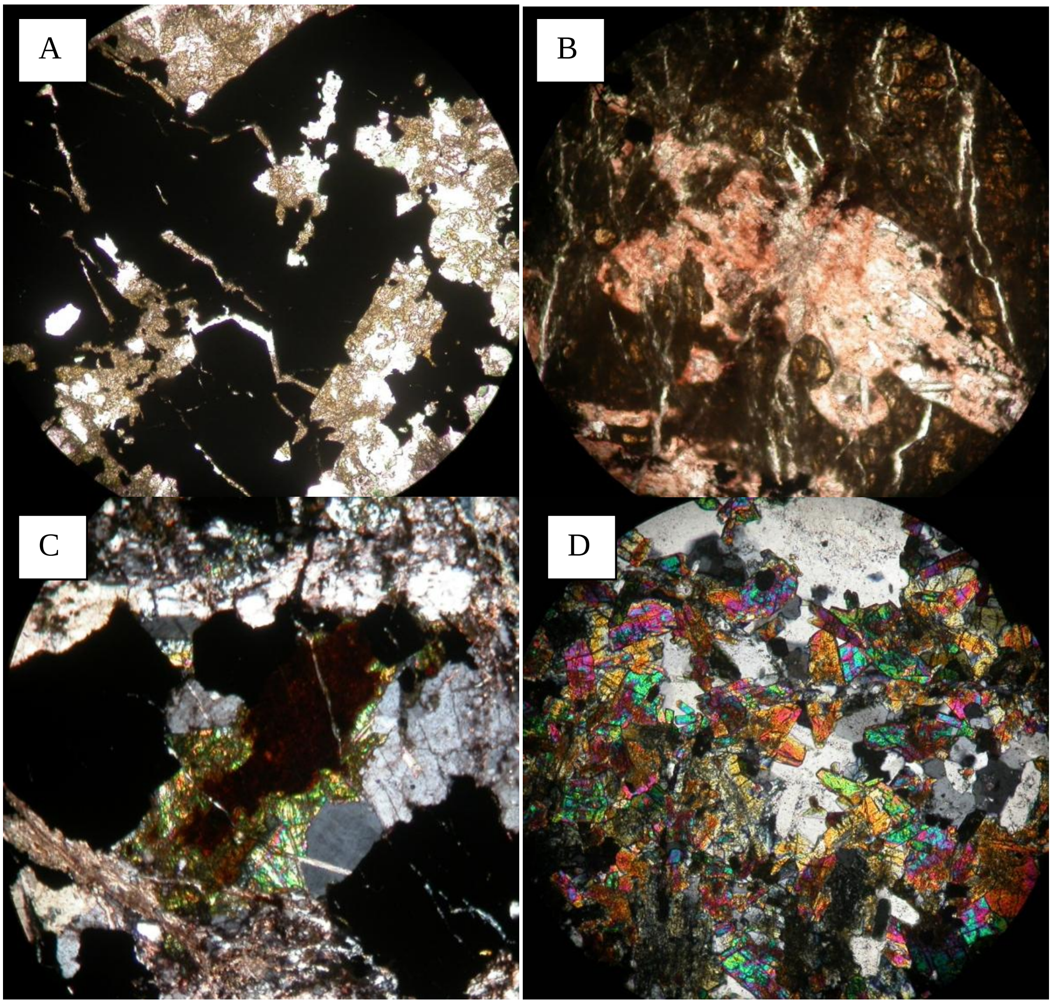

Figure 7

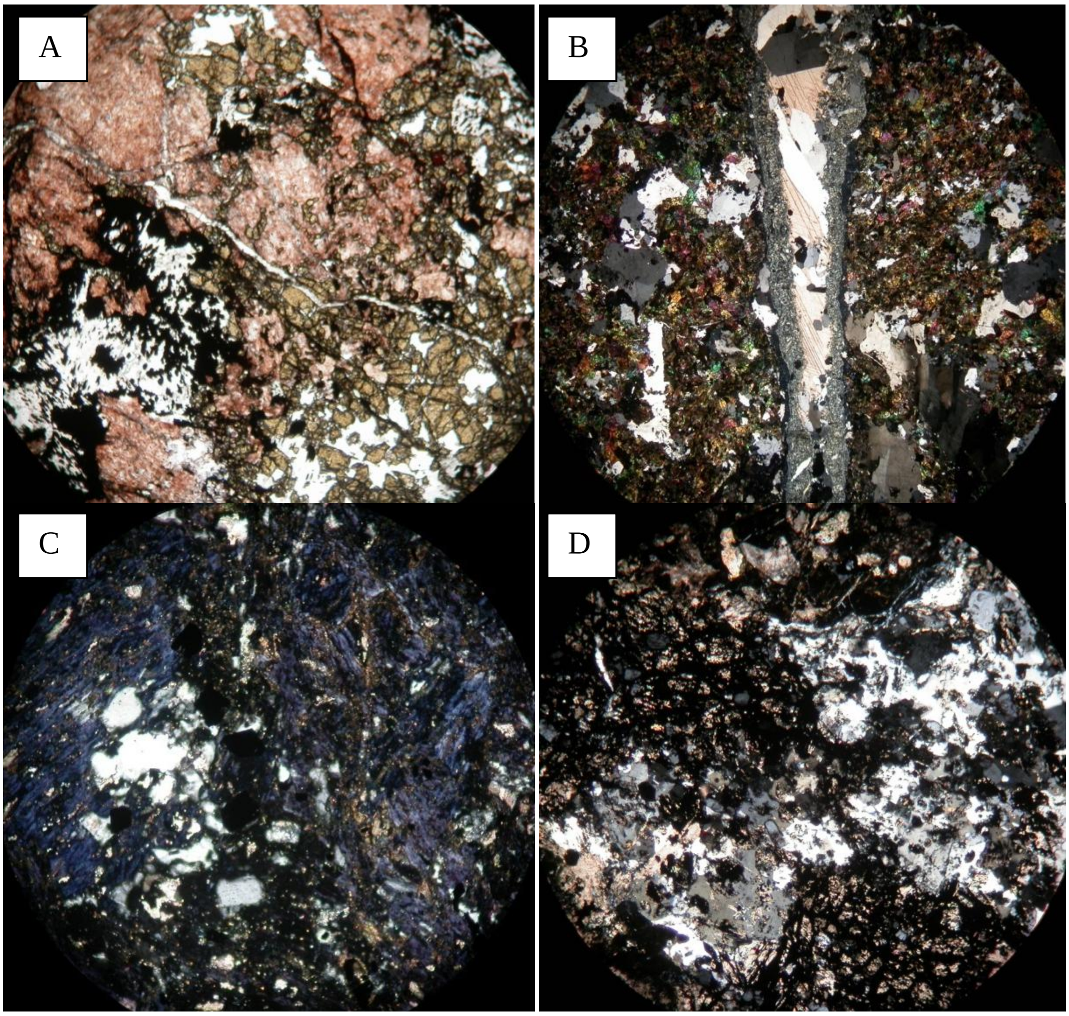

Figure 8

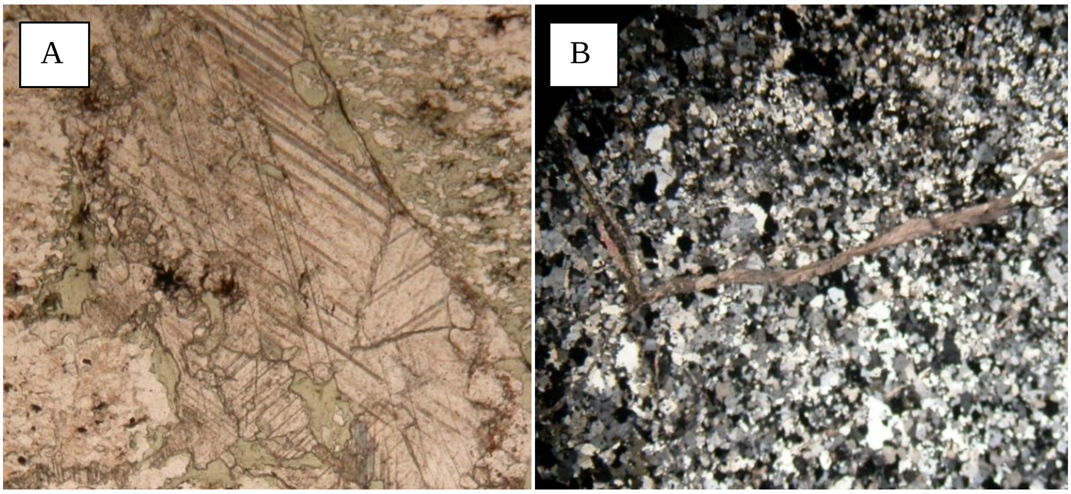

Figure 9

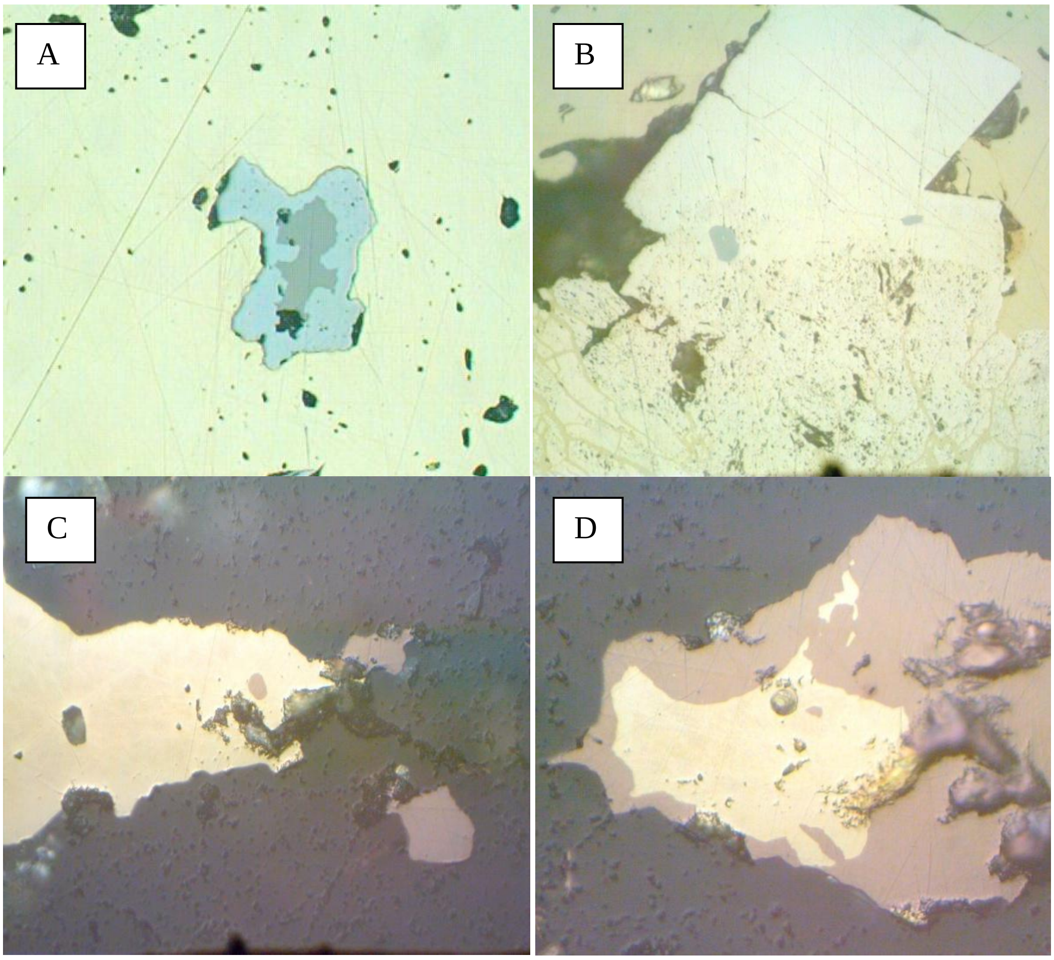

Figure 10

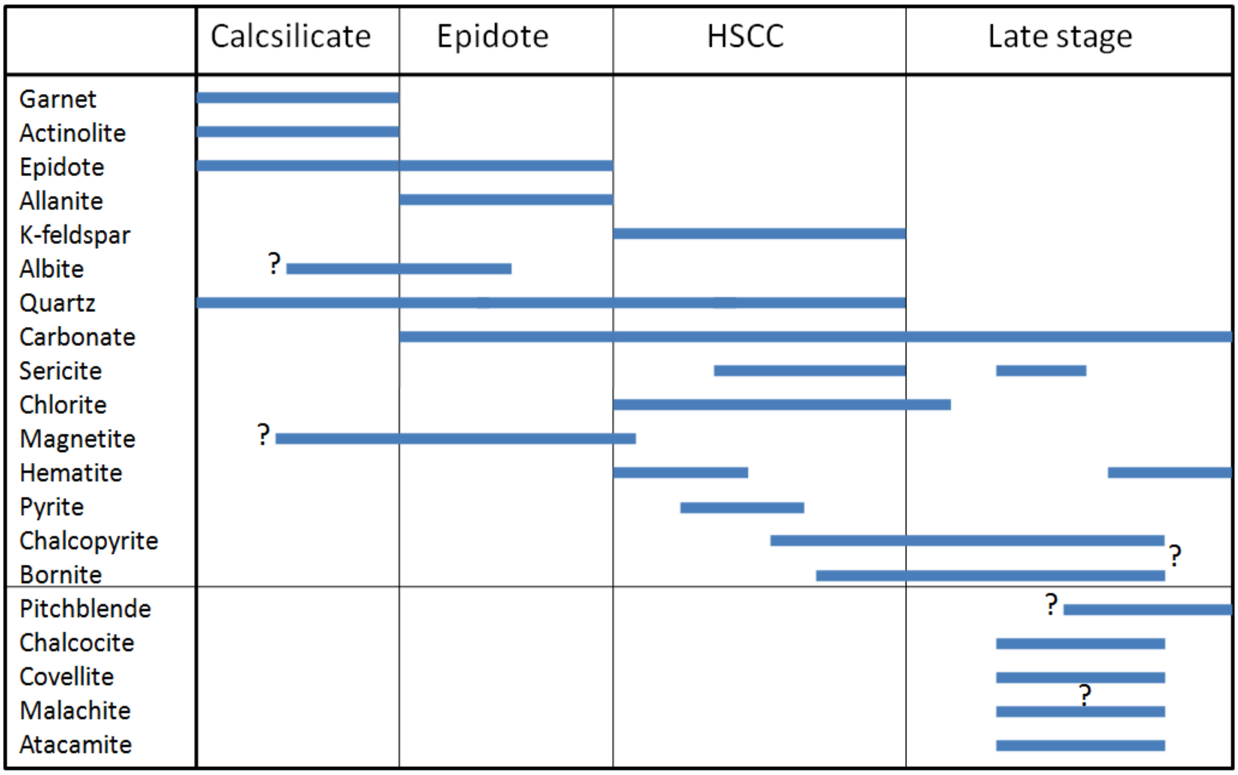
Calcsilicate
Epidote
HSCC
Late stage
Garnet
Actinolite
Epidote
Allanite
K-feldspar
Albite
Quartz
Carbonate
Sericite
Chlorite
Magnetite
Hematite
Pyrite
Chalcopyrite
Bornite
Pitchblende
Chalcocite
Covellite
Malachite
Atacamite
?
?
?
?
?

Figure 11

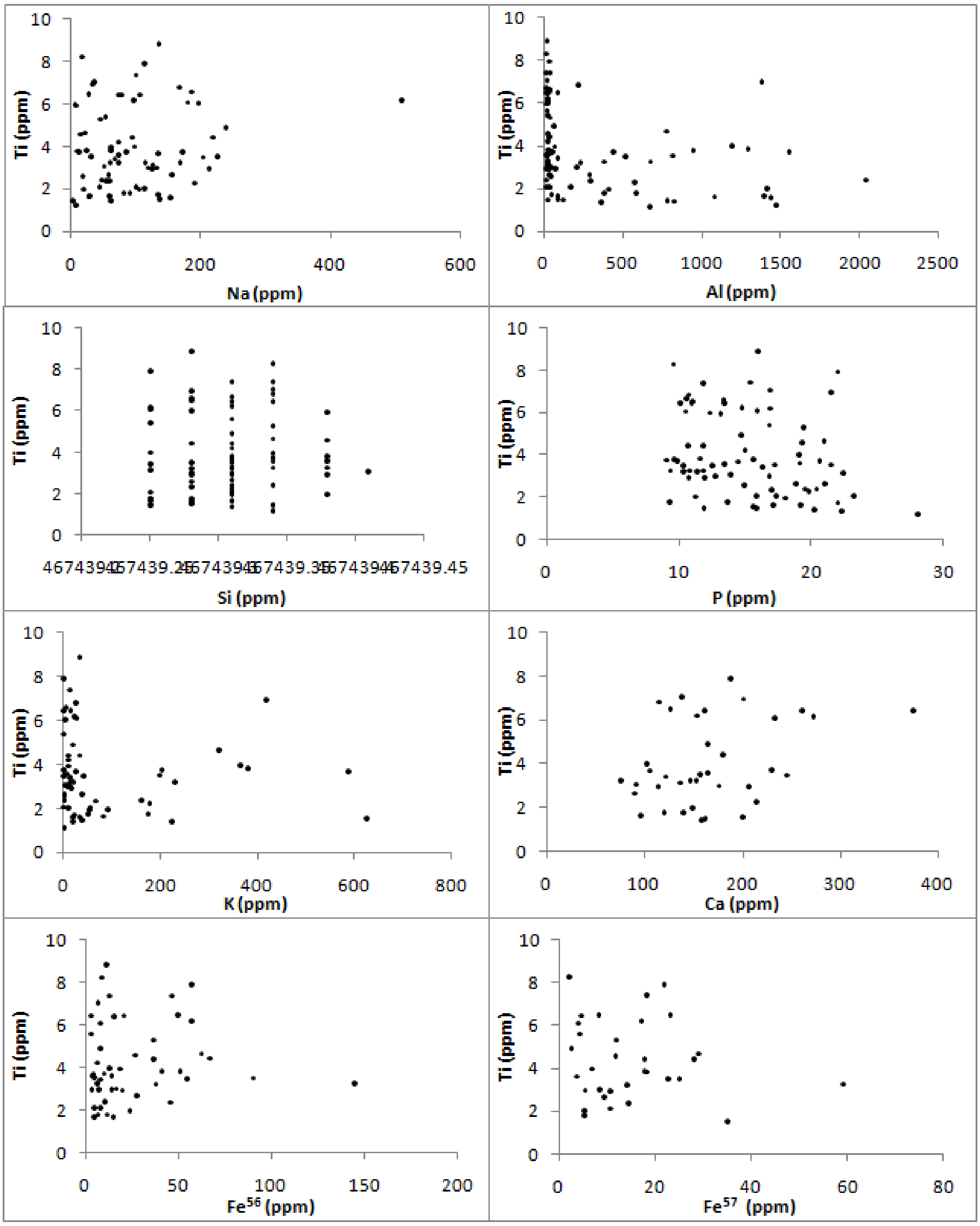
Ti (ppm)
0
2
4
6
8
10
0
200
400
600
Na (ppm)
Al (ppm)
0
500
1000
1500
2000
2500
4674394567439.2567439467439.3567439467439.45
Si (ppm)
P (ppm)
0
10
20
30
K (ppm)
0
200
400
600
800
Ca (ppm)
0
100
200
300
400
Fe⁵⁶ (ppm)
0
50
100
150
200
Fe⁵⁷ (ppm)
0
20
40
60
80

Figure 12

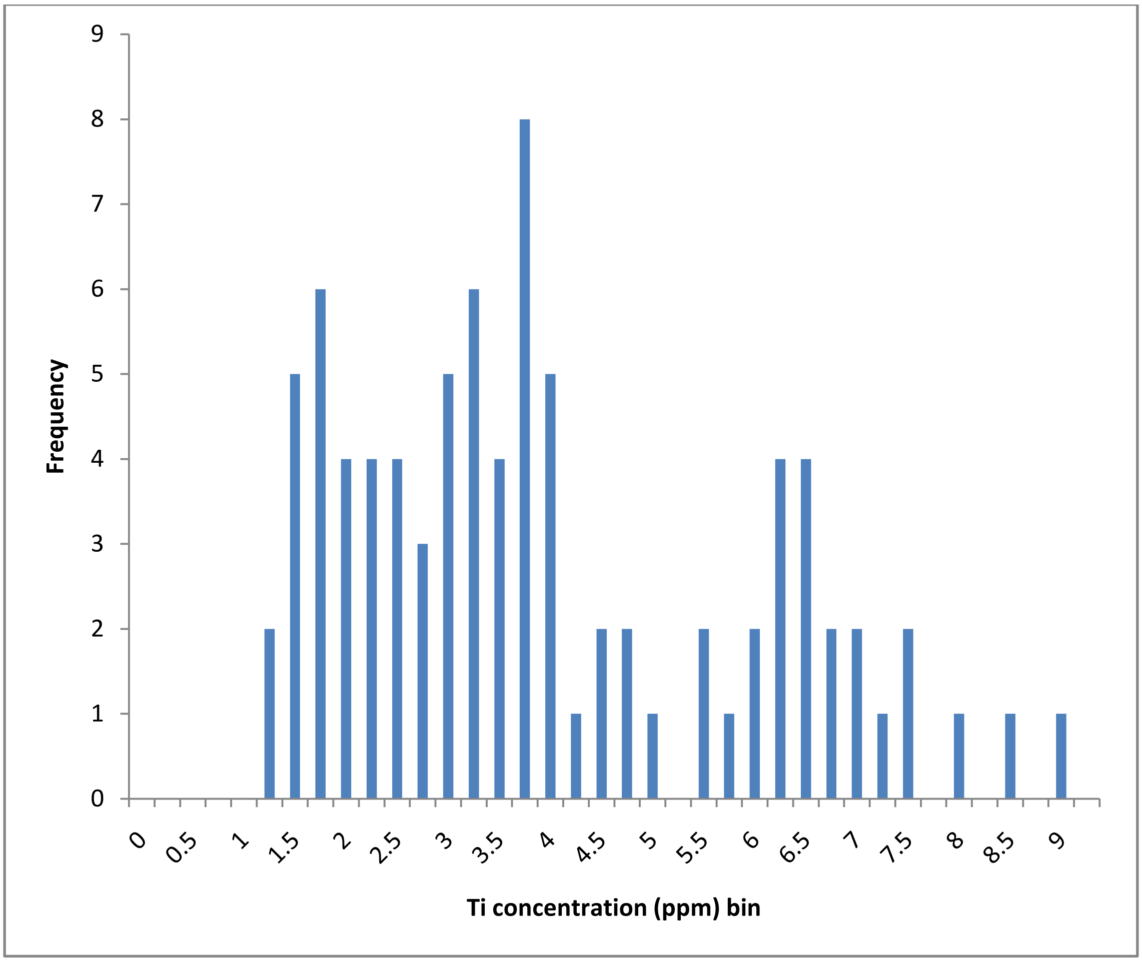
9
8
7
6
5
4
3
2
1
0
Frequency
0
0.5
1
1.5
2
2.5
3
3.5
4
4.5
5
5.5
6
6.5
7
7.5
8
8.5
9
Ti concentration (ppm) bin

Figure 13

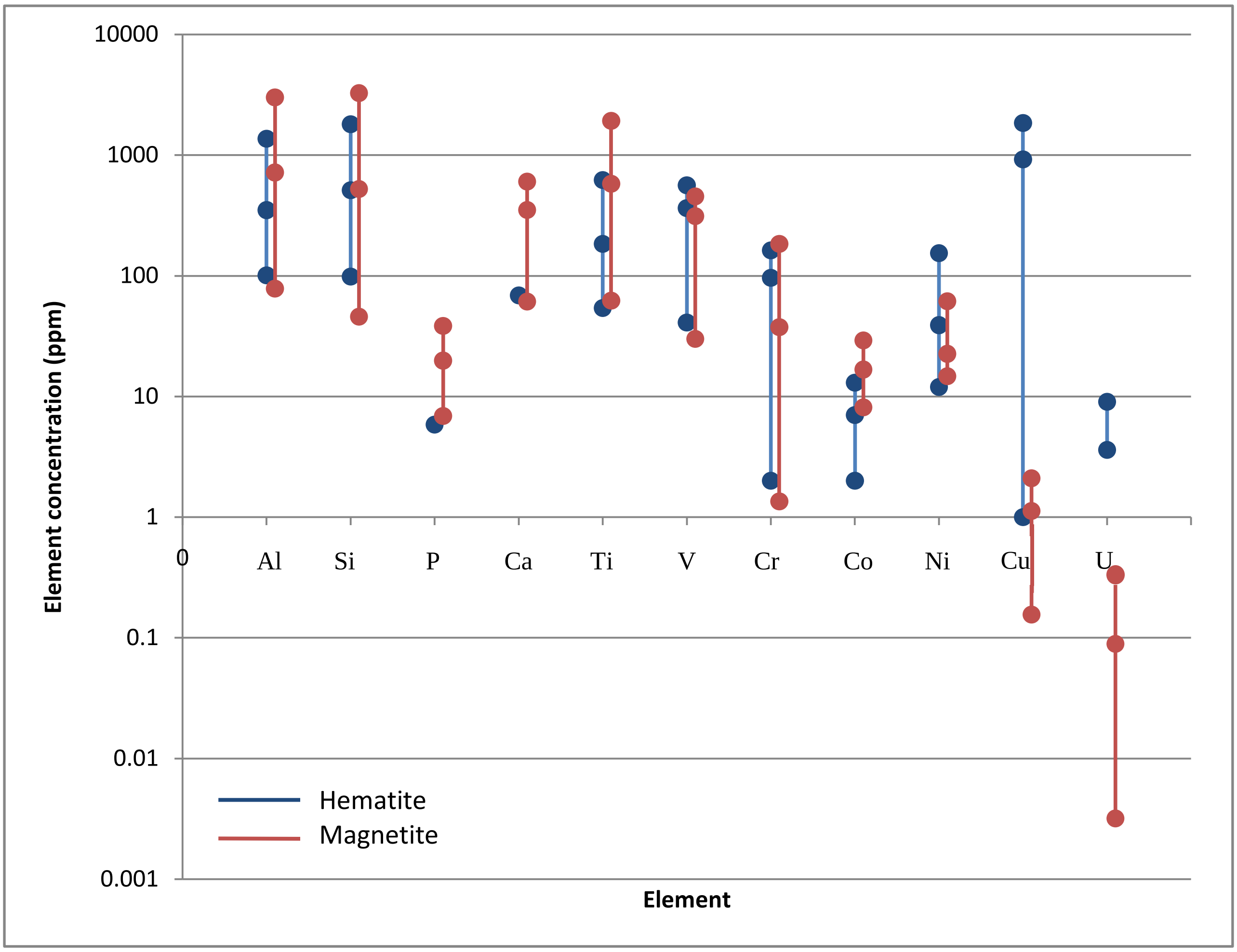
10000
1000
100
10
1
0.1
0.01
0.001
Element concentration (ppm)
0
Al
Si
P
Ca
Ti
V
Cr
Co
Ni
Cu
U
Element
Hematite
Magnetite

Figure 14

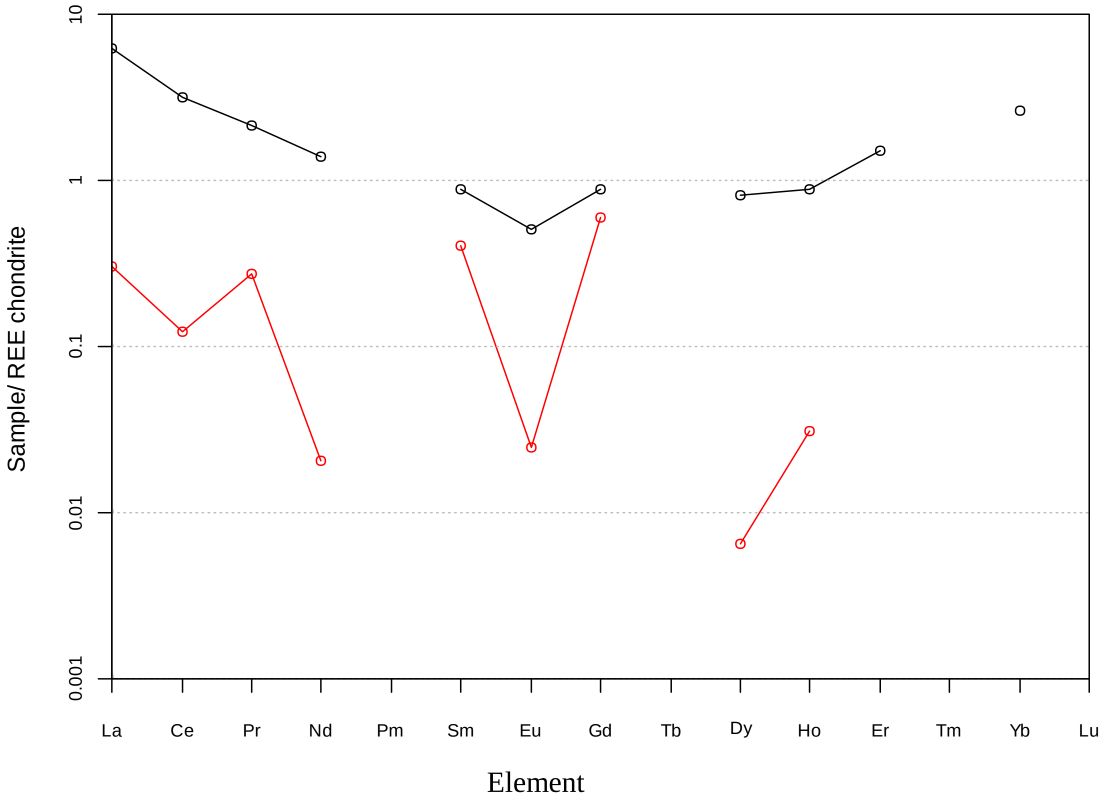
10
1
0.1
0.01
0.001
Sample/ REE chondrite
La
Ce
Pr
Nd
Pm
Sm
Eu
Gd
Tb
Dy
Ho
Er
Tm
Yb
Lu
Element

Figure 15

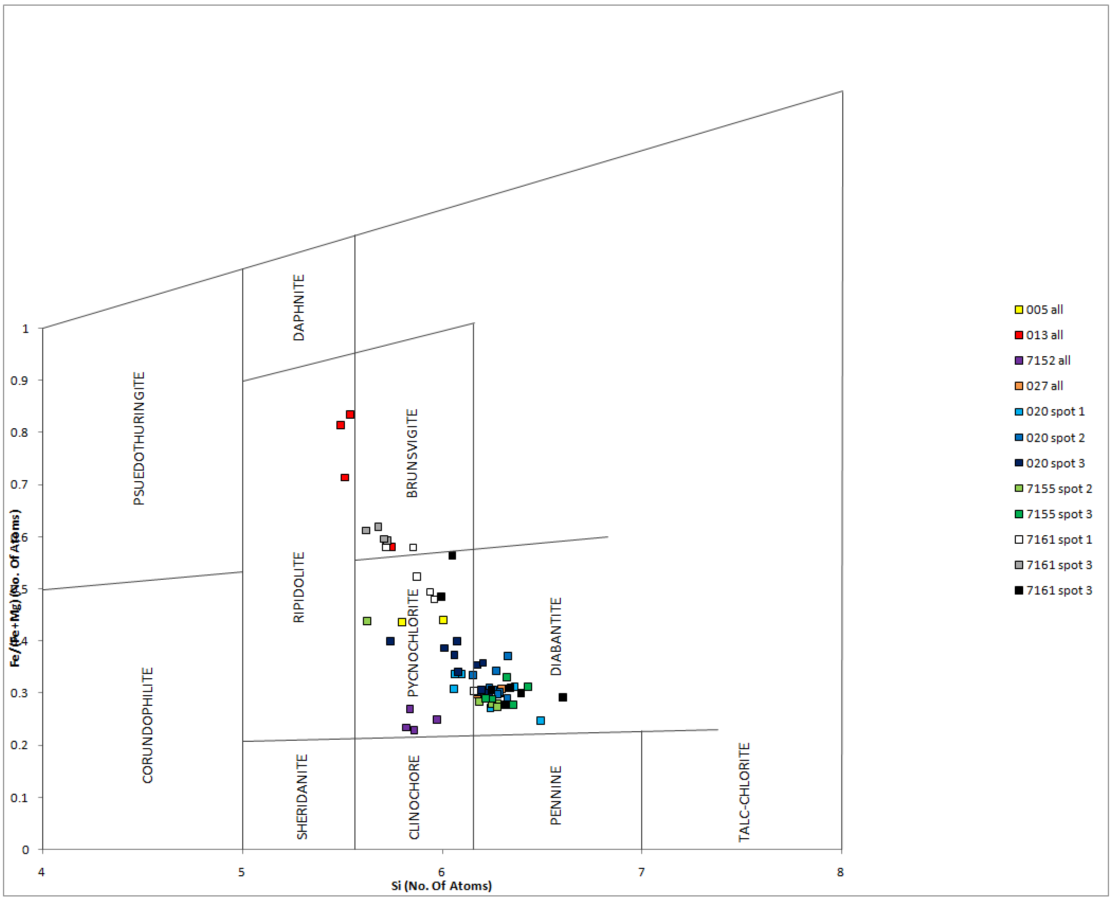
PSUEDOTHURINGITE
CORUNDOPHILITE
DAPHNITE
RIPIDOLITE
SHERIDANITE
BRUNSVIGITE
PYCNOCHLORITE
CLINOCHORE
DIABANTITE
PENNINE
TALC-CHLORITE
Fe/(Fe+Mg) (No. Of Atoms)
Si (No. Of Atoms)
0
0.1
0.2
0.3
0.4
0.5
0.6
0.7
0.8
0.9
1
4
5
6
7
8
005 all
013 all
7152 all
027 all
020 spot 1
020 spot 2
020 spot 3
7155 spot 2
7155 spot 3
7161 spot 1
7161 spot 3
7161 spot 3

Figure 16

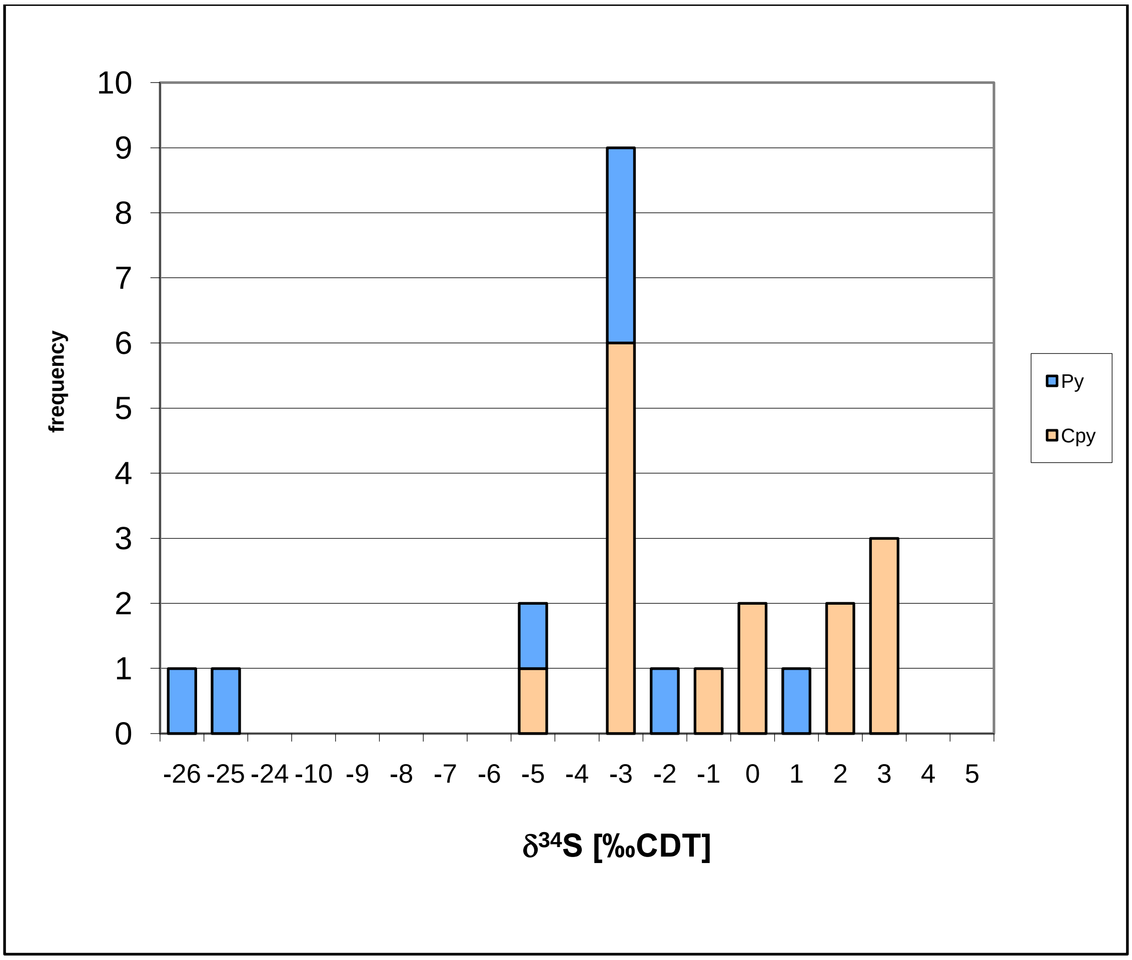
frequency
10
9
8
7
6
5
4
3
2
1
0
-26
-25
-24
-10
-9
-8
-7
-6
-5
-4
-3
-2
-1
0
1
2
3
4
5
δ^{34}S [‰CDT]
Py
Cpy

Figure 17

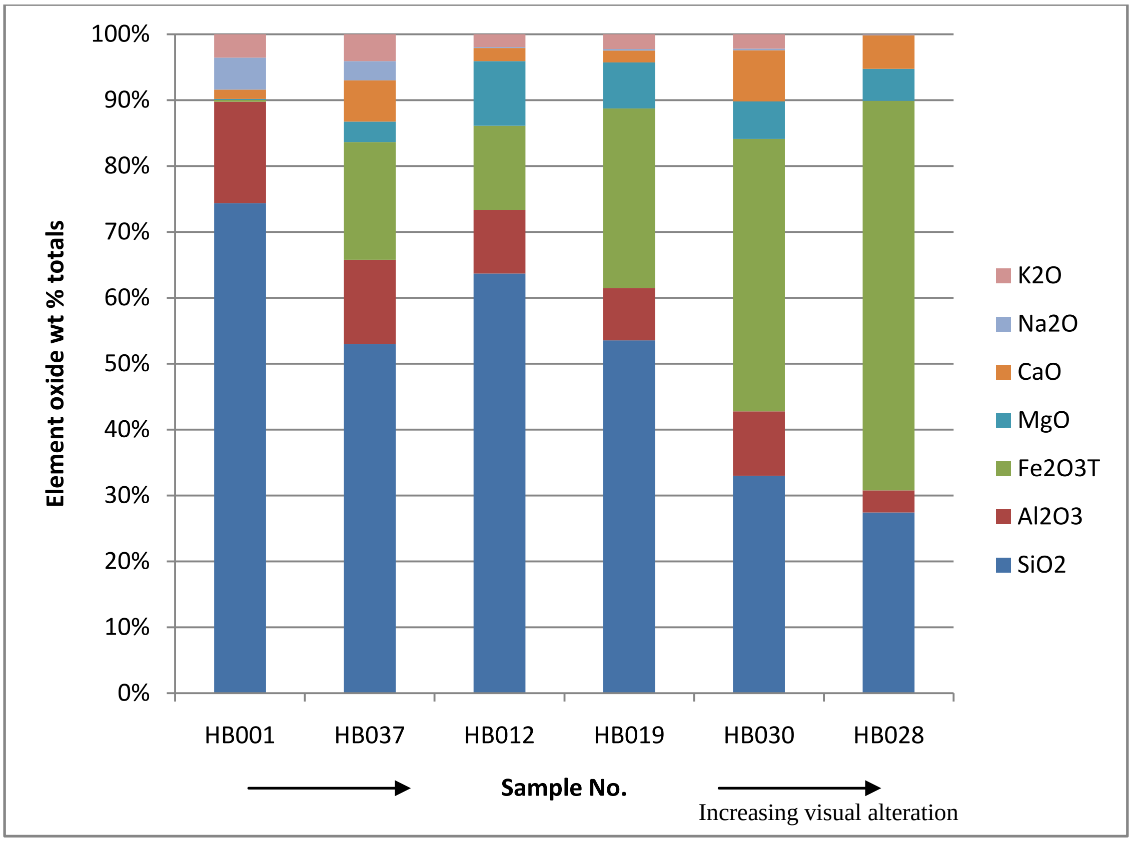
Element oxide wt % totals
100%
90%
80%
70%
60%
50%
40%
30%
20%
10%
0%
HB001
HB037
HB012
HB019
HB030
HB028
Sample No.
Increasing visual alteration
K2O
Na2O
CaO
MgO
Fe2O3T
Al2O3
SiO2

Figure 18

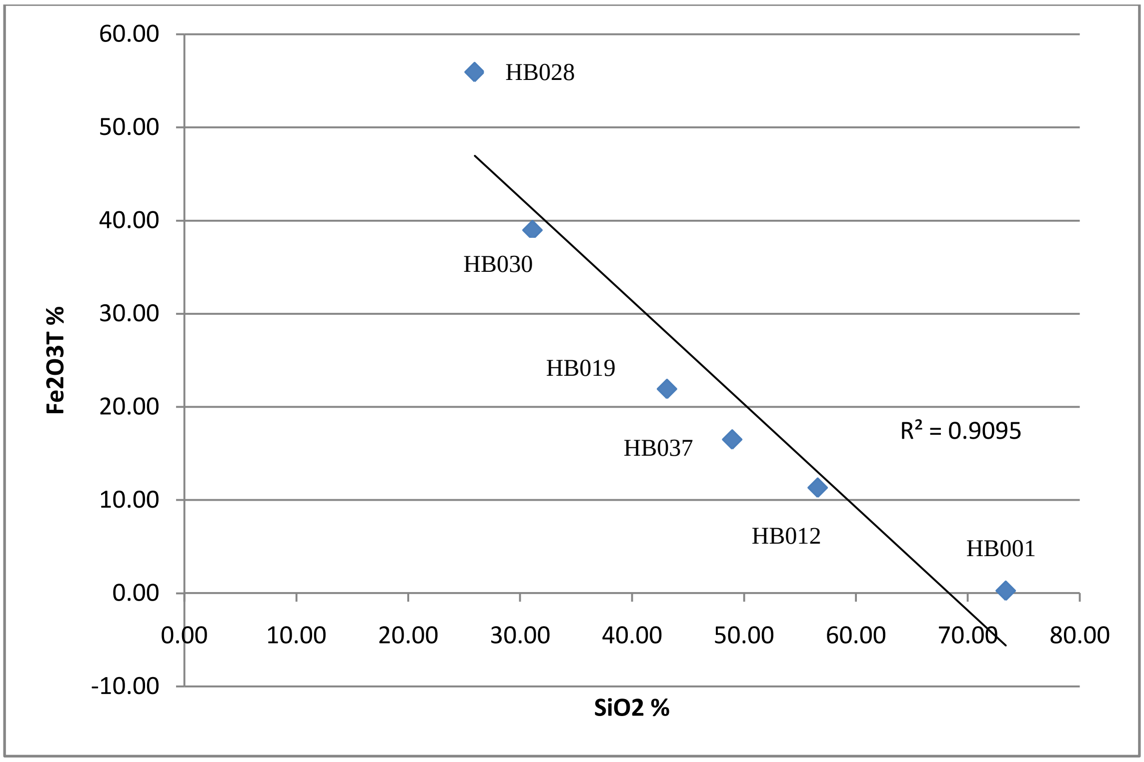
60.00
50.00
40.00
30.00
20.00
10.00
0.00
-10.00
Fe2O3T %
0.00
10.00
20.00
30.00
40.00
50.00
60.00
70.00
80.00
SiO2 %
HB028
HB030
HB019
HB037
HB012
HB001
R² = 0.9095

Figure 19

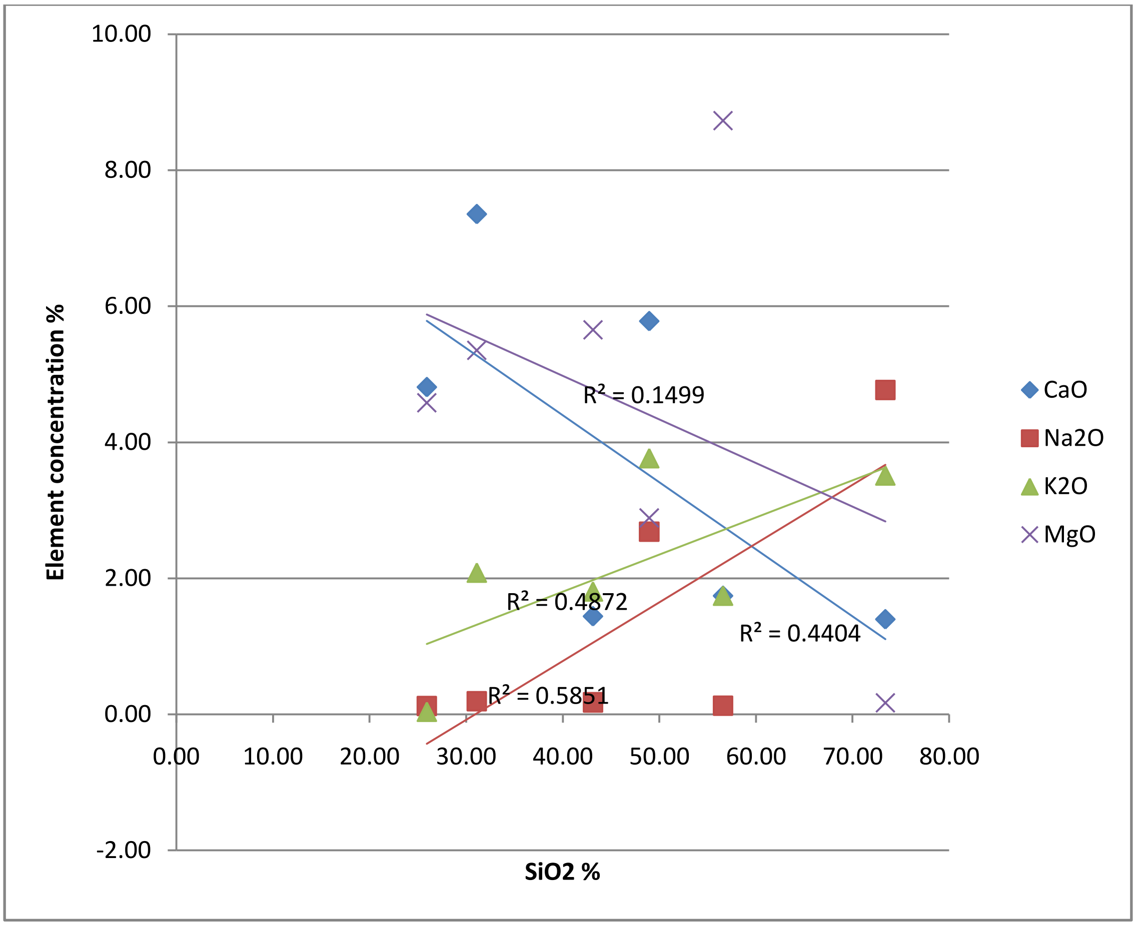

10.00
8.00
6.00
4.00
2.00
0.00
-2.00
Element concentration %
0.00
10.00
20.00
30.00
40.00
50.00
60.00
70.00
80.00
SiO2 %
R² = 0.1499
R² = 0.4872
R² = 0.4404
R² = 0.5851
CaO
Na2O
K2O
MgO

Figure 20

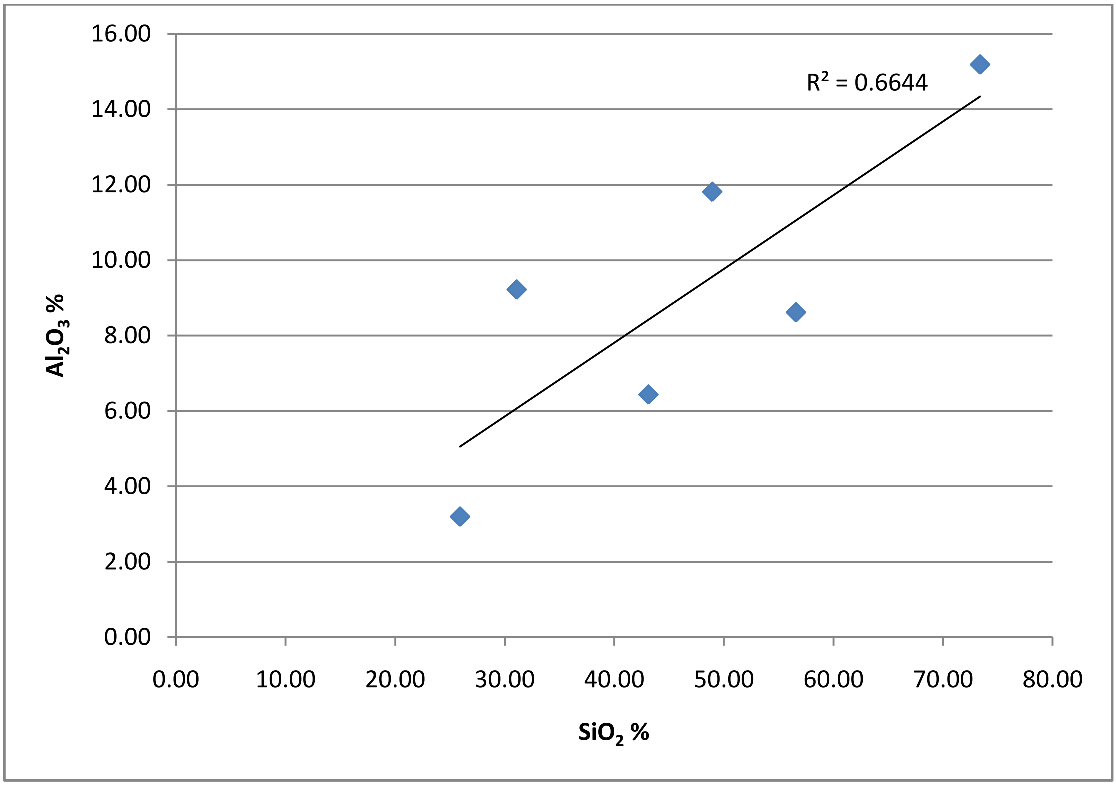
16.00
14.00
12.00
10.00
8.00
6.00
4.00
2.00
0.00
Al_2O_3 %
R^2 = 0.6644
0.00
10.00
20.00
30.00
40.00
50.00
60.00
70.00
80.00
SiO_2 %

Figure 21

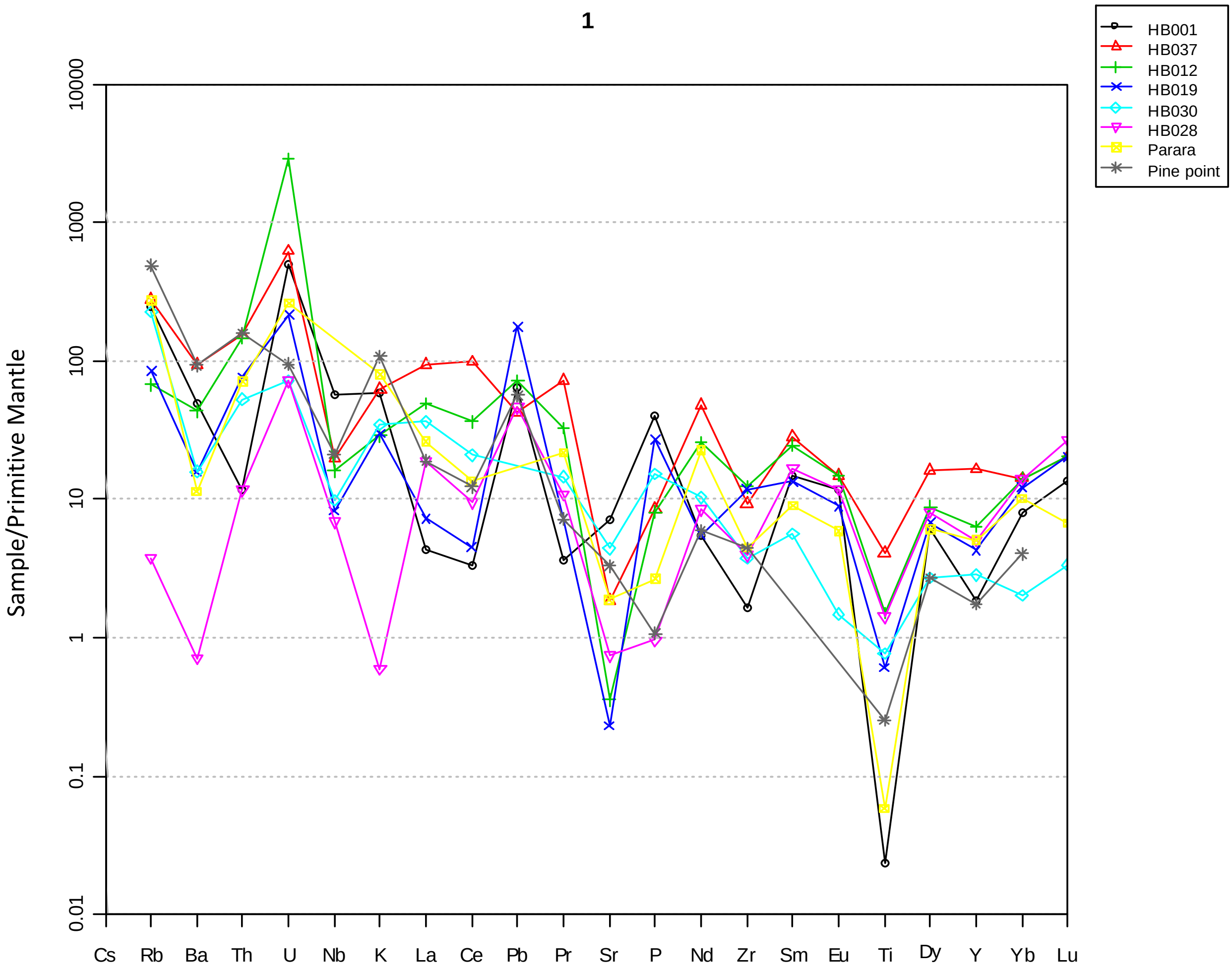
1
HB001
HB037
HB012
HB019
HB030
HB028
Parara
Pine point
Sample/Primitive Mantle
10000
1000
100
10
1
0.1
0.01
Cs
Rb
Ba
Th
U
Nb
K
La
Ce
Pb
Pr
Sr
P
Nd
Zr
Sm
Eu
Ti
Dy
Y
Yb
Lu

Figure 22

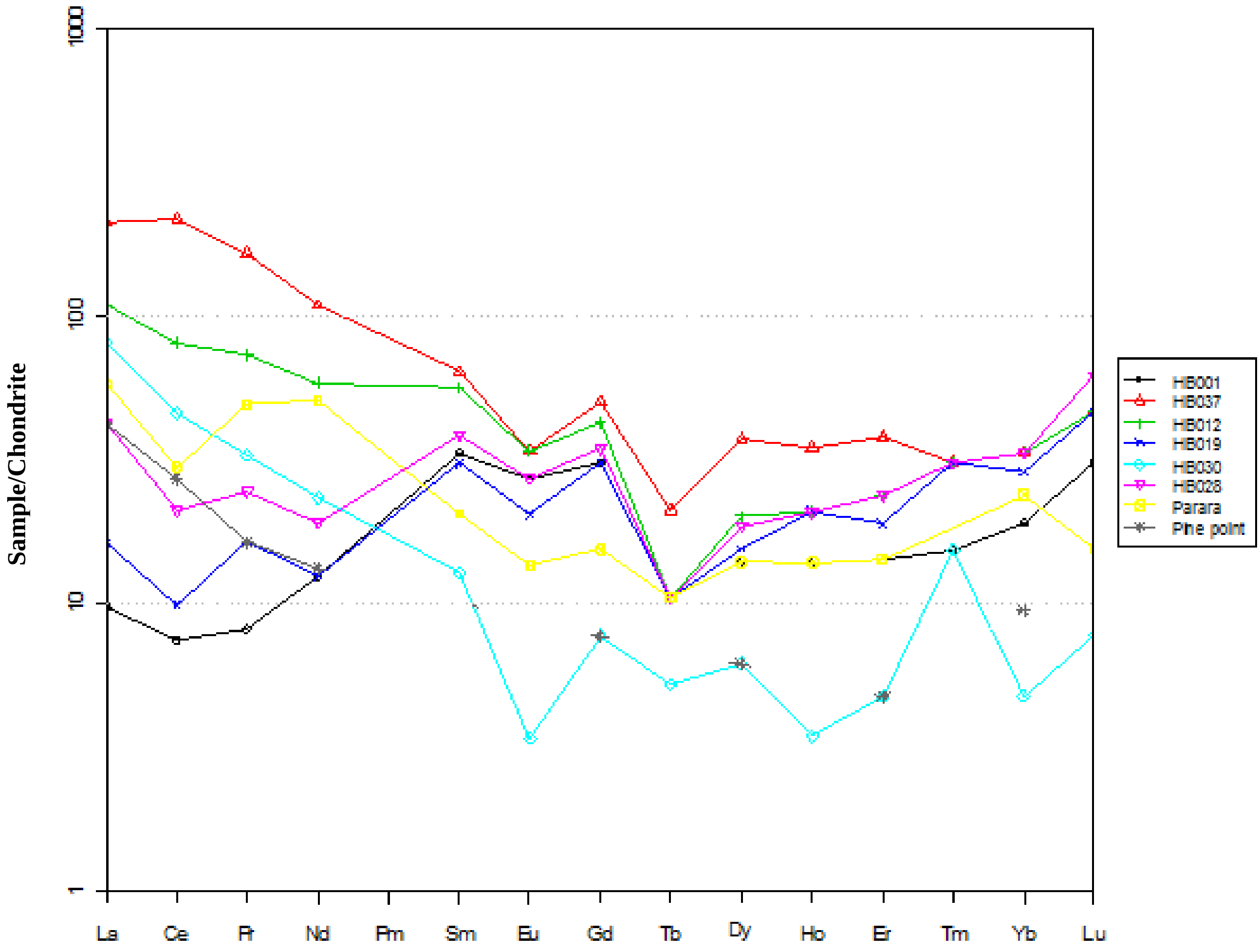
Sample/Chondrite
1000
100
10
1
La
Ce
Pr
Nd
Pm
Sm
Eu
Gd
Tb
Dy
Ho
Er
Tm
Yb
Lu
HB001
HB037
HB012
HB019
HB030
HB028
Parara
Pine point

Figure 23

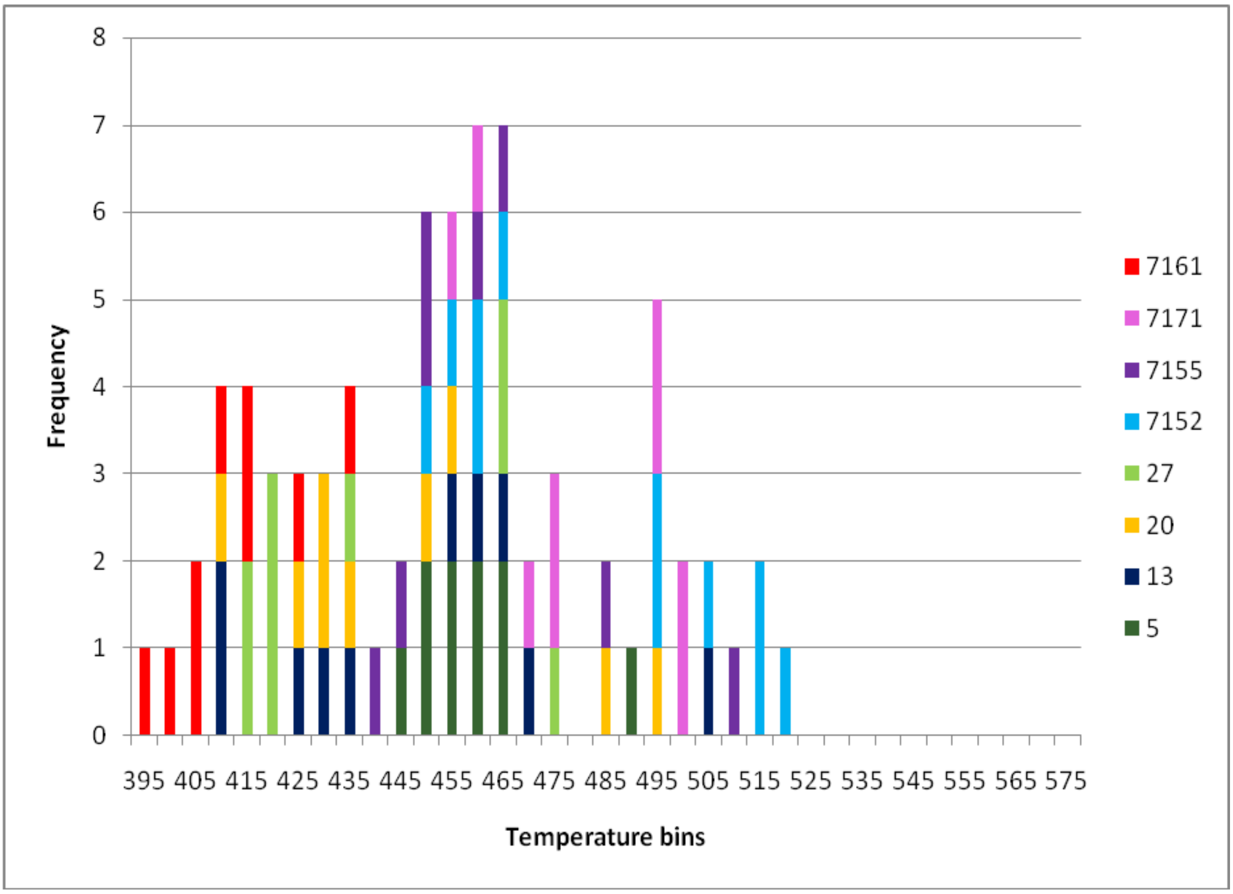
8
7
6
5
4
3
2
1
0
Frequency
395 405 415 425 435 445 455 465 475 485 495 505 515 525 535 545 555 565 575
Temperature bins
7161
7171
7155
7152
27
20
13
5

Figure 24

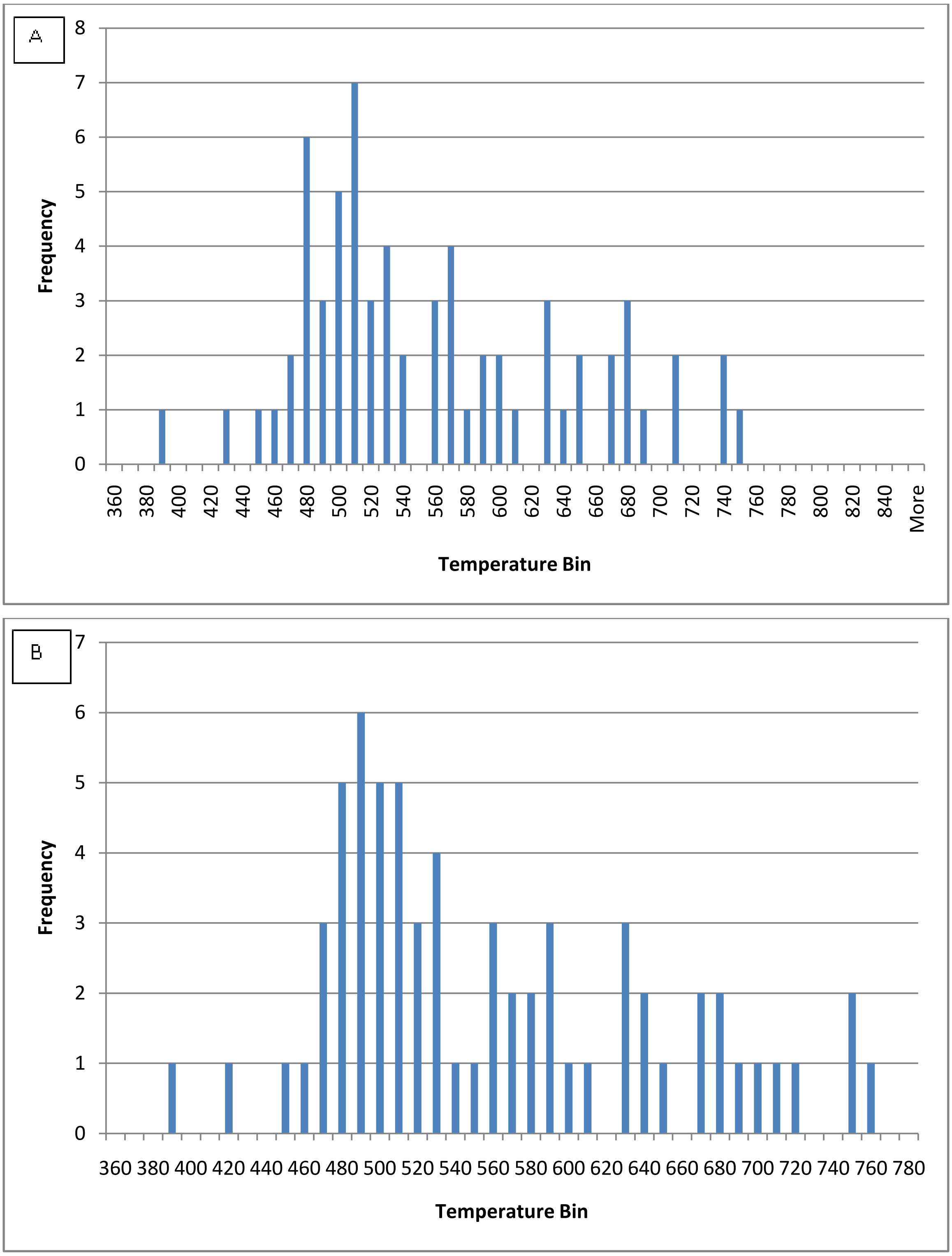
A
Frequency
0
1
2
3
4
5
6
7
8
360 380 400 420 440 460 480 500 520 540 560 580 600 620 640 660 680 700 720 740 760 780 800 820 840 More
Temperature Bin
B
Frequency
0
1
2
3
4
5
6
7
360 380 400 420 440 460 480 500 520 540 560 580 600 620 640 660 680 700 720 740 760 780
Temperature Bin

Figure 25

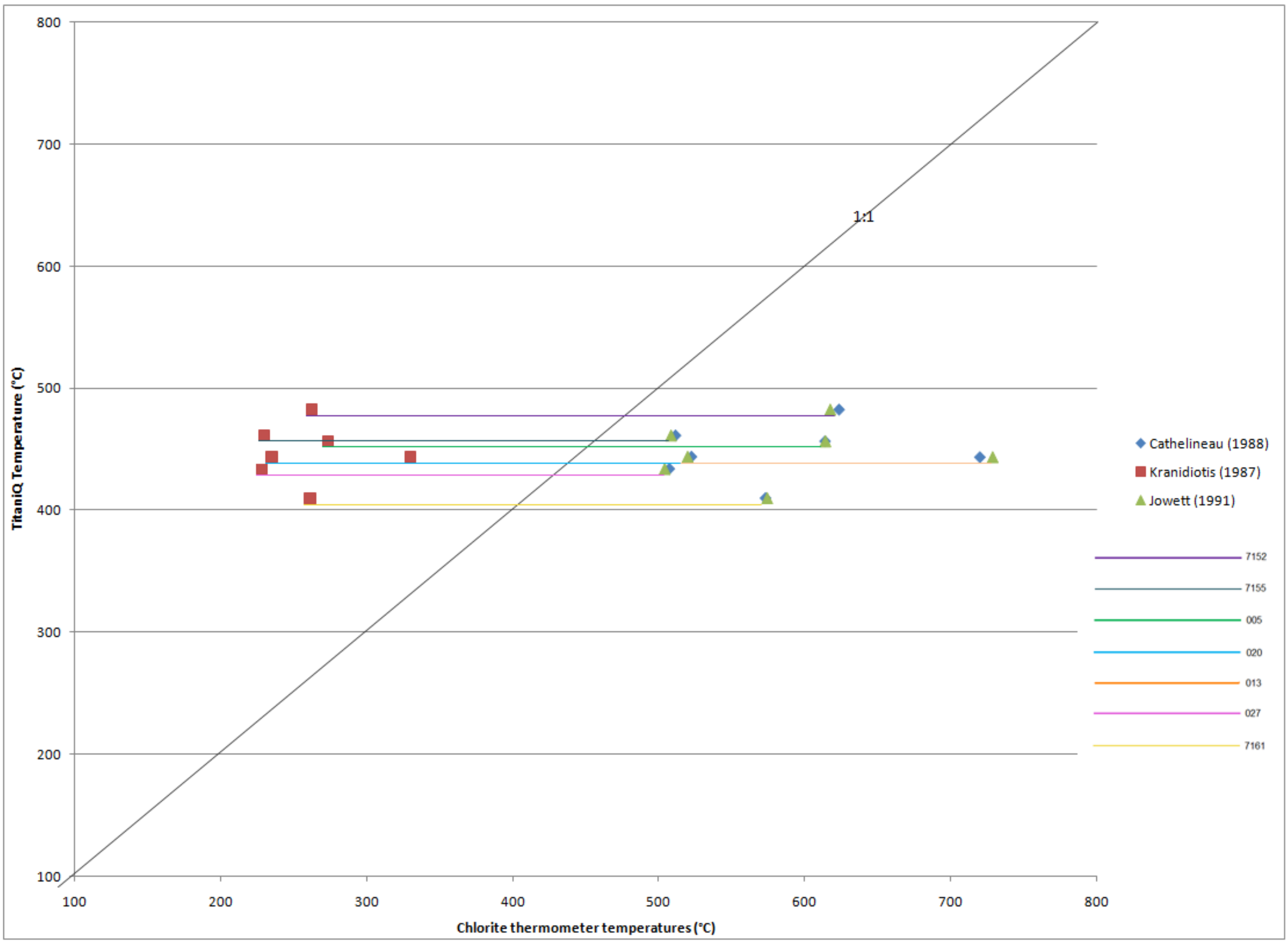
800
700
600
500
400
300
200
100
TitaniQ Temperature (°C)
1:1
100
200
300
400
500
600
700
800
Chlorite thermometer temperatures (°C)
◆ Cathelineau (1988)
■ Kranidiotis (1987)
▲ Jowett (1991)
7152
7155
005
020
013
027
7161

Figure 26

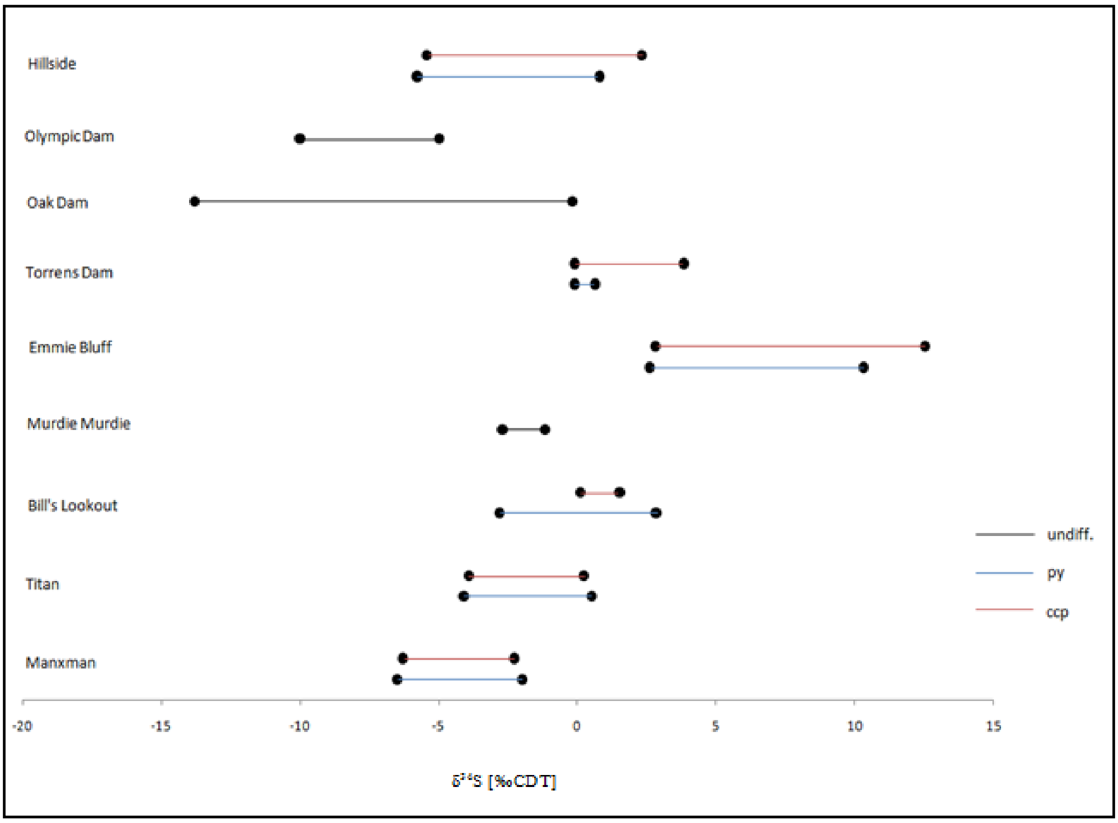
Hillside
Olympic Dam
Oak Dam
Torrens Dam
Emmie Bluff
Murdie Murdie
Bill's Lookout
Titan
Manxman
undiff.
py
ccp
-20
-15
-10
-5
0
5
10
15
δ³⁴S [‰CDT]

Figure 27

Facemap

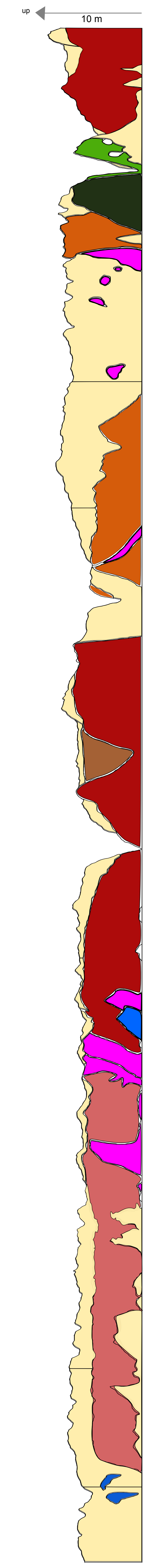

Note all units in facemap are the same as the main Map A, with the exception of the unit below. Also note the vertical exaggeration

🟪	Extremely metasomatised rock, often accompanied by brecciation. Common chlorite, epidote and iron oxide minerals

Map A

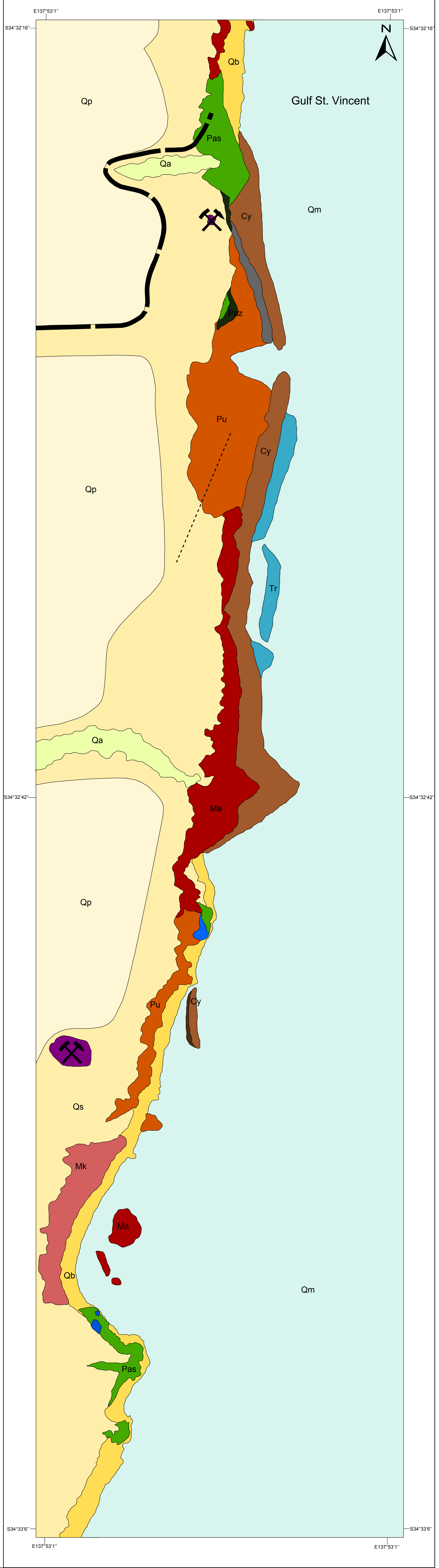

PINE POINT NORTH
COASTAL OUTCROP GEOLOGY

Scale 1:1200

0 50 100 150 200 m

	Unit	Formation	Description
Quaternary	Qa		Recent alluvial sediments including clays, sands and boudres associated with creeks and drainage depressions. Associated with native shrubs and trees and numerous grasses
	Qb		Recent and currently reworked beach sediments dominated by sands with lesser silt and pebbles. Associated with upper intertidal zone and lacking any associated vegetation. Includes magnetite dominated heavy mineral sands
	Qs		Recent slope-face and cliff-top material including regolith and sediment. Material has minimal human disturbance and is associated with medium-size native shrubs and trees, as well as grasses. Includes recent clay deposits (?Hindmarsh Clay) and possibly overlies Rogue Formation in cliff face. Slope deposits characterised by colluvial fan deposits
	Qp		Tilled agricultural paddocks, dominated by grain crops
	Qm		Gulf St. Vincent marine sediments. Includes sand and silt substrates generally associated with several species of seagrass and algae. Includes recent white fossiliferous limestones dominated by molluscs beyond the intertidal zone. Distinguished from Qb by presence of aquatic plants and algae
Tertiary	Tr	Rogue Formation	Ferruginous highly fossiliferous sandstone dominated by several mollusc species, Highly porus and showing irregular weathering patterns. Dominates distal outcrop apparently unconformably overlying Yuruga Formation. Teakle (1982) indicates also present as deposits on cliff-tops (not seen) No obvious bedding or structural features
Cambrian	Cy	Yuguru Formation (Yorke Group)	Pink-red-brown sandstone, arkose, conglomerate and sedimentary breccias. A series of irregular stacked channel conglomerates in surrounding sandstone and arkose deposits. Conglomerate channels dominate lower ~10 m of stratigraphy, becoming more sand dominated at the top. Teakle (1982) suggests stacked fluvial fan depositional environment. Bedding dips ~30-50 deg to the east in mapped section
	Ccy		As above but completely dominated by conglomerates and sedimentary breccias. Possibly fault scarp colluvial fan deposits
Mesoproterozoic	Ma	Arthurton Granite (Hiltaba Suite Granitoid)	White-pink granite ranging from quartz monzonite to adamellite composition with many poorly understood aplite and pegmatite dykes. Often shows only a quartz-K feldspar-minor plagioclase composition with rare hornblende, biotite and magnetite (+ tourmaline in pegmatites) Highly altered to iron oxide-chlorite-epidote assemblages in places (faults?), making almost unrecognisable. Contains small (<1m) enclaves of unaltered dioritic-?gabbroic material
	Mk		As above, but strongly and deeply weathered to kaolin with only residual quartz remaining
	Mm		Black-green amphibolite enclave. Highly weathered outcrops are dominated by clay-altered amphiboles that smear to clays when struck. Presumably a metadolerite or other mafic intrusion. Age poorly constrained - intrudes Wallaroo Group but no clear relationship with granites observed. May post-date or be syn-genetic with granites.
Palaeoproterozoic	Pu		Undifferentiated Proterozoic rocks likely including Aagot Member metasandstone and Arthurton Granite. Similar feldspar-quartz composition coupled with similar deformation, extreme alteration and weathering make distinguishing these units near impossible in these regions. May also include volcanics based on scree, but not directly observed
	Pas	Aagot Member (Wallaroo Group)	White-pink quartzite with variable amounts of feldspar. Outcrop in south of mapped area generally yellowish white with minor alteration (chlorite-iron oxide). Outcrop to the north more feldspar rich and difficult to distinguish from granites. May also contain sections of metarhyolite. Highly iron-oxide-K-feldpar-chlorite-epidote altered in north of mapping area
	Paz		Black-white foliated fine grained siltstone-?calcsilicate rock. Rare; confined to northern section of map area, Appears to be older than Pas and a boulder of Paz lithology in hosted in the quartz-feldspar rock, with discordant foliations between the two units. Processes in this section unclear (dropstone?, fault controlled?, volcanic eruption process?)
	Pab		Extremely iron-oxide altered, possibly hematite brecciated Pas unit. Occurs in small strip, and may be related to fault movement involving thrusting of Cy over basement rocks.
	Fm		Manmade fill and rock brought to surface during mining operations, including mullock heaps and open pits

—	Visible fault
⚒	Historical mine site/working
– –	Beach access track

Map B

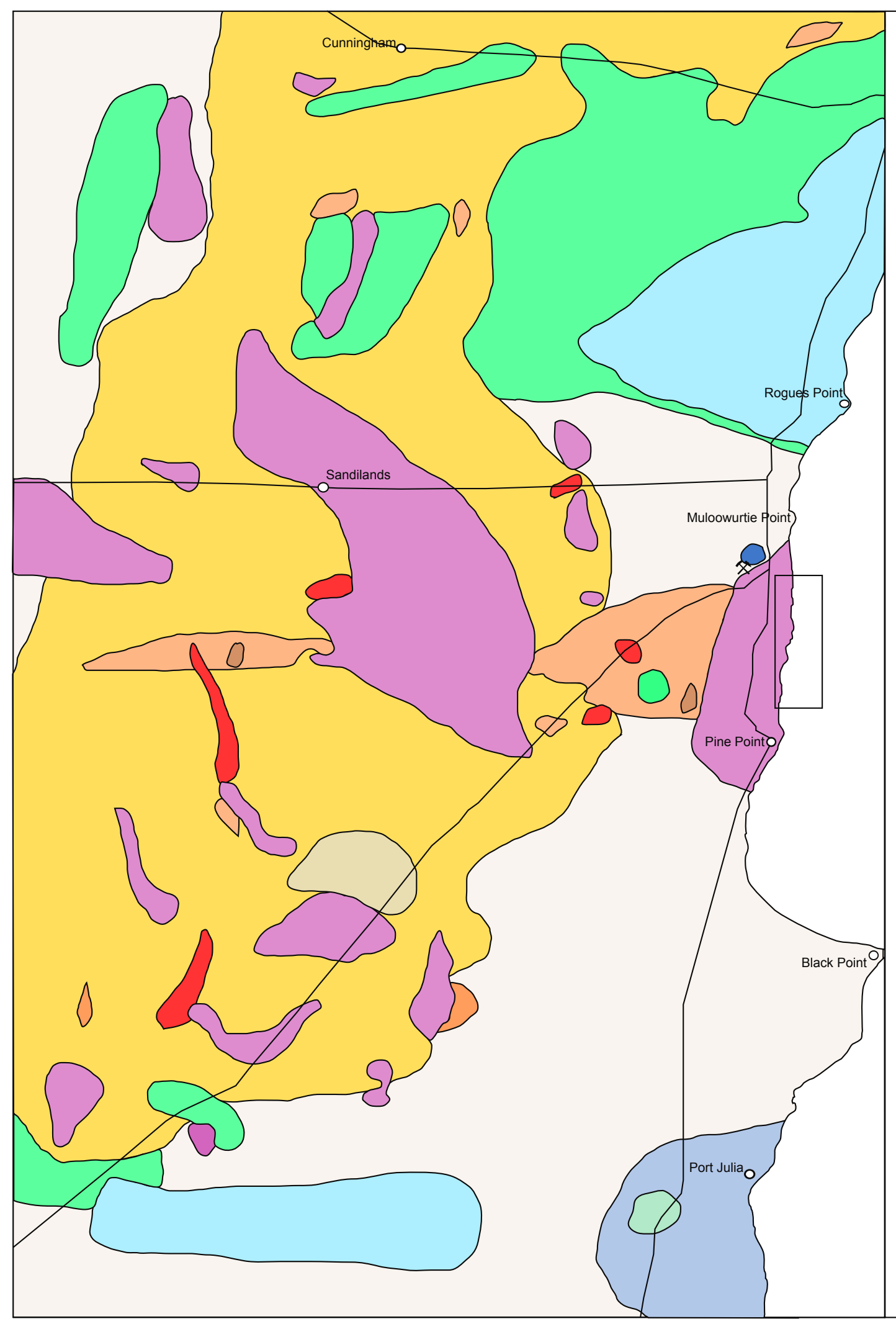

SOUTH ARDROSSAN-PORT JULIA
Subsurface Geology

Scale 1:120000

0 3 km

	Undifferentiated Tertiary and Quaternary sediment and regolith (no solid rock intersected) or no data available (lack of drilling coverage)
	Muloowurtie Formation (Eocene): Silty calcarenite, sandstone and basal conglomerate
Cambrian	Coobowie Limestone: Basal glauconitic sandstone grading upwards to sandy limestone and oolitic limestone
	Ramsay Limestone: Calcareous sandstone grading upwards to silty nodular limestone
	Kulpara Formation: Thick to medium bedded limestone and dolomite
	?Kulpara Formation: Amphibolitic, brecciated and altered limestone/marble, likely attibutable to Kulpara Formation
	Winulta Formation: Basal conglomerate and arkose grading upwards to quartzitic sandstone, siltstone and silty dolomite
Mesoproterozoic	Arthurton Granite: Quartz monzonite-ademellite including aplite and pegmatite dikes. Dominantly quartz, albite, K-feldspar with minor biotite, hornblende, magnetite and tourmaline
	Amphibolite: Dark greenmetamorphic rock (?metadolerite) with minor quartz-feldspar porphyry
	Undifferentiated gneiss: Apparently includes granitic, aplitic and sedimentary gneisses of Wallaroo Group and Arthurton Granite.Wide compositional range, but difficult to differentiate
Palaeoproterozoic	?Doora Member: Muscovite-biotite-hornblende-feldspar-quartz schist (grading to gneiss) of Wallaroo Group. Minor pegmatite intrusions
	?Aagot Member: Logged as Proterozoic fine grained metasandstone. Possibly corresponds to Aagot Member
—	Major connecting roads
⚒	Hillside Mine

Map Notes

Map data taken from RC and diamond drill holes previously drilled along roads in region. Lithology represents first solid rock intersected in core. Map is only a visual guide to areal geology, and no structural interpretation is recommended due to relativley poor drilling coverage and chip/core description

Lithology data sourced from PIRSA SARIG database. Original drilling data presented in Open File Envelope reports by several companies including Esso, BHP, Dampier, CRA, and SA Department of Mines. No new data presented here, only a synthesis of RC and diamond drillhole data

Appendix A

Hole ID: HDD013
Sample Number: 007
Depth: 264.3
Reason For sampling:
Possible albitised dolerite (or fine grained metasediment)
Hand specimen description:
- A grey foliated rock with orange alteration, appearing to stem from central vein or fracture which bisects slide. Green ?chlorite tinges on side of vein. Several smaller orange veins occur in same orientation

Mineral Abundances

Quartz	45%
K-feldspar	35%
Plagioclase (non-vein)	6%
Albite (vein)	3%
Carbonate	3%
Sericite	4%
Biotite	1%
Chlorite	1%
Opaques	3%
Hornblende	Trace

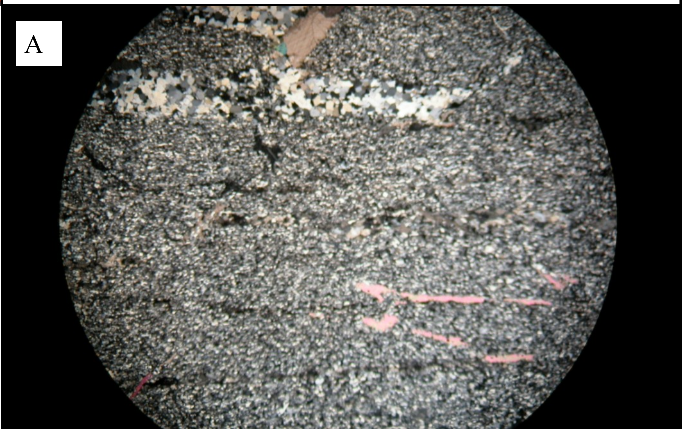

Mineralogical and textural description
-The matrix is dominantly quartz and K feldspar with lesser plagioclase (A). In this section quartz and K-feldspar are difficult to distinguish, however it appears most feldspars are slightly to highly sericitised (B). Plagioclase shows both carsibald and simple twinning.

-The quartz-feldspar matrix is lightly dusted with a light red-brown coated, likely hematite. Trace hornblende and biotite are highly chloritised in the matrix (C). The matrix shows a distinct foliation becoming stronger at the base of the slide. Coincidental with these foliations are bands of coarser grained quartz, possibly recrystallised bands which occurred before metasomatism. Microfaults and associated veins offset some quartz layers. Veins consist mostly of carbonate (D), however rarer zones of quartz and albite. The margins of these albite containing veins are often hevily chloritised or sericitised. The albite within the veins is almost unrecognisable in places due to heavy sericitisation. Where less extensively altered, albite shows perthitic textures in some grains. An opaque and rare biotite appear to be associated with these veins, with biotite often replaced by chlorite. Opaques in the matrix are likely sedimentary in nature.

Interpretation:
-Probably a sedimentary or volcaniclastic rock which has been fractured and veined. The alteration appears to all be of one stage

Rock name
-Quartzofeldspathic metasedimentary rock (possibly volcaniclastic)

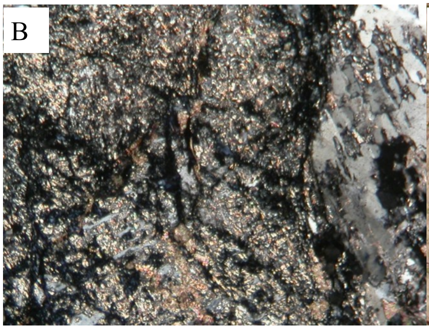

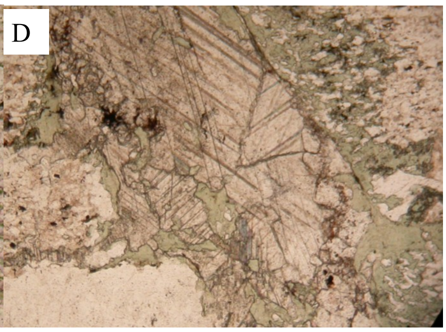

Hole ID: HDD013
Sample Number: 009
Depth: 288.3
Reason For sampling:
Confirm possible andesitic volcanic rock
Hand specimen description:
- A green-grey mostly aphantic rock with several large white phenocrysts. Few opaque minerals scattered through aphantic groundmass. Slide mostly homogenous. Possibly an intermediate volcanic rock or a fine grained breccia.

Mineral Abundances

Carbonate	40%
Chlorite	35%
Quartz/Orthoclase	20%
Hornblende	2%
Opaques	1%
Sericite	1%
Epidote	1%

Mineralogical and textural description

- Aphantic groundmass consists of fine grained (<0.05 mm) matrix of quartz, carbonate, chlorite and possibly feldspar, however the grains are too fine to differentiate between orthoclase or quartz. In this matrix are porphyroblasts of quartz (A), opaques and hornblende.
- Quartz occurs as either large single grains (to 2.5 mm) with recrystallised fine grained margins or aggregates of many small crystals joined together and possibly as inclusions in larger ?orthoclase poikioblasts. These quartz crystals are anhedral and often have a ring of carbonate around them. The hornblende crystals are generally smaller than the quartz, (<0.3 mm). They are green in plane-polarised light (B) and mid-second order birefringence colours in cross-polarised light. In contrast to the quartz they are circular in shape. There also appears to be remnant hornblende or pyroxene crystals in places that have been heavily altered and now are only visible due to a distinct outline with blebs of green-grey material strung throughout. Several rectangular euhedral crystals nearly completely replaced by chlorite, which may have had biotite precursors. Opaques are smaller than 0.4 mm and are subhedral to anhedral and contain inclusions of surrounding groundmass, possibly indicating later stage of growth. In the matrix , chlorite appears to be interstitial to the groundmass grains and contains numerous fine opaques. A single alteration path of fine grained epidote has worked into a margin of the slide. One area of the slide has much more euhedral crystals—may be product of reheating and recrystallisation? Or possibly less sheared. Several larger muscovite/sericite crystals also occur in the altered zone. Several later stage carbonate veins cut the rock, with no apparent relationship with the matrix carbonates.

Interpretation

- Two possibilities

1) A quartz-carbonate metasediment. In this scenario the hornblende and altered remnant ?pyroxene and biotite would be metamorphic products and the carbonate of sedimentary origin.
2) A quartz-feldspar volcanic with rare phenocrysts of hornblende, ?pyroxene and biotite. Carbonate is a replacement feature.

Each has merit—however there are no feldspar phenocrysts (and no plagioclase at all) which would indicate a volcanic rock, so the sedimentary origin is slightly favoured here

Hole ID: HDD013
Sample Number: 010
Depth: 301.4 m
Reason For sampling:
Identify rock and porphyroblasts
Hand specimen description:
Orange aphantic rock with numerous grey-purple ?hematite circular porpyroblasts and many orange bladed porphyroblasts. Contains some carbonate (HCl rxn) Possibly a volcanic rock or hornfels type rock.
No mineralisation or structural features obvious

Mineral Abundances

Carbonate	55%
Quartz	25%
K-feldspar (?Orthoclase)	15%
Opaques	3%
Chlorite	2%
Hornblende	Trace
Sericite	Trace

Mineralogical and textural description

- Thin section appears to contain two domains of different texture but same mineralogy
- First domain is fine-grained (<0.1 mm) quartz-carbonate-opaque. Quartz is subhedral, carbonate anhedral with carbonate being slightly larger than quartz. Opaques very fine (<0.1 mm). This domain has a very ‘messy’ appearance
- Second domain has the same mineralogy as the above section, but is much coarser grained. Carbonate and quartz grains interlock and are euhedral-subhedral. Carbonate grains to 0.6 mm, quartz to 0.5 mm diameter

- Throughout the coarser grained section of the rock are two types of porphyroblast (A,B):

1) A 0.5-10 mm orange dusted ?K-feldspar lathe to equant shaped porphyroblast (C). Appears to now be an aggregate of many fine K-feldspar crystals (recrystallisation?) Throughout these porphyroblasts are small quantities of sericite (alteration) , as well as chlorite ‘veins’ all running parallel to each other. These chlorite veins occur in all blasts but never in the quartz-carbonate groundmass
2) An equant 0.4-0.7 mm carbonate and opaque porphyroblast, again containing the chlorite ‘veining’ (D). The direction of chlorite ‘veining’ does not always match that of the veining in the K-feldspar porphyroblast

- Several small carbonate veins cut both the groundmass and the porphyroblasts. One corner of the slide contains a chloritic overprint associated with an opaque mineral (?hematite). Brick red-brown hematite is further distributed along narrow stockwork veins, with this appearing to be the last stage of alteration.

Interpretation

- Protolith likely a carbonate-quartz sediment (sandy limestone) or less likely a carbonate altered volcanic rock. Protolith was foliated and possibly sheared during early events, leaving a chlorite defined fabric. K-feldspar possibly authigenic or alteration product; less likely volcanic-derived. Carbonate-opaque porphyroblasts also probably authigenic or alteration-associated. Protolith partially recrystallised in contact aureole with nearby Hiltaba Suite granite, destroying most primary textures except in porphyroblasts. Later carbonate and chlorite-hematite overprinted rock in places.

Rock Name: Porphyroblastic carbonate-quartz hornfels OR porphyroblastic quartz bearing marble

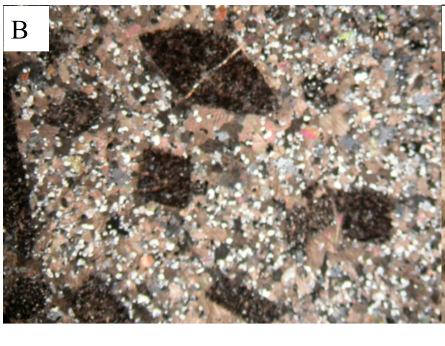

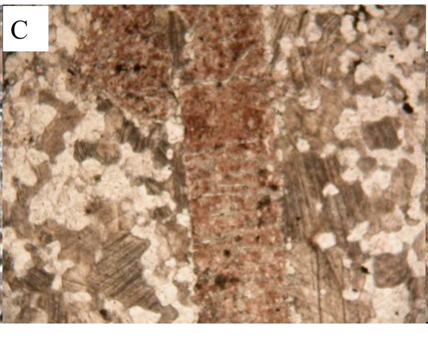

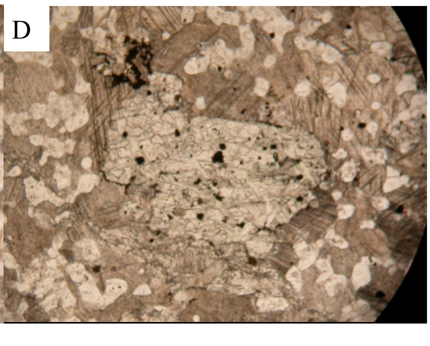

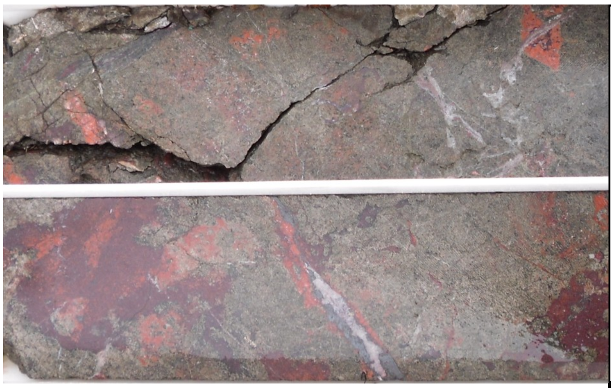

Hole ID: HDD013
Sample Number: 025
Depth: 537.4
Reason For sampling:
Unusual metasomatised rock, appeared to contain allanite.
Hand specimen description:
- A mottled brown/orange/green rock. Appears the brown mineral is replacing the green mineral. Later stage white (carbonate?) veins cut the previous two mineral zones. Green mottling is 3mm to 2cm diameter zones, with brown zone 'infilling'.

Mineral Abundances

Opaque	45%
Garnet	20%
Carbonate	15%
K-feldspar/albite	15%
Quartz	3%
Chlorite	2%
Epidote	Trace
Actinolite	Trace

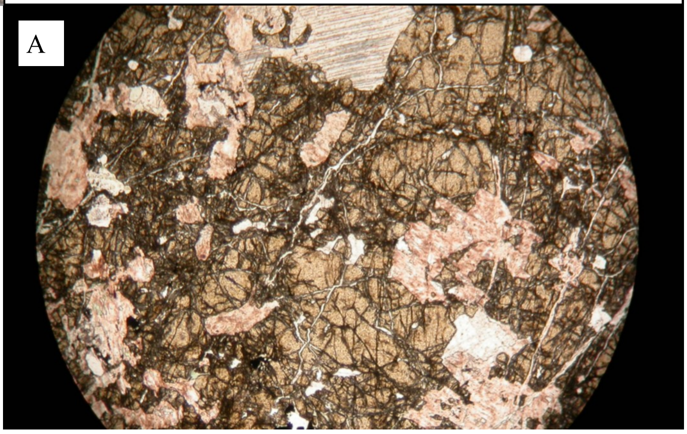

Mineralogical and textural description
- A rather homogenous green garnet with rare 0.2-0.5 mm epidote crystals, Garnet appears to have been lose to 100% of early rock composition (A,D). Trace actinolite appears to be either coeval with garnet or at some undetermined later stage. Opaques are not part of this early stage. The green garnet sections are 0.5-15 mm in diameter

- Following stages rather obscure, however carbonate, feldspar, quartz, opaques, chlorite and possibly sericite are involved (C) Large areas, possibly veins, consist of coeval opaque (hematite), quartz, feldspar and chlorite. In these 'veins', hematite accounts for 50% of the minerals by abundance. Quartz is subhedral in these veins, all other minerals are anhedral (max. 0.1 mm in size) in a rather amorphous mass. These qz-fd-chl-cb-hm 'veins' appear like small intrusive bodies in most cases, but have vein networks protruding into the surrounding garnetiferous rock.

-Early euhedral epidote associated with garnet has been cut and replaced by amorphous masses of murky Epidote (B). Both the garnet and later epidote stages are cut by the qz-fd-chl-cb-hm veins.

Interpretation:

Garnet unlikely to be igneous in origin, as no garnet is reported in such quantity in the Arthurton Granite. Most likely an early metamorphic/metasomatic event. The precursor rock is then completely obscured and unknown. This was followed by the later alteration ans previously described

Rock name
- Metasomatite (Garnet bearing skarn?)

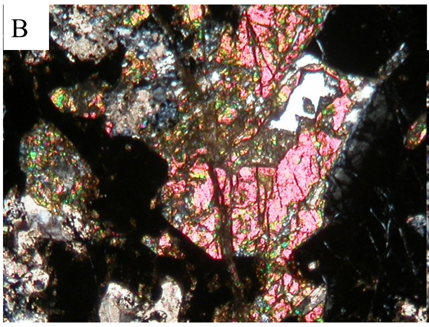

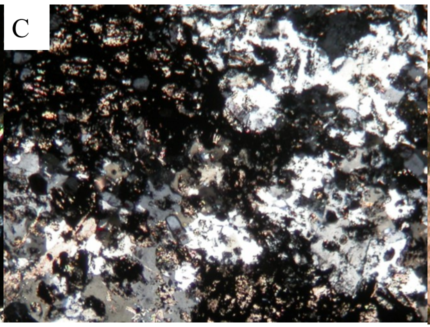

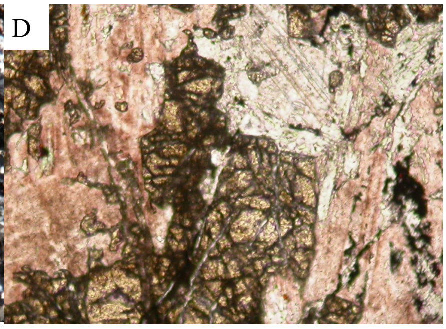

Hole ID: HDD013
Sample Number: 026
Depth: 540
Reason For sampling:
Possible allanite occurrence in unusual highly metasomatised rock
Hand specimen description:
- A heterogenous rock; sections of green, orange/pink and grey/green rock

Mineral Abundances

K-feldspar	45%
Sericite	25%
Opaques	10%
Rutile	7%
Epidote	5%
Quartz	5%
Sphene	3%
Chlorite	2%
Plagioclase	1%
Carbonate	1%

Mineralogical and textural description
- There are two obvious mineralogical domains in this rock; a coarse grain, unaltered section and a fine grained, possibly brecciated section The coarse grained section contains ~40% quartz, 20% K-feldspar (microcline and orthoclase), 20% plagioclase, 10% rutile, 7% opaques and 3% sphene (B). Quartz ranges from 0.5 to 4mm long and is anhedral. K-feldspar and plagioclase are difficult to distibguish due to extensive sericitisation. The feldspar grains are large, ranging from 3-4mm. Feldspar also is being altered to epidote, with fine, often discontinuous veins cutting through crystals and being filled with sericite and Epidote (A). Rutile is common as large 0.5-4 mm crystals of anhedral crystallinity. Opaques are present as sub-anhedral 0.3-1mm grains. Some sericite crystals are relatively large (to 2mm) and appear to cut into some quartz as large lathes. The coarse grained nature of this domain suggests it to be a granite, although lacking biotite or amphiboles. The second domain in the slide is an extremely altered version of the above rock. This zone consists mostly of a brick red feldspar due to hematite dusting and its altered equivalent, a fine grained sericiete-chlorite matrix with strong epidote alteration in places. Amongst the alteration products are remnant rutile, opaques, sphene and quartz which have avoided alteration. Fine grained veins of carbonate and chlorite appear to be the latest stage in alteration, with many of the large primary crystals cut by these veins. It appears a second fine grained stage was added with the alteration which commonly forms anhedral masses that fill interstitial spaces. Epidote appears to replace feldspar and is the only minerals to replace rutile (C).

Interpretation:
- Rock was initially a coarse grained felsic intrusive containing abundant rutile an minor sphene, however was extensively altered by a feldspar-chlorite-carbonate-opaque assemblage

Rock name
- Metasomatised granite

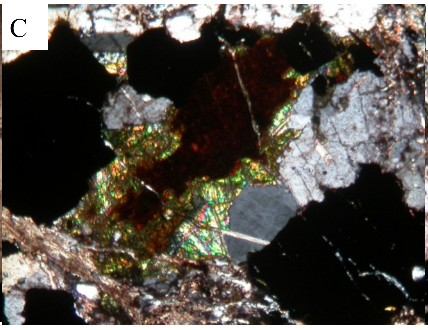

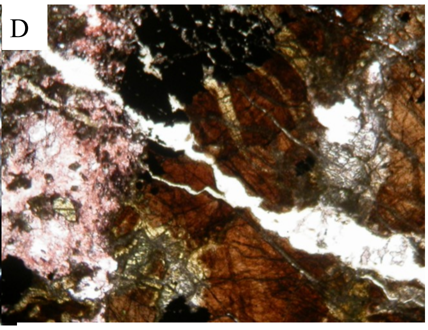

Hole ID: HDD013
Sample Number: 028
Depth: 522.4
Reason For sampling:
Large hematite/magnetite sections in ?granitic breccia.
Hand specimen description:
- A layered green and opaque containing rock. Opaques appear to be hematite or magnetite. Several carbonate bearing veins cut the slide

Mineral Abundances

Opaque	55%
Chlorite	15%
Quartz	15%
Carbonate	14%
Epidote	1%

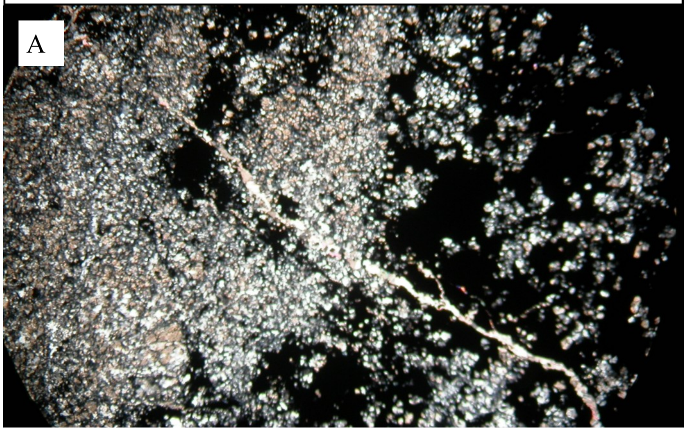

Mineralogical and textural description
- Slide dominated by opaque mineral (magnetite-hematite). The clear anisotropic groundmass (A) is fine (less than 0.1mm) and consists of carbonate, quartz and chlorite. Quartz and carbonate are sub-anhedral grains while chlorite fills interstitial spaces. Epidote is rare and associated wtih the opaque minerals. Chloritisation may predate the opaque-epidote alteration– diagenetic chlorite? Opaques are large and irregular and have grains of anisotropic minerals (qz, chl) within them (B). Two later carbonate vein stages

Interpretation:

-Likely a calcarenite precursor rock had chlorite introduced during diagenesis. Later alterations created the currently seen assemblage

Rock name
- Metasomatised metacalcarenite

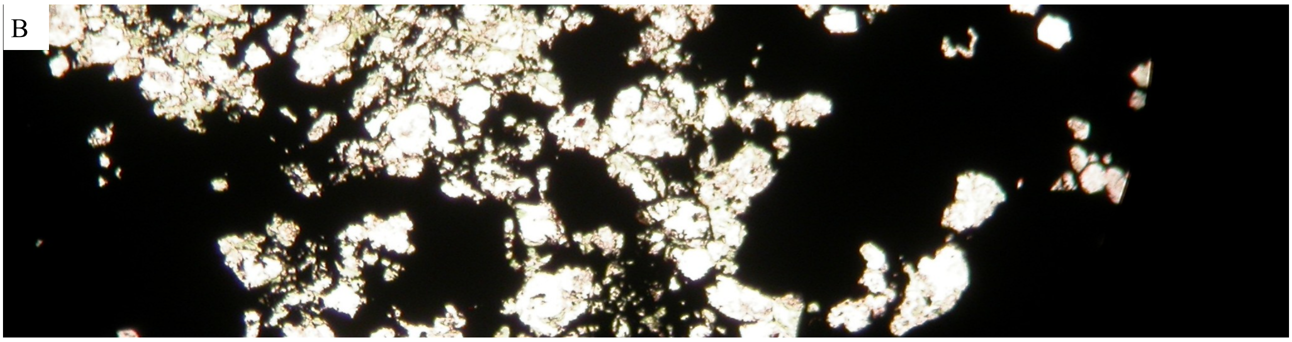

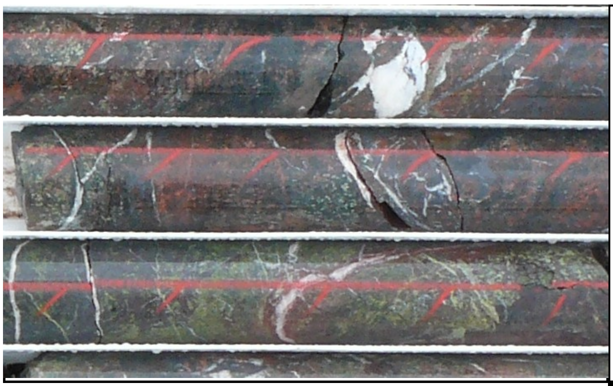

Hole ID: HDD013
Sample Number: 030
Depth: 586.1 m
Reason For sampling:
Identify rock and unusual green-orange alteration texture
Hand specimen description:
- A mottled black-grey-green-orange-white rock of apparently completely altered character. 1-2 mm grains of white-green-orange mineral grains are surrounded by black-grey ?hematite-magnetite matrix. White ?carbonate veins commonly cut rock

Mineral Abundances

Opaque	40%
Quartz	15%
Epidote	15%
Carbonate	10%
Chlorite	12%
K-feldspar	8%
Sphene	Trace
Sericite	Trace

A

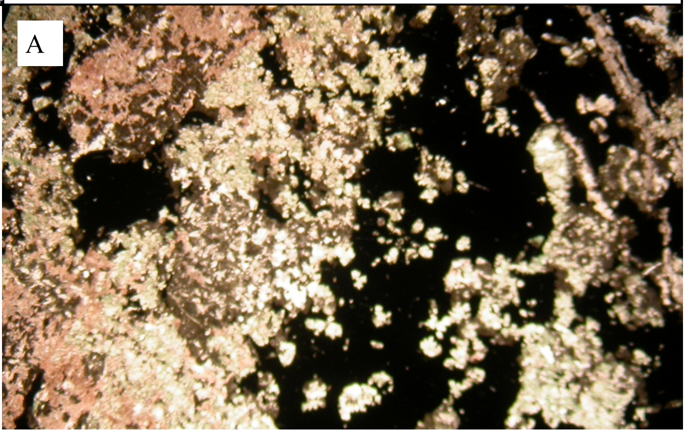

Mineralogical and textural description

- Slide is roughly divisible into two sections—a fine grained quartz-carbonate domain and a highly altered ?equivalent

- The fine grained zone is dominantly quartz (<0.05 mm) with interlayered finer carbonate. This zone also contains large (now sericite altered) either authigenic or volcanic-detrital K-feldspar (B). Remnant outlines indicate these feldspars were 3 to 4 mm in diameter. Chlorite is quite abundant in this section, however does not define a prominent foliation plane.

- Alteration assemblage characterised by an opaque mineral (C), garnet (D), epidote, carbonate and chlorite. This alteration overprints the previously described fine grained rock so that is unrecognisable in most places. The opaque is anhedral and contains inclusions of country rock as well as chlorite and epidote altered material. Epidote and chlorite appear to 'ring' the opaque. Large feldspar porphyroblasts highly altered by epidote, chlorite and sericite. Large (>1 mm) euhedral carbonate crystals occur within this altered zone, and must be part of this alteration assemblage.

- Later carbonate veins cross cut the earlier alteration assemblages.

Interpretation

- Protolith rock most likely a carbonate-bearing sandstone that may contain intercalated volcanics or alternatively contains authigenic K-feldspar phenocrysts. Chlorite likely diagenetically produced throughout sediment. Hydrothermal alteration may have been two-stage with epidote, chlorite and carbonate being followed by the opaque mineral.
A later carbonate stage cut the earlier alteration assemblage.

Rock Name: Metasomatised quartz-carbonate metasediment

B

C

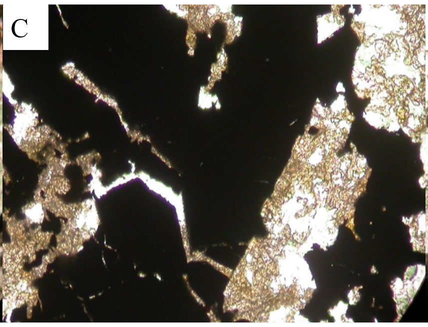

D

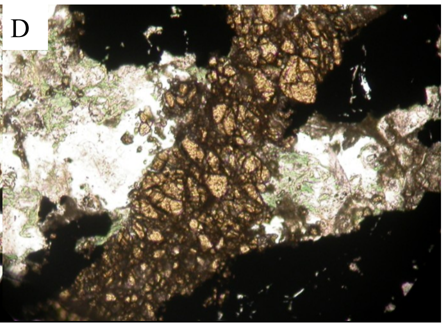

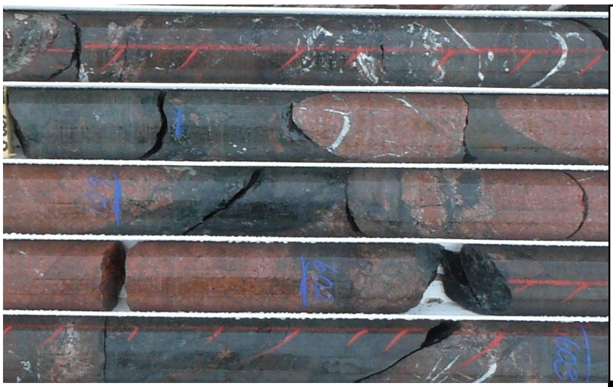

Hole ID: HDD013
Sample Number: 031
Depth: 599.6
Reason For sampling:
Possible mafic dyke for petrographic description and classification
Hand specimen description:
- A brown/green/grey aphantic rock with two veins cross cutting, both in the same orientation. Groundmass is green with fine black-brown spots (A). Vein 1 is clear with few opaques and abundant chlorite also present, Vein 2 opaques

Mineral Abundances

Chlorite	35%
K-feldspar	30%
Plagioclase	7%
Quartz	7%
Biotite	7%
Opaques	7%
Epidote	3%
Carbonate	3%
Sericite	2%
Sphene	1%
Spinel, Monzonite?	Trace

Mineralogical and textural description
- The groundmass consists primarily of K-feldspar (mostly orthoclase, minor microcline) (C) and chlorite. Plagioclase (with simple twinning), quartz, opaques and biotite also relatively common in the groundmass.Spinel, Epidote, sphene and ?monzonite are present but rare in the groundmass. K-feldspar is anhedral and less than 0.5 mm diameter. Feldspar is being highly altered to sericite and contains high levels of brown hematite dusting. Plagioclase occurs in subhedral lathes of the same size as K-feldspar, with biotite also showing this texture. Biotite is often replaced by chlorite. Quartz shows similar textures to plagioclase. Chlorite is a later stage than than biotite-quartz-feldspar and appears to be alteration (B,D). There is one stage of euhedral to subhedral opaques in the groundmass, and a later chlorite associated anhedral opaque (B).

-The two veins are chlorite dominated and also contain abundant phenocrysts of quartz, K-feldspar and rare albite. Sphene, Epidote and opaques are also present as small inclusions in these veins (reworked from older vein?) No evidence of shearing is present. It appears the feldspar is recrystallised based on the murky appearance, and shows a weak foliation plane.

Interpretation:
- The protolith likely is a felsic to intermediate volcanic rock with a feldspar dominated composition which included quartz, biotite, plagioclase and opaques. Appears chlorite-carbonate-opaque stage overprinted an earlier epidote-? sphene alteration stage. Carbonate veins are obvious but disjointed. It appear chlorite infiltrated the groundmass in fine networks

Rock name
- Chloritised rhyolite (based on IUGS volcanic classification)

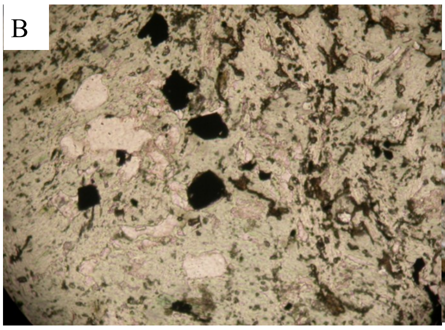

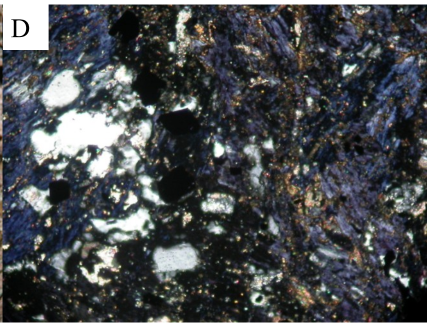

Hole ID: HDD013
Sample Number: 032
Depth: 666
Reason For sampling:
Contanct between granite and surrounding metasediment or ? mafic volcanic.
Hand specimen description:
- A felsic intrusive (granite) intruding an opaque rich rock. Intrusive rock is orange with few opaques and later clear veins. Boundary is mostly opaques with green chlorite. Country rock has both opaques and clear minerals.

Mineral Abundances
(Country rock)

Quartz	50%
Opaques	40%
Chlorite	7%
Feldspar	2%
Carbonate	1%

(Intrusive rock)

K-feldspar	35%
Plagioclase	30%
Quartz	15%
Opaques	7%
Chlorite	7%
Sericite	5%
Sphene	1%
Zircon	Trace

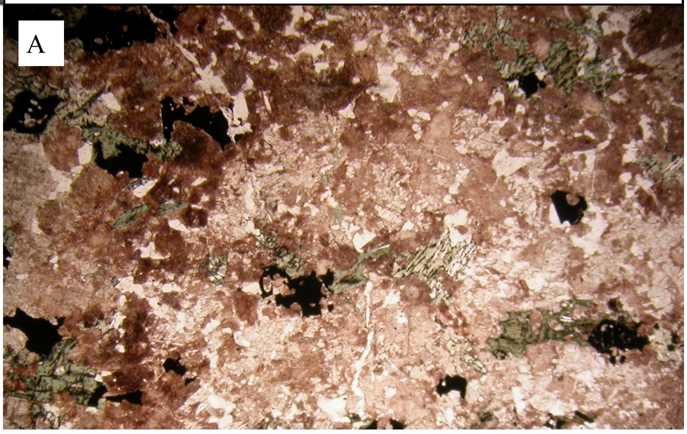

Mineralogical and textural description
- Intrusive rock is dominated by K-feldspar, plagioclase, quartz and chlorite replaced biotite or amphibole (A,B), and is a granitoid of some sort. Plagioclase is euhedral-subhedral and between 0.5 and 2mm in typically lather to equant crystals. K-feldspar is sub-anhedral and is 0.4-3mm in size, with composition dominantly orthoclase and microcline. Perthitic textures are present but rare in feldspars. All feldspars are well altered, with both sericite alteration and hematite dusting prevalent. Quartz is finer grained (<1mm) and appears to fill interstitial spaces between the feldspars and is anhedral with the exception of a few needle shaped crystals. Opaques range from anhedral to subhedral and are 0.3 to 1.7 mm in diameter. Anhedral crystals tend to grow around earlier plagioclase crystals. Sphene appears to have grown with/or earlier than this opaque mineral as a small sub-euhedral crystal. The chlorite replaced biotite (assumed based on remnant brown pleochroism) has grown around feldspar, opaques and sphene. Remnant biotite appear to contain remnant zircon. Two stages of alteration. 1) a quartz-chlorite fine vein network which networks with the chlorite-replaced biotite crystals. 2) a carbonate veining with large (to 3mm) carbonate crystals. This stage appears in the corner of the slide and has created selvages of fine grained opaque and ?Epidote (dirty green mineral)

-The contact zone between the country and intrusive rocks is dominated by a magnetite-chlorite zone (C), although again judging by a prominent remnant single cleavage that this was once biotite. Magnetite occurs as 0.3-2.7 mm crystals—mostly euhedal to subhedral crystals commonly with small sphene inclusions. Quartz occurs as small crystals in a few areas. Chlorite appears to have been later alteration stage.

-The country rock is nearly 50% magnetite and 50% quartz. These minerals and lesser carbonate are interlocking and subhedral ranging from 0.05 to 0.5 mm grains, suggestive of recrystallisation (D). Veins of carbonate-chlorite-K-feldspar cut this section and are probably linked to the veins associated with the granite. Again, what looks like remnant biotite is present in low amounts.

-Investigation of a thich section of the country rock revealed the opaques to be a magnetite core surrounded by hematite (martite)

Interpretation: A contact between intrusive granitoid (quartz monazite) and a metasedimentary rock

Rock name: Aplitic quartz monzonite/quartz-martite hornfels

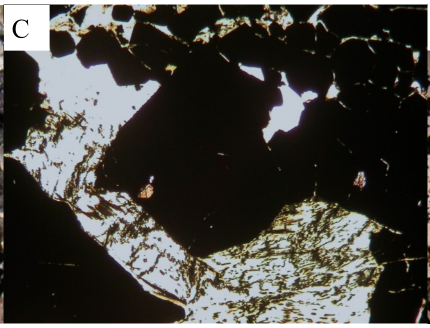

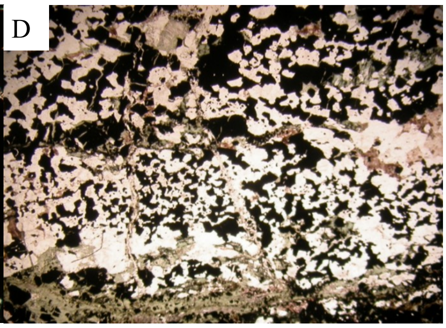

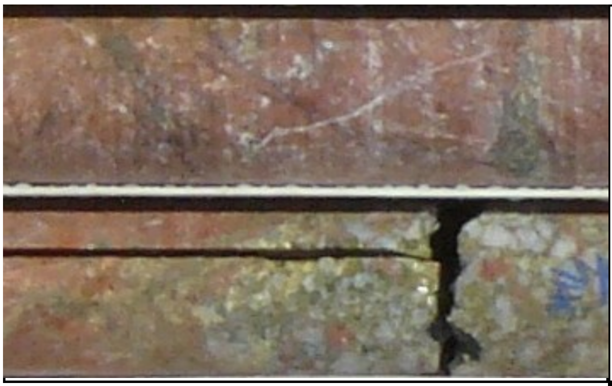

Hole ID: HDD013
Sample Number: 035
Depth: 744.7
Reason For sampling:
Identify micaceous/epidote? alteration of granite. Further classify granite type
Hand specimen description:
- fine grained green-pink rock. A few large pink feldspar crystals visible. Several clear veins running through slide, some with numerous fine opaques.

Mineral Abundances

K-feldspar	45%
Sericite	40%
Plagioclase	5%
Carbonate	5%
Opaques	3%
Quartz	2%

Mineralogical and textural description
- Rock dominantly composed by remnant coarse grained K-feldspar, predominantly orthoclase and microcline. These feldspars are being heavily altered to sericite (the green mineral in hand specimen). No epidote is present. Sericite is very fine grained, however several larger crystals are present. These show obvious pastel blue-green-pink pleochroism. Hematite staining of feldspar is rare, and most feldspars are fractured along their cleavage and are replaced by sericite. Feldspars were coarse grained (>3mm) in the primary rock. The rock has later been fractured and brecciated in places. Carbonate veins occur and appear to overprint the earlier sericite, however are discontinuous. Opaques mostly occur as veinlets in the sericite. Some opaques have a needle-lathe like composition, and possibly are hematite based on similar lathes identified in polished section

Interpretation:
-A feldspar rich granite (syenite) which has been extensively fractured and altered to sericite

Rock name
-Sericite altered synenite

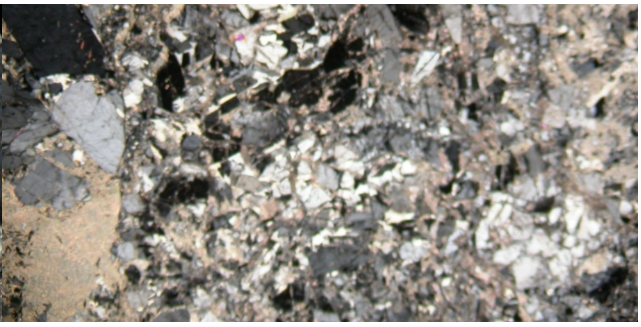

Hole ID: HDD013
Sample Number: 037
Depth: 688
Reason For sampling:
Intensely seriticised granite, however preserved patches of fresh rock
Hand specimen description:
- A fine grained, clear-pink-green coloured rock, with fine opaques. Second section appears to be opaque and chlorite filled breccia. Chlorite and carbonate veins run throughout the rock

Mineral Abundances

• K-feldspar	50%
• Quartz	18%
• Opaques	12%
• Plagioclase	10%
• Chlorite	3%
• Epidote	3%
• Sericite	2%
• Sphene	1%

Mineralogical and textural description

- A fine grained rock consisting primarily of K-feldspar (microcline and orthoclase), quartz and plagioclase groundmass with trace sphene. Plagioclase is relatively euhedral in shape, while K-feldspar and quartz are anhedral. Grains interlock quite well. Grain size between 0.05 and 0.1 mm on average for quartz and feldspars, while sphene is finer. Feldspars are usually altered to sericite and chlorite, especially near veins. Opaques are eu-subhedral and are likely part of the primary rock (not alteration), Epidote alteration is minor, but occurs in several strong bands. Both chlorite and later carbonate veins cut the epidote section. Part of the rock is strongly brecciated—the clasts are the same composition as above, but matrix is an opaque mineral. Breccia margin immediate, not gradual, however some chlorite-sericite-carbonate veins extend out of the breccia zone into the matrix, along with several smaller branches of the breccia (probably paths the opaque-laden fluid used as opposed to mechanical breccias). Several stages of vein-chlorite and carbonate appear to reuse the zone of weakness at the margin of the breccia.

Interpretation:

Based on the fine grained crystalline nature of the rock, it is likely the primary rock was an aplite of quartz-feldspar composition. Later brecciation with fluid flow formed the main opaque breccia, and later chlorite and carbonate rich fluid reused the breccia margins.

Rock name

- Metasomatised aplite

TtaniQ LA-ICPMS Samples and spots

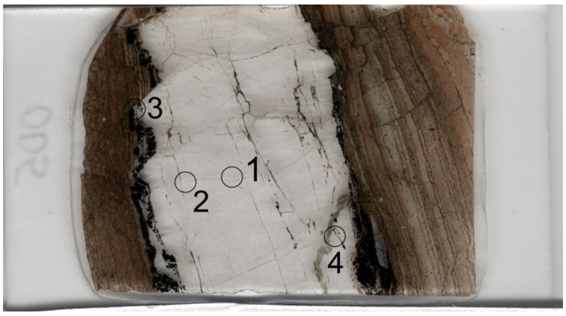

005:Polished thick section

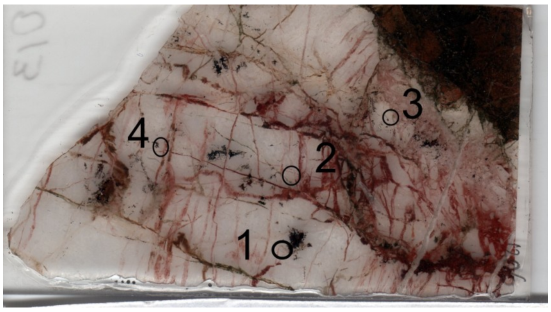

013:Polished thick section

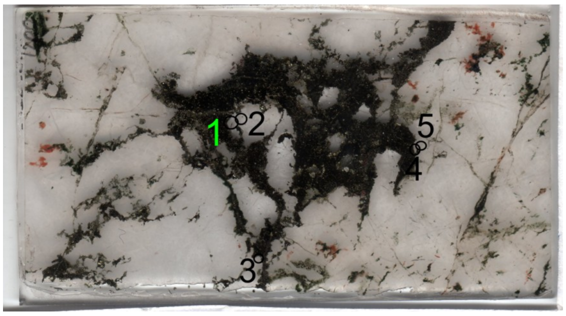

020:Polished thick section

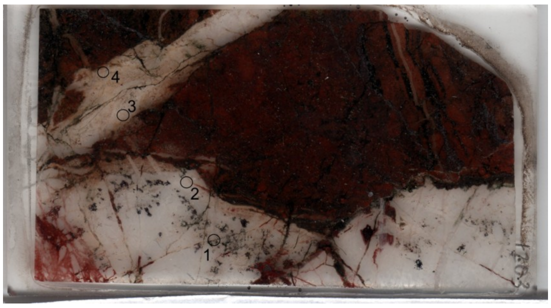

027:Polished thick section

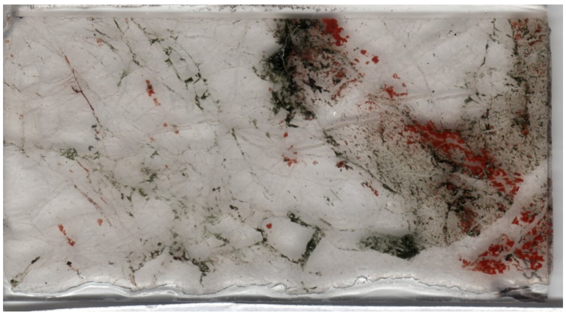

7152:Polished thick section

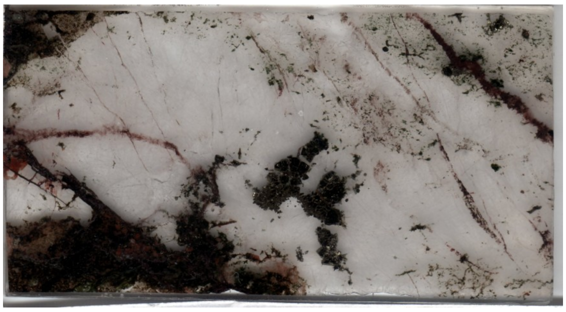

7155:Polished thick section

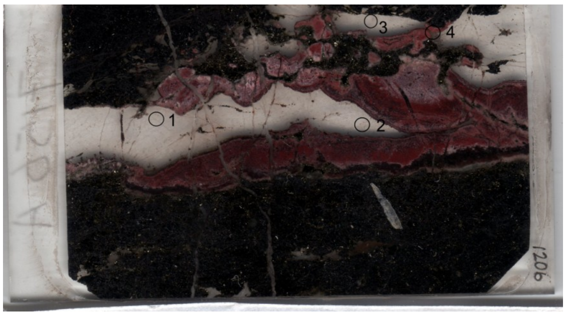

7156A:Polished thick section

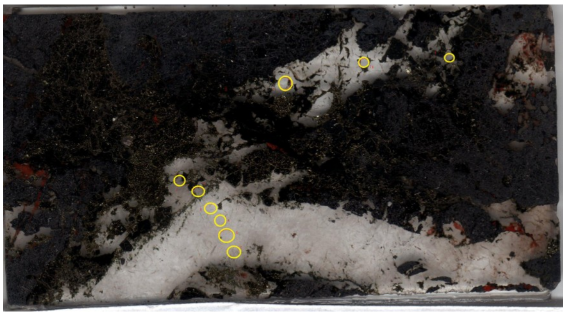

7161:Polished thick section

TtaniQ LA-ICPMS Samples and spots

7171:Polished thick section

Chlorite microprobe Samples and spots

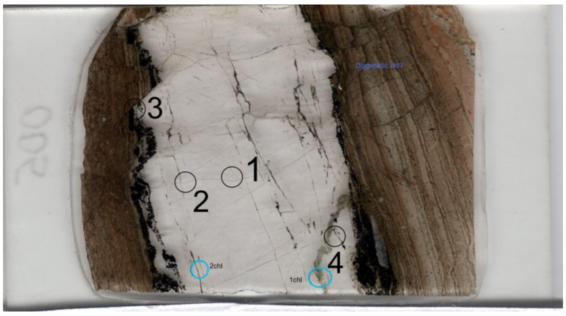

005:Polished thick section (Note blue circles are chlorite, others are TitaniQ spots

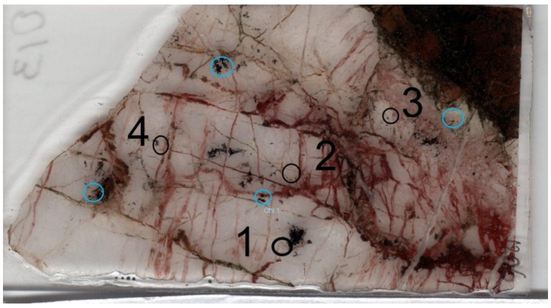

013:Polished thick section Polished thick section (Note blue circles are chlorite, others are TitaniQ

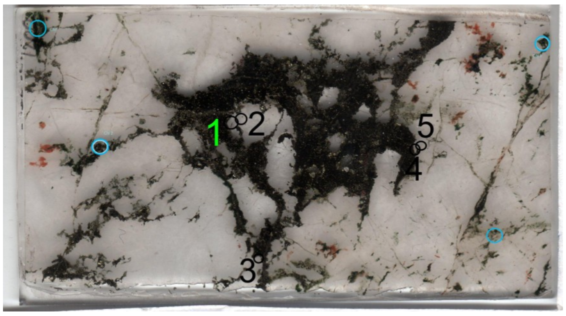

020:Polished thick section (Note blue circles are chlorite, others are TitaniQ spots

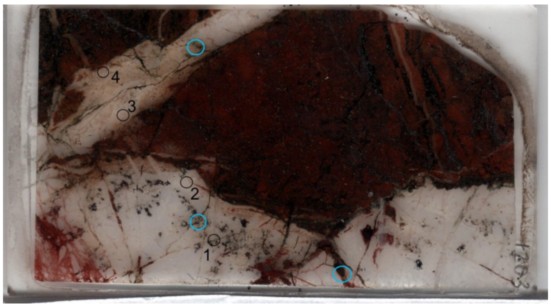

027:Polished thick section Polished thick section (Note blue circles are chlorite, others are TitaniQ

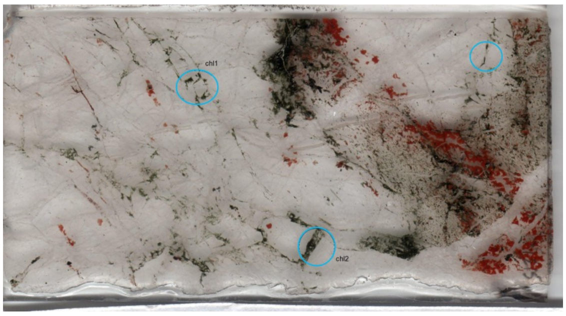

7152:Polished thick section (Note blue circles are chlorite, others are TitaniQ spots

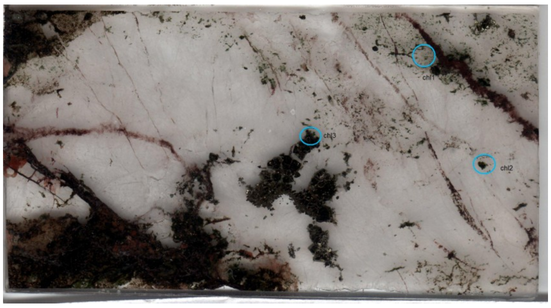

7155:Polished thick section Polished thick section (Note blue circles are chlorite, others are TitaniQ